CENTRO INTERNACIONAL DE ESTUDOS
DE DOUTORAMENTO E AVANZADOS
DA USC (CIEDUS)

TESE DE DOUTORAMENTO

SUPERCRITICAL TECHNOLOGY APPLIED TO THE DEVELOPMENT OF DRUG DELIVERY SYSTEMS FOR BONE REGENERATION

Leticia Goimil García

ESCOLA DE DOUTORAMENTO INTERNACIONAL

PROGRAMA DE DOUTORAMENTO EN INVESTIGACIÓN E DESENVOLVEMENTO DE MEDICAMENTOS

SANTIAGO DE COMPOSTELA

ANO 2019

USC
UNIVERSIDADE
DE SANTIAGO
DE COMPOSTELA

DECLARACIÓN DO AUTOR/A DA TESE

Supercritical technology applied to the development of drug delivery systems for bone regeneration

D./Dna. Leticia Goimil García

Presento a miña tese, seguindo o procedemento axeitado ao Regulamento, e declaro que:

1) A tese abarca os resultados da elaboración do meu traballo.
2) De selo caso, na tese faise referencia ás colaboracións que tivo este traballo.
3) A tese é a versión definitiva presentada para a súa defensa e coincide coa versión enviada en formato electrónico.
4) Confirmo que a tese non incorre en ningún tipo de plaxio doutros autores nin de traballos presentados por min para a obtención doutros títulos.

En Santiago de Compostela, 31 de Maio de 2019

Asdo.

USC
UNIVERSIDADE
DE SANTIAGO
DE COMPOSTELA

AUTORIZACIÓN DO DIRECTOR / TITOR DA TESE

Supercritical technology applied to the development of drug delivery systems for bone regeneration

Dna. Carmen Álvarez Lorenzo
D. Carlos A. García González

INFORMA/N:

Que a presente tese, correspóndese co traballo realizado por Dna. ***Leticia Goimil García****, baixo a nosa dirección, e autorizamos a súa presentación, considerando que reúne os requisitos esixidos no Regulamento de Estudos de Doutoramento da USC, e que como director desta non incorre nas causas de abstención establecidas na Lei 40/2015.*

En Santiago de Compostela, 31 de Maio de 2019

Asdo. Asdo

USC
UNIVERSIDADE
DE SANTIAGO
DE COMPOSTELA

"...Human beings, little bags of thinking water held up briefly by fragile accumulations of calcium..."

— Terry Pratchett

USC
UNIVERSIDADE
DE SANTIAGO
DE COMPOSTELA

El “hacerse a uno mismo” es un concepto muy extendido —generalmente ligado al triunfo del esfuerzo (uni)personal— y, sin embargo, también muy erróneo. Son muy pocas las cosas que se pueden conseguir enteramente en solitario, si es que hay alguna. Tampoco debe ser el objetivo. Pedir ayuda no es una muestra de debilidad; una tarea que parecía inabarcable se vuelve menos intimidante al tener a alguien a nuestro lado. Especialmente en investigación, donde el fin último son las personas, no se debe minimizar la importancia de lo humano. A veces son nuestra inspiración, nuestra guía o nuestra motivación. Un empujón cuando crees que no puedes más. Una sonrisa en la que apuntalarse para seguir adelante. La realización de una tesis es uno de esos trabajos imposibles en apariencia, tan inmensos que a veces es difícil no desistir, no perder el rumbo.

Por suerte, no estamos solos.

El día que comencé la carrera de Farmacia, paseando con mi abuelo Manolo por la zona vieja, él señaló una tienda y dijo “Cuando termines la carrera te compro uno de esos anillos”. No pudo llegar a verme licenciarme. El día de la graduación llevé unos pendientes que me había regalado años atrás; aunque no significaba nada para el resto del mundo, era un detalle importante para mí. Una forma de tenerlo presente a mi manera. Tampoco ha podido acompañarme hasta aquí mi abuela Maru, a quien recuerdo en su cocina contándome la historia de El Cid y enseñándome que “arisco” es una de las peores cosas que se pueden ser. Tal vez ya no estén, pero este logro también es en parte suyo, y sencillamente no podía no dedicárselo. Gracias por tanto.

Huelga decir que la realización de esta tesis hubiese sido irrealizable sin la dirección y la dedicación de *Carmen Álvarez Lorenzo* y *Carlos García González*, sin la inestimable colaboración del profesor *José Luis Gómez Amoza* o sin la oportunidad del profesor *Hermínio C. de Sousa* y la doctora *Mara E.M. Braga* para realizar una estancia de investigación en su laboratorio.

Tampoco estaría aquí de no ser por la profesora *Begoña Seijo* y el amor por la Tecnología Farmacéutica que transmitía en sus clases. Por supuesto, también agradezco a los demás profesores del departamento, particularmente a *Ángel Concheiro, Mariana Landín, Ramón Martínez*

Pacheco y *Francisco Otero Espinar*, su orientación, su cercanía y su disposición para conversar sobre lo que hiciera falta.

En todos estos años también he podido contar con excelente compañía en el laboratorio. Aquellos que al principio de todo me enseñaron a moverme por el laboratorio —y no morir en el intento—: *Clara, Isa, Sonia, Luis* y *Lidia*. Los que conocí en el máster y siempre tienen un oído, un comentario o una sonrisa que ofrecer —*María, Rubén, Ana, Tamara, Marta*. Gente con quien pude compartir unos pocos (pero grandes) meses tanto en Santiago —*Xelhua, Maira, Ibeth, Jesús*— como en Coímbra —*Mariana, Akel, Luisa, Sofía, Rita*. A los compañeros del día a día, tanto los que estuvieron desde el principio como los que llegaron luego para quedarse —*Fer, Víctor, Mirian, Patri, Clara López, Víctor Santos* y *Xián*, entre otros muchos. Y, por supuesto, quienes ya son amigos y, prácticamente, familia —*Lorena, Helena, Jorge*; me alegro infinito de conoceros.

También hubo momentos en los que alguien tenía que poner un poco de locura en la cordura. Esas personas maravillosas que creen en mí más que yo, que me soportan, que me animan. Que me ayudan a desconectar y a la vez a descubrir otras partes de mí. Hablo de *Daniel* y *Adrián*. De *Carol, Isa, Naza* y *Estela*. De *María Torres*. De *Sara, Nati, Nereida, Zeltia* y *Marilu*. Y más recientemente, pero no por ello menos importantes, de *Alba, Dara* y *Jeannette*. Gracias. Por hacerme sentir cómoda siendo yo. Por compartir momentos e ideas. Por inspirarme. Por empujarme a alcanzar sueños que creía perdidos. Por estar ahí para escuchar, aunque sea a trescientos, mil o diez mil kilómetros, sólo a un mensaje de distancia, y conseguir que todo valga la pena.

Pero, sobre todo, gracias a mi familia. A mi hermano. A mis padres. Especialmente a mis padres. Por vuestro apoyo, por el cariño, por enseñarme a querer saber, a pensar e intentar ver más allá. Os debo todas las oportunidades que he tenido y que me han traído hasta aquí.

Es una larga lista. Me alegra que lo sea. Me alegro de haber encontrado a tanta gente increíble en mi camino. No importa si es por un trecho largo o corto. A todos, GRACIAS POR ESTAR AHÍ.

USC
UNIVERSIDADE
DE SANTIAGO
DE COMPOSTELA

INDEX

USC
UNIVERSIDADE
DE SANTIAGO
DE COMPOSTELA

I. RESUMEN

La medicina regenerativa está experimentando un creciente auge con un enorme desarrollo en los últimos años. Esta tendencia se halla ligada a la creciente demanda de soluciones sociosanitarias para problemas derivados de los procesos naturales de envejecimiento y de las necesidades de reparación de lesiones asociadas no sólo a accidentes laborales y de tráfico sino también a nuevos hábitos de vida, como la práctica generalizada del deporte. Las aproximaciones clásicas para hacer frente al deterioro o la pérdida de un tejido se basan, principalmente, en incorporar un material con capacidad para suplir la pérdida física pero sin recuperar la función completa de ese tejido. Un buen ejemplo de ello son las prótesis metálicas que se implantan en sustitución de huesos o porciones de hueso en el caso de fracturas grandes o resecciones quirúrgicas asociadas a tumores. El principal problema de las prótesis inertes es que, aunque sirven de puente entre los extremos de la lesión, también actúan como obstáculo frente a la regeneración natural del tejido. En el caso de una persona en crecimiento, esto obliga incluso a intervenciones periódicas para sustituir la prótesis por otra de dimensiones mayores. En el caso de un adulto, la durabilidad de la prótesis puede resultar insuficiente dada la creciente esperanza de vida de la población.

El estudio del proceso de regeneración natural de los tejidos en los seres vivos encierra un gran interés para solventar estas limitaciones ligadas a las prótesis inertes. Se pretende aprovechar el conocimiento sobre las cascadas de curación y reparación para plantear aproximaciones biomiméticas. La gran mayoría de los tejidos de nuestro organismo se encuentran en un proceso continuo de regeneración para suplir el desgaste natural que permite que las pequeñas lesiones se reparen espontáneamente. Cuando la lesión supera un cierto tamaño denominado crítico (que depende de cada tejido), los mecanismos de regeneración fallan y el organismo para

mantener la homeostasis desencadena procesos de cicatrización que dan lugar a tejidos de prestaciones inferiores a las del tejido no lesionado. Si la herida es muy grande, puede ocurrir que no se produzca la cicatrización, convirtiéndose en una lesión crónica.

La regeneración natural de los tejidos se basa, a grandes rasgos, en la formación de un nicho o soporte adecuado en el que se puedan asentar, diferenciarse y proliferar las células. Para imitar este proceso resulta necesario, por lo tanto, contar con materiales que puedan servir de andamios (*scaffolds*, en la terminología inglesa), que alberguen las células adecuadas o las sustancias activas necesarias para atraerlas y regular su crecimiento. La utilización de porciones sanas del mismo tejido como scaffold en una zona lesionada ha sido ampliamente investigada. El injerto de hueso del propio paciente (autólogo) reúne las tres características deseables para la regeneración de lesiones de tamaño superior al crítico: osteoconducción, es decir, sirve de guía (andamio) en el proceso de reparación del hueso natural; osteoinducción, contiene las sustancias necesarias para fomentar que las células no diferenciadas se conviertan en osteoblastos activos; y osteogénesis, aporta células de hueso que deben contribuir a la remodelación ósea. A pesar de los buenos resultados clínicos que se obtienen, el injerto autólogo tiene los inconvenientes de requerir una intervención adicional para extraer tejido de la zona dadora, que en pacientes mayores o con alguna patología crónica puede ser un área muy limitada y de curación lenta, e implica el riesgo de infecciones. Las alternativas naturales con injertos procedentes de donantes (aloinjertos) o de animales (xenoinjertos) tienen riesgo de rechazo, de transmisión de enfermedades y su disponibilidad es limitada. Además hay que tener en cuenta que sólo el injerto autólogo es osteogénico, ya que en las alternativas mencionadas el tejido se debe descelularizar antes de la implantación.

El tejido óseo es, después de la sangre, el tejido con mayor demanda lo que ha motivado un mayor esfuerzo investigador en el diseño de scaffolds sintéticos específicos para hueso. Los scaffolds sintéticos deben tener una estructura 3D porosa que guie y promueva el crecimiento de los tejidos, que facilite la difusión de nutrientes y oxígeno y la eliminación de productos de desecho de las células, y que

cuente con propiedades mecánicas similares al tejido a reemplazar. La porosidad debe ser de entre el 65 y el 80 %, y debe combinar microporos (~ 10 µm) que faciliten la adhesión celular y macroporos (~ 350 µm) que permitan la colonización celular no sólo en superficie sino también en profundidad. Además de ser biocompatible –es decir, que ni los materiales ni los productos de degradación pueden resultar tóxicos para las células– el scaffold debe biodegradarse a la misma velocidad a la que se forma el nuevo tejido, de manera que proporcione soporte mecánico sin impedir la regeneración completa del tejido. El scaffold sintético no debe desempeñar un papel meramente pasivo en la regeneración sino que debe modular la respuesta del organismo al daño y también el comportamiento de las células que lo colonicen. En este sentido, se ha ensayado la incorporación de una amplia variedad de sustancias activas, principalmente factores de crecimiento con capacidad osteoinductiva.

Desde un punto de vista tecnológico, los dos principales retos que plantea la preparación de scaffolds rígidos porosos son: a) conseguir que su arquitectura porosa interna se ajuste a las características de la estructura del hueso, con una población bimodal de poros interconectados; y b) mantener la cantidad y la actividad de los factores de crecimiento o de los fármacos necesarios para promover la adhesión, diferenciación y proliferación celular. Los procedimientos clásicos de preparación de materiales porosos implican, en su mayoría, la exposición de polímeros y porógenos a disolventes orgánicos volátiles, la aplicación de calor hasta alcanzar temperaturas relativamente elevadas para fundir el polímero y/o evaporar el porógeno, o la lixiviación con disolventes que arrastren el porógeno. Ninguna de estas técnicas permite un control preciso de la estructura porosa. Además, tienen el riesgo de que las sustancias activas se pierdan por degradación o por arrastre, lo que redunda en un bajo rendimiento de carga.

En los últimos años, la tecnología de fluidos supercríticos y comprimidos se está revelando como una herramienta capaz de dar respuesta a los retos principales de la medicina regenerativa. Si bien esta tecnología se viene utilizando desde hace tiempo en campos muy variados, tan sólo recientemente ha empezado a ensayarse con

biomateriales. Los fluidos alcanzan condiciones supercríticas cuando la temperatura y la presión se sitúan por encima de las del punto crítico, caracterizados por su temperatura (Tc) y presión crítica (Pc), respectivamente. Los fluidos supercríticos están dotados de propiedades fisicoquímicas singulares que los hacen muy útiles para el procesado de materiales, destacando su elevada difusividad, que permite que penetren en materiales con morfologías y texturas complejas. El CO_2 supercrítico ($scCO_2$) es el fluido supercrítico más empleado debido a que las condiciones moderadas de su punto crítico (73,8 bar, 31,1 ºC) son adecuadas para materiales lábiles. Además, no es inflamable, es económico, relativamente inerte y está considerado como seguro (GRAS). El interés en el $scCO_2$ para la preparación de scaffolds porosos se basa en su capacidad para disolverse en polímeros amorfos y semicristalinos. El $scCO_2$ actúa como plastificante, reduciendo el punto de fusión y la temperatura de transición vítrea de los polímeros. Los poros se forman en el material durante la despresurización cuando la remoción del CO_2 da lugar a una inestabilidad termodinámica que provoca la expansión de la matriz polimérica. La porosidad del producto resultante depende de la cantidad de CO_2 que se adsorbe durante el espumado, y se puede ajustar regulando la temperatura, la presión y el tiempo de procesado. La interconectividad de los poros depende de la velocidad de despresurización y de la velocidad de enfriamiento como parámetros de procesado principales. La evaporación completa del CO_2 resulta en un producto sólido poroso libre de disolventes y de impurezas. Resulta una técnica muy versátil que se puede aplicar al diseño de sistemas de diferente composición (orgánicos e híbridos), morfología (esponjas, micro y nanopartículas, monolitos), porosidad (meso y macroporosidad) y arquitectura interna (homogénea, multicapa, multicomponente).

Esta Tesis Doctoral se planteó con el objetivo general de diseñar scaffolds porosos útiles en regeneración ósea. Para ello, se seleccionaron como componentes principales poliésteres biodegradables, tales como la poli(ε-caprolactona), PCL, y el ácido poli(láctico-co-glicólico), PLGA. Se implementaron procedimientos de procesado utilizando $scCO_2$ o CO_2 comprimido para obtener tres

tipos de scaffolds: (1) scaffolds de PCL y PLGA con almidón pregelificado para cesión controlada de dexametasona; (2) scaffolds de PCL conteniendo aerogeles de almidón para cesión sostenida de ketoprofeno para regeneración ósea; y (3) scaffolds de PCL y aerogeles de fibroína de seda para cesión controlada de dexametasona.

De acuerdo con estos objetivos, el trabajo se llevó a cabo en tres etapas:

1. Preparación de scaffolds, mediante espumado con CO_2 comprimido, de PCL y PLGA con almidón pregelificado y cargados con dexametasona para regeneración ósea, y evaluación de su estabilidad durante el almacenamiento. Esta etapa de la Tesis se centró en dos objetivos principales: evaluar las posibilidades que ofrece la incorporación de almidón pregelificado para modular la estructura porosa y la cesión de sustancias activas a partir de los scaffolds; y obtener información sobre la estabilidad de los scaffolds en condiciones de almacenamiento controladas que reflejan las condiciones climáticas de la zona II según el International Council for Harmonization (ICH). Este último es un aspecto crítico para determinar el periodo de vida útil del scaffold una vez preparado y establecer las características requeridas para el material de acondicionamiento. No obstante, hasta la fecha se ha prestado muy poca atención a la estabilidad de los scaffolds por lo que la información disponible es muy escasa. Para llevar a cabo este estudio se contó con la colaboración de Ph. Jaeger de la compañía Eurotechnica GmbH, que evaluó la capacidad de absorción de CO_2 en las matrices poliméricas mediante balanza de suspensión magnética, y de I. Ardao del grupo BioFarma de la Universidade de Santiago de Compostela, que realizó los estudios de modelización de la cesión *in vitro* de dexametasona.

En primer lugar, se prepararon mezclas de PCL y PLGA (50:50) de baja viscosidad inherente con y sin almidón pregelificado y dexametasona. Las mezclas se compactaron utilizando una máquina de comprimir excéntrica para obtener compactos de 400 mg de masa (14x10x2.6 mm). A continuación, se aplicó un protocolo de espumado asistido por CO_2 comprimido previamente patentado en el grupo I+D

Farma, y que se adaptó a los compactos. Los compactos se expusieron a CO_2 a 26 ºC y 60 bar durante 30 min. Posteriormente, la presión se redujo a 30 bar a una velocidad de 10 bar/min, y se volvió a incrementar de nuevo a 60 bar mediante la incorporación de CO_2 líquido a 1 ºC. Este protocolo se repitió tres veces antes de proceder a la despresurización a 10 bar/min. Se eligieron estas condiciones de temperatura y presión suaves para hacerlas compatibles con la estabilidad de moléculas activas lábiles como la dexametasona, y también para evitar un espumado descontrolado del PLGA de baja viscosidad inherente contenido en el scaffold.

A continuación, los scaffolds se caracterizaron en cuanto a características morfológicas, comportamiento frente a la temperatura, biodegradabilidad y propiedades mecánicas. El proceso de espumado hizo que el volumen de los scaffolds aumentara cuatro veces con respecto al volumen de los compactos no procesados, lo que supone valores de porosidad total de 68-75 %. Los poros presentaron dos poblaciones de macroporos, una de tamaño comprendido entre 50 y 200 µm, y otra de unas 10 µm de tamaño medio. El efecto de la composición de los scaffolds sobre la velocidad de erosión se evaluó en tampón fosfato salino de pH 7,4. La velocidad de erosión fue similar en todos los scaffolds durante los primeros 14 días, con una pérdida de peso de ~25 % y que está asociada a la degradación del PLGA. La incorporación tanto de dexametasona como de almidón pregelificado dio lugar a valores de pérdidas de masa más elevadas a partir de los 14 días, y que se justifican por la formación de poros mayores a medida que se disuelven/dispersan en el medio acuoso.

Para evaluar la estabilidad, los scaffolds (no embalados) se mantuvieron en una cámara a 25 ºC y 65 % de humedad relativa, imitando las condiciones climáticas de la zona II según la ICH (Europa, Estados Unidos y Japón). Se monitorizaron los cambios en la estructura de los scaffolds, sus propiedades fisicoquímicas y mecánicas, y los perfiles de cesión de dexametasona al cabo de 1 y 3 meses. Se observaron disminuciones significativas del volumen de los scaffolds, debido a procesos de densificación, que fueron más marcadas en el caso de aquellos preparados con dexametasona y almidón. Al cabo de tres meses, los scaffolds preparados con almidón

mostraron un descenso muy notable de la porosidad y el volumen total de los poros, lo que puede ser atribuido al hinchamiento de la fracción de amilopectina del almidón por efecto de la humedad. También se observaron cambios en las propiedades mecánicas y en los perfiles de cesión. En conjunto, los resultados obtenidos indican que la exposición directa de los scaffolds a 25 ºC y 65 % de humedad relativa causa efectos negativos sobre las propiedades de los scaffolds, de distinta magnitud dependiendo de la composición. La dexametasona y el almidón conducen a estructuras menos cristalinas y más sensibles a la humedad ambiental. La velocidad de cesión de dexametasona se produce mayoritariamente por la erosión de la matriz. El posible control del almidón pregelificado sobre la cesión de la dexametasona se reduce cuando los scaffolds se almacenan durante un período de tiempo prolongado.

2. Procesado supercrítico de aerogeles de almidón y de scaffolds de PCL conteniendo aerogeles para cesión sostenida de ketoprofeno para regeneración ósea. El objetivo principal de esta etapa de la Tesis fue preparar scaffolds porosos de poli(ε-caprolactona), PCL, conteniendo ketoprofeno y micropartículas de aerogel de almidón. El ketoprofeno es un anti-inflamatorio no esteroídico (AINE) que se administra por vía oral durante el período postoperatorio para aliviar el dolor y reducir la inflamación. El ketoprofeno no inhibe el proceso de curación del hueso, por lo que la cesión localizada podría permitir regular la respuesta inflamatoria que está normalmente asociada al proceso de implantación utilizando dosis bajas y minimizando efectos secundarios. Por su parte, las micropartículas de aerogel de almidón se caracterizan por una elevada mesoporosidad y pueden incorporar sustancias activas. La hipótesis del trabajo fue que la incorporación de micropartículas de aerogel de almidón debe permitir modular la estructura porosa del scaffold y la velocidad de cesión del ketoprofeno. Esta parte de la Tesis se llevó a cabo en colaboración con el grupo de H. C. de Sousa del Chemical Engineering Department, FCTUC, de la Universidade de Coimbra en el marco de una estancia predoctoral de 5 meses.

En primer lugar se puso a punto, por primera vez, un procedimiento de preparación de microesferas de aerogel de almidón del tamaño de una micra. Para ello se desarrolló un procedimiento de emulsión-gelificación en el que se partió de una emulsión de fase interna acuosa (dispersión de almidón al 15 %) y de fase externa oleosa (aceite de parafina) utilizando un agente emulsificante adecuado. La mezcla se llevó a autoclave, se aplicaron ultrasonidos manteniendo la mezcla a 95 ºC y después se enfrió para la completa gelificación del almidón. Las microsferas de hidrogel de almidón obtenidas se sumergieron en etanol y el alcogel resultante se secó en condiciones supercríticas para obtener las microesferas de aerogel. Parte de las microesferas se cargaron con ketoprofeno utilizando también $scCO_2$ mediante impregnación supercrítica.

Se prepararon lotes de scaffolds de PCL sin/con aerogel y sin/con ketoprofeno libre en el scaffold o previamente incorporado al aerogel. Las mezclas de los componentes se expusieron a $scCO_2$ a 37 ºC y 140 bar, durante 60 min en condiciones estáticas. La despresurización se llevó a cabo a una velocidad de venteo de 1,8 g/min hasta presión atmosférica. Todos los scaffolds se caracterizaron en cuanto a sus propiedades morfológicas, físico-químicas y mecánicas mediante análisis de adsorción-desorción de N_2, microscopía electrónica de barrido, porosimetría de intrusión de mercurio, modelado 3D, análisis mecánico dinámico y calorimetría diferencial de barrido. Los andamios preparados con aerogeles de almidón presentaron mayor porosidad e interconectividad de los poros, lo que debe facilitar la penetración de células madre mesenquimales, aunque a costa de un pequeño debilitamiento de las propiedades mecánicas.

Los estudios de cesión de ketoprofeno se llevaron a cabo sumergiendo piezas de scaffold en tampón fosfato salino de pH 7,4, en condiciones sink, a 37 ºC y bajo agitación. La monitorización de la concentración de ketoprofeno en el medio de cesión reveló que todos los scaffolds podían sostener la cesión durante varios días. No obstante, la cesión fue más rápida desde los scaffolds preparados con aerogeles de almidón, probablemente debido a la más alta accesibilidad del agua a la estructura interna del scaffold.

En su conjunto, los resultados de esta etapa ponen de manifiesto que la combinación de PCL con microesferas de aerogel de almidón y el procesado de las mezclas mediante espumado supercrítico permite obtener scaffolds cargados con ketoprofeno que cuentan con una estructura porosa, en términos de porosidad total, distribución de tamaños de poro e interconectividad, adecuada para el crecimiento celular y capaz de proporcionar perfiles de cesión sostenida de sustancias activas.

3. Preparación de scaffolds de PCL y aerogeles de fibroína de seda con dexametasona, mediante espumado con $scCO_2$, para regeneración ósea. En estudios previos, se ha observado que la fibroína de seda promueve la adhesión y el crecimiento de células madre mesenquimales en scaffolds. Sin embargo, su utilización en forma de partículas de aerogel no ha sido investigada previamente. Por otra parte, es conocido que la dexametasona base y la dexametasona-21-fosfato de sodio presentan una solubilidad distinta en medios acuosos, lo que puede condicionar su velocidad de cesión. Tomando como base estas premisas, en la última etapa de la Tesis, se prepararon scaffolds a partir de mezclas de PCL, micropartículas de aerogel de fibroína de seda y dexametasona con el objetivo de contrastar las hipótesis siguientes: (i) las micropartículas de aerogel de fibroína de seda pueden mejorar la estructura porosa del scaffold y facilitar la infiltración celular y el transporte de fluido biológico; y (ii) la incorporación de dexametasona en forma de base o en forma de sal puede llevar a diferentes perfiles de cesión y, por lo tanto, a diferentes resultados de regeneración ósea. Para llevar a cabo este estudio se contó con la colaboración del grupo de J.L. Cenis del Instituto Murciano de Investigación y Desarrollo Agrario y Alimentario (IMIDA), que proporcionó fibroína de seda fresca obtenida en condiciones GMP, y del grupo de C. Evora de la Universidad de La Laguna, donde se llevaron a cabo los estudios *in vivo*.

En primer lugar, se prepararon aerogeles de fibroína de seda a partir de una emulsión de fase interna disolución de fibroína de seda (8 %) y fase externa aceite de parafina, utilizando un agente emulsificante adecuado. Se ensayaron distintas condiciones de

procesado y se seleccionaron las que dieron lugar a partículas de tamaño submicrométrico tras aplicar secado supercrítico.

Para preparar los scaffolds, mezclas físicas de los componentes en polvo se compactaron manualmente y se expusieron a $scCO_2$ (37 ºC, 140 bar) durante 1 hora en condiciones estáticas. A continuación, se despresurizó a una velocidad de 1.8 g/min hasta presión atmosférica. Todos los scaffolds se caracterizaron en cuanto a morfología, comportamiento frente a la temperatura, biodegradabilidad, propiedades mecánicas, modelización *in silico* de la infiltración celular y capacidad para regular la cesión de dexametasona y promover la osteodiferenciación celular.

Los scaffolds de PCL presentaron forma cilíndrica y elevada porosidad (56-63 %), con poros en el intervalo de 100 a 200 μm de superficie lisa e interconectados. La presencia de aerogeles de fibroína de seda dio lugar a un incremento de la porosidad, del tamaño de los macroporos, que se situó entre 150 y 400 μm, y de la rugosidad de los poros debido a la localización preferente de los aerogeles en las proximidades de su superficie. Estos cambios dieron lugar a incrementos notorios de la permeabilidad al agua y la capacidad de infiltración celular.

Los perfiles de cesión resultaron ser muy dependientes de la forma química de la dexametasona (base o sal). Los scaffolds preparados con la dexametasona sal mostraron un burst en la primera hora seguido de cesión sostenida durante tres semanas. Por el contrario, los scaffolds preparados con dexametasona base proporcionaron cesión más sostenida, con perfiles ajustados a la cinética de Higuchi.

Las prestaciones de los scaffolds para regeneración ósea se evaluaron *in vivo* utilizando un modelo murino de defecto calvar de tamaño crítico (diámetro: 8 mm). Todos los scaffolds ensayados mostraron una excelente biocompatibilidad y, en comparación con el grupo control en el que no se colocó scaffold, favorecieron la reparación del tejido dando lugar a focos de osificación. La regeneración más efectiva se observó para los scaffolds preparados con los aerogeles de fibroína de seda y dexametasona sal. Este resultado se explica por la cesión rápida de la dexametasona que debe

proporcionar niveles terapéuticos de fármaco de manera rápida, pero que se mantienen en el tiempo.

En conjunto, las actividades llevadas a cabo en esta Tesis Doctoral han dado lugar a la implementación de nuevos protocolos de procesado de biomateriales y sustancias activas para la obtención de scaffolds porosos con utilidad potencial en regeneración ósea.

USC
UNIVERSIDADE
DE SANTIAGO
DE COMPOSTELA

II. ABBREVIATION LIST

ATR-FTIR: Attenuated Total Reflection–Fourier Transform Infra-Red
BET: Brunauer-Emmett-Teller
BJH: Barrett-Joyner-Halenda
BMP-2: bone morphogenetic protein-2
DS: dexamethasone 21-phosphate/dexamethasone salt
DSC: differential scanning calorimetry
DX: dexamethasone base
EMA: European Medicines Agency
FDA: Food and Drug Administration
FDM: fused deposition modeling
GMP: good manufacturing practices
GRAS: generally recognized as safe
HA: hydroxyapatite
HPLC: high performance liquid chomatography
ICH: International Council for Harmonisation
K: ketoprofen
LSD: least significant difference
MIP: mercury intrusion porosimetry
MSC: mesenchymal stem cell
NSAID: nonsteroidal anti-inflammatory drug
PBS: phosphate buffered solution
P_c: critical pressure
PCL: poly(ε-caprolactone)
PCL_{raw}: non-processed poly(ε-caprolactone)
PGA: poly(glycolic acid)
PGPR: polyglycerol polyricinoleate
PLA: poly(lactic acid)
PLGA: poly(lactic-co-glycolic acid)
PLLA: poly(L-lactic acid)
SA: silk fibroin aerogel

$ScCO_2$: supercritical CO_2
SEM: scanning electron microscopy
SF: silk fibroin
St: starch
StA: starch aerogel
St_p: pre-gelified starch
St_{raw}: starch in the native form
T_c: critical temperature
T_g: glass transition temperature
$T_m/T_{m,1}/T_{m,2}$: melting temperature values

USC
UNIVERSIDADE
DE SANTIAGO
DE COMPOSTELA

USC
UNIVERSIDADE
DE SANTIAGO
DE COMPOSTELA

1. INTRODUCTION

1.1. BONE FUNCTIONS, PROPERTIES AND REQUIREMENTS

Bone is a connective tissue with an extracellular matrix composed by a mineral phase of hydroxyapatite (HA) as main component and responsible for its compressive strength, and an organic phase that mainly consists of collagen type I, which represent 65 and 35 % of dry weight, respectively (Fig. 1.1) *(Henkel et al. 2013)*. This composition provides not only compressive strength and stiffness, but also enough ductility to withstand repetitive impacts without being fractured. Bone tissue has various functions in the organism: serves as point of attachment for skeletal muscles, provides support and protection for soft tissues and organs, contributes to mineral homeostasis by storing and releasing calcium and phosphate, and accommodates red bone marrow, which produces blood cells, and yellow bone marrow, a reservoir of triglycerides *(Doblaré et al. 2004, Tortora and Derrickson 2012, Florencio-Silva et al. 2015)*.

According to their dimensions and morphology, bones can be classified into long (e.g., femurs), short (carpals and tarsals), flat (cranial bones), sesamoid (kneecaps) and irregular (vertebrae). Bone shapes are interlinked to their mechanical functions: while long bones support body weight and help movement, flat and irregular bones protect internal organs, short bones provide stability and fine movement, and sesamoid bones protect tendons from stress *(Tortora and Derrickson 2012)*.

Bone structure can be divided into cancellous and cortical bone. Cortical bone is structured in osteons or haversian systems, composed by concentric lamellae surrounding a harvesian canal, which contains blood vessels, lymphatic vessels and nerves. There are spaces, lacunae, between the layers of lamellae containing the osteocytes, connected by canals with diameters ranging from 0.13 to 0.39 μm denominated canaliculi (Fig. 1.1) *(You et al. 2004)*. This wide net of

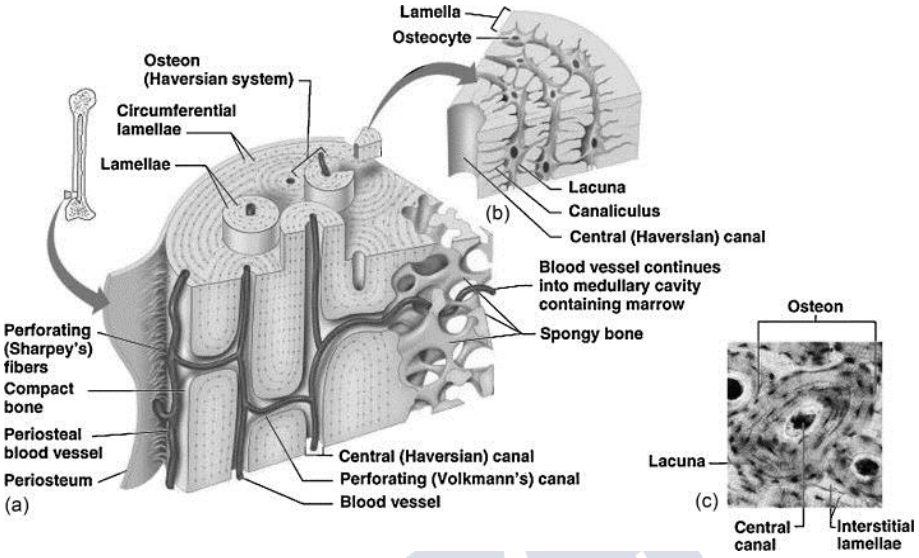

Fig. 1.1: Structure of cortical bone: (a) 3D sketch of cortical bone, (b) cut of a Haversian system and (c) micrograph of a Haversian system. Reproduced from Sprio et al. (2011) with permission of Elsevier.

canaliculi is filled with extracellular fluid, which provides osteocytes with nutrients and oxygen and removes waste products.

Cancellous bone is built by the bone marrow and presents a lamellar architecture with a high porosity, up to 90 %. Cancellous bone is always surrounded by a layer of varying thickness of cortical bone, which possesses higher density and stiffness; compressive strength and Young modulus of cortical bone can reach up to 230 MPa and 30 GPa respectively, while the values for cancellous bone are 12 MPa and 0.5 GPa. This combination of cortical and cancellous bone confers enough resistance to bones, capable of absorbing impacts and resisting deformation, without adding too much weight to the structure *(Velasco et al. 2015, Osterhoff et al. 2016).*

Despite its inert appearance, bone is a highly vascularized tissue with a constant remodeling that allows a high regenerative capacity of the tissue without scarring due to the action of bone cells: osteogenic cells, osteoblasts, osteocytes and osteoclasts (Fig. 1.2). Osteogenic cells, stem cells derived from mesenchymal stem cells, are the only bone cells that experiment cellular division, and differentiate into

osteoblasts. Osteoblasts are located on the bone surface and are responsible for bone formation synthesizing and secreting the organic components of bone matrix, such as collagen fibers, and initiate calcification. Once they are surrounded by the growing bone matrix, osteoblasts turn into osteocytes, and acquire the function of regulating bone metabolism through the exchange of nutrients and metabolic wastes between blood and bone tissue. Lastly, osteoclasts are large macrophage-like cells that take part in bone resorption and calcium homeostasis by secreting enzymes and acids that decompose bone matrix.

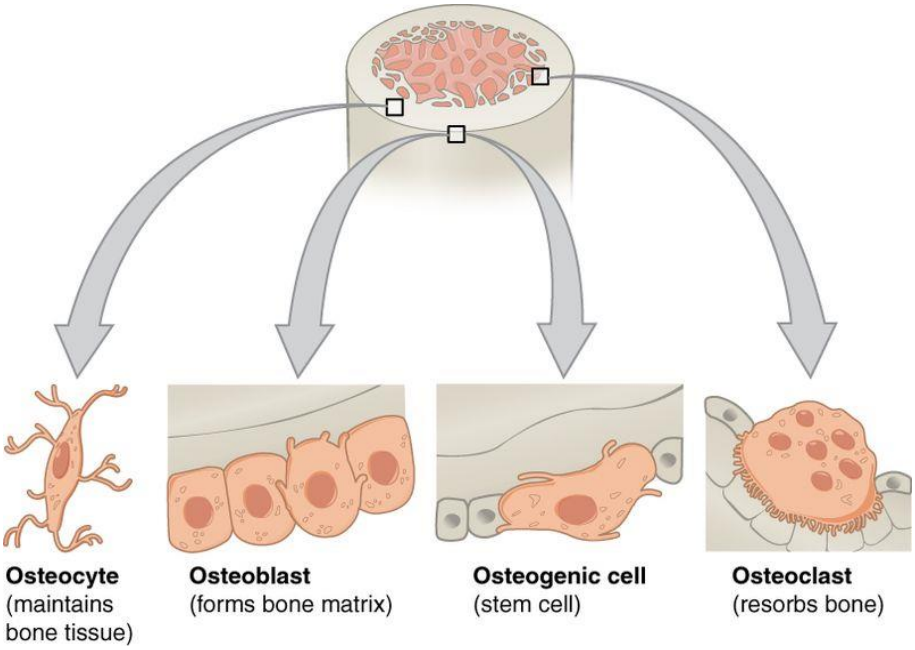

Fig. 1.2: Types and morphology of bone cells: osteocytes, osteoblasts, osteogenic cells and osteoclasts. OpenStax College - Anatomy & Physiology http://cnx.org/content/col11496/1.6/.

The activity of osteoblasts and osteoclasts varies through life. Bone production is regulated by insulin like growth factor (IGF) and thyroid hormones, which promote cell division and stimulate the activity of the osteoblasts. This results in a predominance of bone formation over bone resorption in childhood. Androgens and estrogens increase the activity of osteoblasts in puberty and slow bone

resorption during adulthood. In the later years of life, as the production of androgens and estrogens decays, bone resorption prevails. This bone resorption, and sequent decline of bone density, is more notable in women, since the decrease in estrogens is more pronounced *(Marsell and Einhorn 2011, Tortora and Derrickson 2012, Florencio-Silva et al. 2015).* In addition to hormones, mechanical stimulus also has a big impact on bone formation and maintenance. The added pressure when walking, jumping or weight-lifting leads to an increment in bone production, enhancing bone strength. Insufficient mechanical stimulus, due to either a lack of activity (sedentary lifestyle) or a low gravity environment (astronauts), causes a loss of bone mass up to 1 % a week *(Tortora and Derrickson 2012, Alghadir et al. 2015).* Apart from declining bone density, modifications in bone ductility also increase its brittleness. These changes are not only due to the lower production of proteins in the later stages of life, but also because of modifications in the structure of the collagen matrix regarding the kind of cross-linking of the fibers: enzymatic cross-links, produced by lysyl hydroxylase and lysyloxidase, and non-enzymatic cross-links, formed for example by glycation- or oxidation-induced non-enzymatic processes. This second mode of cross-linking increases with age, while enzymatic cross-linking decays, and has been found to be linked to lower toughness and resistance to crack propagation of bone tissue *(Boskey and Coleman 2010).*

The healing of bone fractures can be naturally achieved when the size of the defect does not exceed the ability of self-repair. In these cases, the fracture can be resolved through either direct or indirect bone healing. Direct bone healing happens when the gap between the ends of the fracture is lower than 1 mm and requires anatomical stabilization so that lamellae, Harvesian canals and blood vessels can be repaired without the formation of callus. Indirect bone healing is the most common bone healing process and is favored by micro-motion and weight-loading, so it does not need a rigid fixation. Indirect bone healing takes place following five steps: I) haematoma and inflammation, II) soft callus formation, III) fibrous tissue formation, IV) hard callus formation and V) callus resorption and

remodeling (Fig. 1.3) *(Marsell and Einhorn 2011, Einhorn and Gerstenfeld 2015)*. Haematoma is formed immediately with peripheral and intramedullary blood cells and is coagulated as a response to the inflammatory process, creating a support for callus formation. During the initial inflammation, which has its peak at 24 hours after the damage, the release of pro-inflammatory factors (tumor necrosis factor-α (TNF-α), interleukin-1 (IL-1), IL-6, IL-11 and IL-18) attracts inflammatory cells and promotes angiogenesis. Also, TNF-α is capable of inducing osteogenic differentiation of mesenchymal stem cells (MSCs). Nevertheless, despite the role of inflammation during bone regeneration, a sustained or chronic process has a negative impact since it is associated with a decreased angiogenesis and delayed osteoclast recruitment, apart from the direct tissue damage derived from inflammation *(Abou-Khalil et al. 2014, Loi et al. 2016)*.

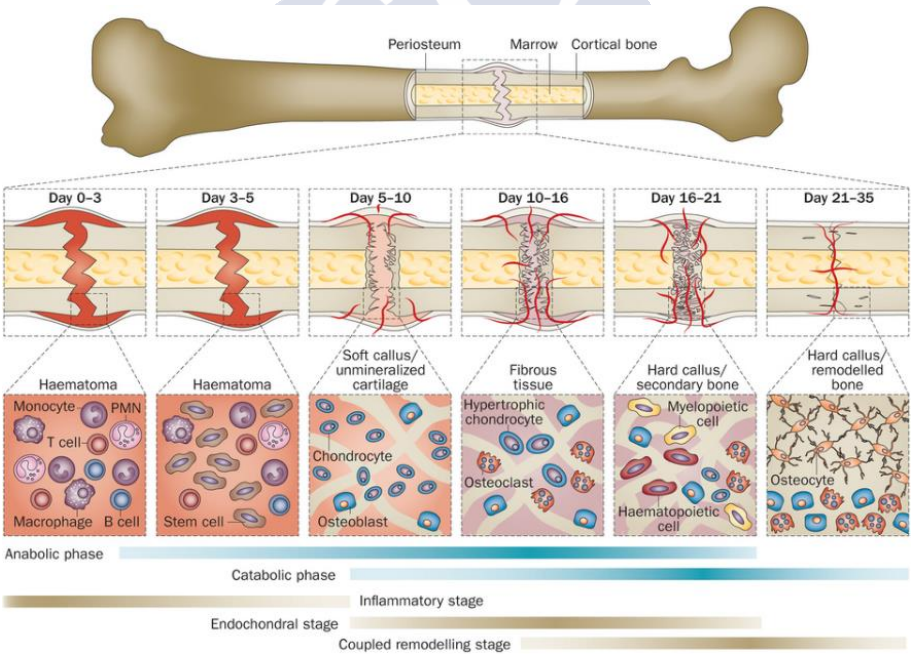

Fig. 1.3: Steps of indirect fracture healing. Reproduced from Einhorn and Gesterfield (2015) with permission of Springer Nature.

The reconstruction of bone tissue starts with the growth of a cartilaginous callus that helps stabilize the structure and its following ossification, starting at the ends of the fracture, until a hard callus is formed. As the mineralized cartilage is replaced with woven bone, the callus becomes more rigid and capable of bearing weight. However, this structure does not completely fulfill the original properties of the tissue. Remodelling starts 3-4 weeks after the injury, and it consists of the resorption of the hard callus and the deposition of lamellar bone carried by osteoclasts and osteoblast, respectively. This process usually takes years to complete until mature bone tissue is obtained *(Marsell and Einhorn 2011)*.

Critical size is the limit upon which a bone injury cannot spontaneously heal during a lifetime. Thus, this kind of damages requires the implantation of grafts that bind the ends of the fracture and enable bone healing to take place. The size for a bone defect to be considered critical sized in humans is generally considered to be above 1-3 cm and comprising at least 50 % loss of bone circumference. However, this value can differ since successful fracture healing not only depends on the amount of tissue lost, but also on bone regeneration capacity, which at the same time varies with the condition of the patient and the location of the defect, since regions such as the tibial diaphysis present low blood supply and soft tissue covering *(Schemitsch 2017)*. The variability in the prognosis regarding full recovery of bone tissue implies that there is a need for grafts with different properties that suit the prospected healing timeline.

1.2. STRATEGIES FOR BONE REGENERATION

Bone is the second most transplanted tissue, only surpassed by blood transfusions, with an incidence of over 2 million of procedures annually worldwide *(Campana et al. 2014)*. Life expectancy in Europe has greatly increased from 40 to 80 years through the last century due to the advances in medicine, hygiene and nutrition, along with a decrease in natality. In Spain the population above 65 years represented an 18.8 % of total in 2017, and it is prospected to increase up to a 34.6 % by 2066 *(Abellán García et al. 2018)*. Given that age is one of the main risks for fractures and post-surgical complications,

researches aimed at preventing and treating bone fractures are of paramount importance in order to favor healthy and active ageing.

1.2.1. Biological grafts: autograft, allograft, xenograft and decellularized matrix

The history of prosthesis goes back thousands of years ago, with the use of materials like shells, metals or wood to replace lost or damaged tissues; 2500 years BC the Egyptians implemented the use of gold wires to stabilize teeth and around 500 BC the Etruscans combined gold bands and bovine bones to fix oral problems.

Bone grafts aim at repairing bone defects by both providing a structure for tissue to grow and stimulating cell growth and differentiation. Biological grafts are the current gold-standard in the clinical practice and can be classified according to their origin as: *autografts*, pieces of bone harvested from a healthy bone of the patient; *allografts*, from donors different from the patient; and *xenografts*, from animals. The use of bone grafts to repair bone tissue was firstly reported in 1668, when the Dutch surgeon Job van Meek'ren filled a defect in the cranium of a soldier using a canine xenograft *(Klosterhoff et al. 2017)*. This intervention was considered blasphemous and the soldier was excommunicated; but when he tried to get the graft removed it was already incorporated into his cranium. It was not until 1820 that the first autologous bone grafting was performed by Philips von Walter to repair a cranium after trepanation *(Von Walter 1821, Pryor et al. 2009)*.

A survey of patients that suffered fracture nonunions and were treated with either autografts or allografts revealed the use of autografts led to statistically significant shorter healing procedures (172–225 days) compared to allografts (290–543 days). The patients whose fractures were repaired with autografts also had the lowest rate of surgical revisions (17 %) and incidence of postoperative infections (12.4 %), compared to those treated with allografts (47 % and 26.3 %, respectively) *(Flierl et al. 2013)*. These factors have an economic impact derived from the costs of longer treatments and rehabilitation programs, but also on the quality of life of patients.

Even though autologous bone grafts are the preferred clinical option due to their superior performance, their use implies longer surgical procedures, damage to healthy bone structures and post-surgical pain, so their application is limited (Table 1.1). Allografts and xenografts are restricted by their availability in tissue banks not able to give response to the growing demand and by possible immunological responses from the host. Decellularization appears as an alternative strategy to obtain scaffolds from allogenic or xenogenic tissues without generating this response by removing cells through a combination of mechanical, chemical and enzymatic techniques. This approach aims at obtaining the protein structure of the tissue, but a complete removal of the cells of a tissue or organ is difficult to attain and the processing technique usually alters the architecture of the extracellular matrix, leading to a high variability in studies regarding their application *(Gilbert et al. 2006, Crapo et al. 2011).*

Table 1.1: Advantages and disadvantages of biological bone grafts.

Bone graft	Advantages	Disadvantages
Autograft	Osteoinduction Osteoconduction Compatibility	Availability Second surgical site Post-surgical complications
Allo/xenograft	Availability	Immunological reactions Disease transmission Lower osteoinduction and osteoconduction
Decellularized matrix	Availability Compatibility	Complex preparation High variability

1.2.2. Synthetic grafts

The design of synthetic bone grafts aims to overcome the problems of availability and immunogenic reactions of biological grafts (Table 1.1). These artificial scaffolds must fulfill some basic requirements to be suitable for bone tissue engineering. First and foremost, they shall be biocompatible, meaning neither the materials nor their degradation products can be toxic to the cells, and also biodegradable, with a degradation rate that matches the growth of the new tissue. They need a high porosity, from 65 to 80 %, and a proper pore size distribution, with a microporosity of about 10 μm, that improves cell attachment, and a macroporosity ideally reaching up to

350 μm *(Lee et al. 2010)* to allow cell proliferation. Since mechanical stimulus is an important factor for bone formation and mechanical stresses are inherent to the physiological function of bones, bone grafts should have mechanical properties similar to those of bone tissue. Lastly, the synthetic matrix should not merely be an inert structure, but also be endowed with bioactive properties such as promoting cell growth (*osteoconductivity*) and differentiation (*osteoinductivity*). This can be attained combining materials with different properties or by loading bioactive materials into the matrix that are locally delivered after implantation.

1.3. MATERIALS FOR BONE GRAFTS

A wide range of materials has been tested for the fabrication of synthetic bone grafts, aiming to replicate the properties of bone tissue regarding porosity, strength or even composition.

1.3.1. Ceramics

The development of bone grafts using calcium phosphate ceramics, such as HA or tricalcium phosphate (TCP), in their composition is a common approach since bone matrix is mainly composed by HA *(Ghassemi et al. 2018)*. HA has a high biocompatibility and poor resorbablility, but this feature can be tuned with the incorporation of salts of zinc and manganese. TCP is also biocompatible, with a faster biodegradation than HA by dissolution and osteoclastic resorption *(Chai et al. 2011)*. Apart from osteoconduction and osteoinduction, ceramic scaffolds show high compression resistance (up to 160 MPa). Nevertheless, the stiffness of bioceramics alone leads to poor fracture resistance, so composites combining ceramics with ductile components like collagen, the main component of bone extracellular matrix, have been designed to overcome this drawback *(Fernandez de Grado et al. 2018)*.

1.3.2. Natural polymers

Natural polymers have the intrinsic capacity of promoting cell attachment and differentiation, as well as degrading into non-toxic products *in vivo*; however, the resulting scaffolds often lack in

mechanical properties, so they are mainly used in combination with ceramics *(Lee et al. 2010).* Apart from being matrix constituents, natural polymers can also be engineered in the form of microparticles and added to the scaffolds to function as drug delivery systems, control drug release or enhance porosity and cell attachment *(Silva et al. 2007, Melke et al. 2016).*

Starch (St) is a versatile and inexpensive polysaccharide composed by amylose and amylopectin (Fig. 1.4) that can be obtained from different sources –cereals (corn, rice, amaranth, quinoa), legumes (peas, beans) and root vegetables (potatoes, cassava)– with a variety of compositions regarding the amylase-amylopectin ratio and the trace amount of proteins, lipids and phosphorous *(Roslan et al. 2016).* St is widely used in tissue engineering, since it is biocompatible and naturally degraded by enzyme α-amylase present in blood plasma, often in combination with other materials to obtain more suitable mechanical properties *(Koski et al. 2018).*

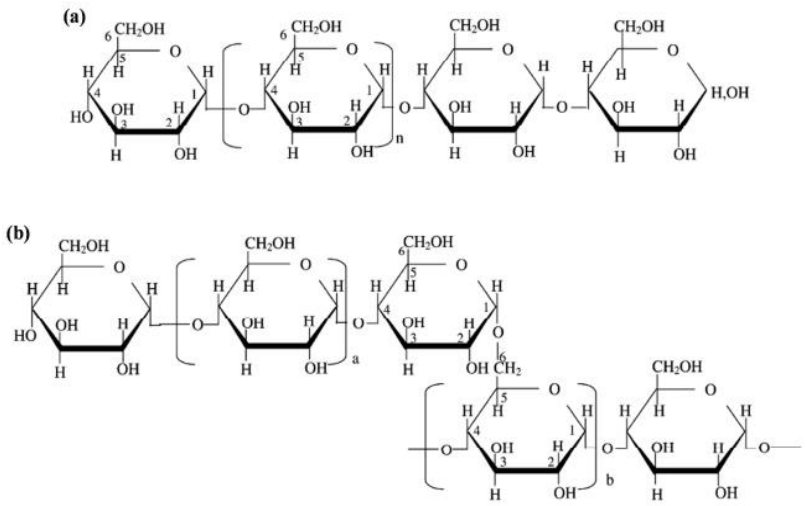

Fig.1.4: Structures of (a) amylose and (b) amylopectin. Reproduced from Amagliani et al. (2016) with permission of Elsevier.

Silk fibroin (SF) is a protein formed by a sequence of glycine, serine and alanine (Fig. 1.5) obtained from the silk fibers of spiders and silkworm cocoons. SF is well known for its biocompatibility and

mechanical strength, widely used as suture material. When in β-sheet conformation, silk fibroin has slower *in vivo* degradation times compared to other biopolymers such as collagen, thus being suitable for long-term regeneration processes, as in bone tissue *(Melke et al. 2016)*.

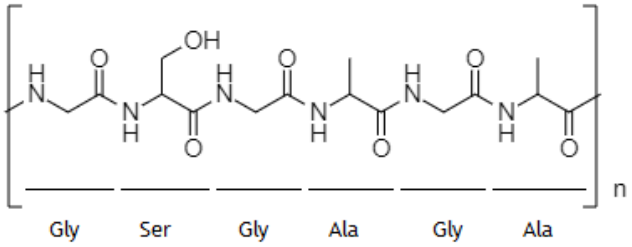

Fig. 1.5: Chemical structure of silk fibroin.

1.3.3. Synthetic polymers

Conversely to natural polymers, synthetic polymers offer higher mechanical strength and reproducibility, and do not present antigenicity like some natural materials, but generally provide lower cell attachment rates *(Lee et al. 2010)* and osteoconductivity *(Gentile et al. 2014)*. These disadvantages can be solved either with the incorporation of other materials or by tuning the structure of the matrix. This group includes polyesters, which have interesting properties regarding mechanical strength, are well tolerated and undergo *in vivo* hydrolytic degradation, a process that depends on the length of the chains, branching and crystallinity.

Poly(lactic-co-glycolic acid) (PLGA) is an EMA- and FDA-approved polyester obtained by copolymerization of poly(lactic acid) (PLA) and poly(glycolic acid) (PGA) found in commercialized resorbable sutures, like Vicryl©, and drug delivery systems, such as Nutropin Depot©. PLGA has attracted special attention due to the wide range of degradation rates available by varying the ratio between its monomers. PLGA is usually combined with other materials for bone regeneration purposes to make up for its low osteoconductivity and load-bearing strength *(Gentile et al. 2014)*.

Poly(ε-caprolactone) (PCL) is a polyester obtained by opening and polymerization of ε-caprolactone rings. Various medical devices containing this polymer, such as Monocryl© resorbable sutures, have already been approved for their use in humans. Regarding tissue engineering, the lower frequency of ester-bonds per monomer compared to polylactides endows PCL with higher stability and longer degradation times (order of several months), which makes it suitable as a replacement for hard tissues *(Malikmammadov et al. 2018)*.

1.3.4. Bioactive compounds

Bioactive molecules can be loaded into the matrix to promote bone regeneration. Namely, growth factors, anti-inflammatory drugs or antimicrobial agents can enhance cell growth and differentiation or mitigate post-surgical complications. The incorporation of growth factors has been proven effective when it comes to promote tissue formation. Bone morphogenetic protein-2 (BMP-2) is a potent osteoinductive factor approved by FDA, but its use entails severe side effects such as inflammation, osteoclast activation that leads to bone resorption and ectopic bone formation *(James et al. 2016)*. Besides, stability is often an additional concern when incorporating bioactive proteins into a formulation, since they can be sensitive to minor changes in their environment *(El Bialy et al. 2017)*.

The use of synthetic drugs appears as a promising alternative due to their higher stability and the well-studied side effects. Among them, anti-inflammatory drugs are particularly interesting when implanting synthetic grafts because, despite being part of the healing process, a prolonged inflammation due to foreign body response might delay, or even impede, proper bone regeneration. Besides, local drug delivery requires lower doses than systemic administration, which helps diminish secondary effects *(Vacanti et al. 2012)*.

Ketoprofen (Fig. 1.6) is a non-steroidal anti-inflammatory drug (NSAID) that can be orally administered after surgery to reduce pain and inflammation without inhibiting bone regeneration *(Nyangoga et al. 2010)*.

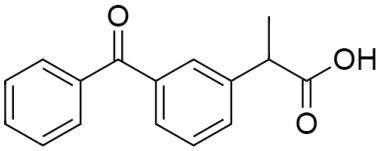

Fig. 1.6: Chemical structure of ketoprofen.

Dexamethasone (Fig. 1.7) is a glucocorticoid that, apart from its anti-inflammatory properties, can induce the differentiation of MSCs into osteoblasts *(Yoon et al. 2003)*.

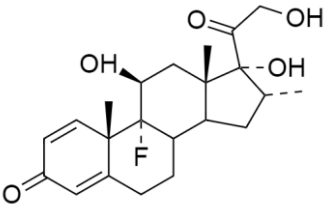

Fig. 1.7: Chemical structure of dexamethasone.

1.4. TECHNIQUES FOR THE PREPARATION OF POLYMERIC GRAFTS

The methods developed for the processing of polymeric scaffolds comprise two main groups: 1) methods using solvents to solubilize the polymer and 2) methods processing the polymer under a viscous behavior (usually working with temperatures above glass transition or melting point).

The suitability of a processing technique is evaluated regarding their reproducibility, easy scale-up, cost and the number of steps required, all of which will affect the quality of the resulting material, health and environmental safety and the economy of the process.

In the case of medicated scaffolds, the loading yield and the predictability of the release profiles after implantation are also critical parameters, since they will not only determine the cost of production, but also the *in vivo* performance. For example, techniques including leaching or solvent extraction steps lead to a dramatic removal of the bioactive agent along with the presence of residual porogens or toxic organic solvents. Besides, the use of solvents generally hampers the

control of the spatial distribution of the bioactive agent in the porous structure of the scaffolds upon processing and under storage.

Solvent-free methods arise as an auspicious strategy to overcome these problems and obtain scaffolds with suitable and reproducible properties.

1.4.1. Solvent-based processing techniques

1.4.1.1. Solvent casting-particle leaching

This technique is employed for the fabrication of polymeric scaffolds, and consists of the dissolution of the polymer in an organic solvent and the dispersion of a porogen, usually a salt, into the solution. The solvent is evaporated and the porogen is removed with water to obtain a porous matrix (Fig. 1.8a) *(Turnbull et al. 2018)*. Despite allowing to control pore size by selecting the particle size of the porogen, the use of organic solvents implies further purification steps to avoid cytotoxicity. Moreover, leaching limits the incorporation of bioactive compounds, which might be partly washed out together with the porogen *(Walker and Santoro 2017)*.

1.4.1.2. Freeze drying

This technique consists of freezing the formulation, usually a polymer dispersed in water, to temperatures from −70°C to −80°C and then submit it to vacuum in order to remove the water by sublimation (Fig. 1.8b). The low processing temperatures of the freeze-drying technique is compatible with the processing of thermolabile materials, and it also avoids the use of organic solvents *(Lu et al. 2013)*. Freeze-drying is suitable for the processing of scaffolds with controlled pore size (50–240 μm) and porosity (30–70 %) by regulating the freeze-drying pressure profile. However, the preparation of hierarchical structures still remains a challenge *(Autissier et al. 2010)*.

1.4.1.3. Phase separation

Even though phase separation can be induced either thermally or with the addition of a nonsolvent, the latter often leads to heterogeneous structures not suitable for tissue engineering purposes.

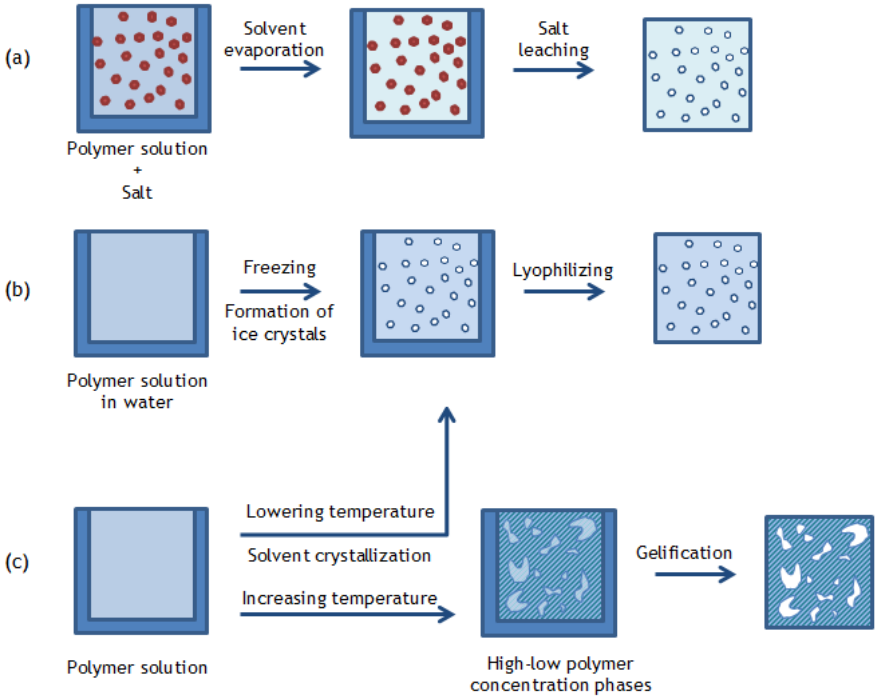

Fig. 1.8: Diagram of (a) solvent casting-particle leaching, (b) freeze-drying and (c) thermally induced phase separation processes.

Thermal-induced phase separation (Fig. 1.8c) consists of submitting a polymer solution to temperature conditions where an homogeneous solution becomes thermodynamically unstable, resulting in separation of different phases with high and low polymer concentrations. The polymer-rich phase solidifies forming the matrix, while the phase with the lower concentration is removed to create pores *(Lu et al. 2013)*.

1.4.1.4. Electrospinning

This technique consists of applying a high voltage to a polymeric solution or melt that is pumped through a capillary tube or nozzle to create nano or micrometric fibers (Fig. 1.9). The electrical current generates charge repulsion forces in the polymer solution able to overcome the surface tension forces and the solution flows in the direction of the electrical field. Polymer concentration, distance

between the tip of the capillary and the collector and the voltage of the electric field are among the processing parameters to tune the size of the fibers *(Walker and Santoro 2017)*. Electrospining allows the incorporation of bioactive molecules into the blends of polymers, and is suitable for obtaining fibrous wound dressings and scaffolds for ligaments and tendons, but the use of solvents or high temperatures to liquefy the polymer can be a limit to its use *(Lu et al. 2013)*.

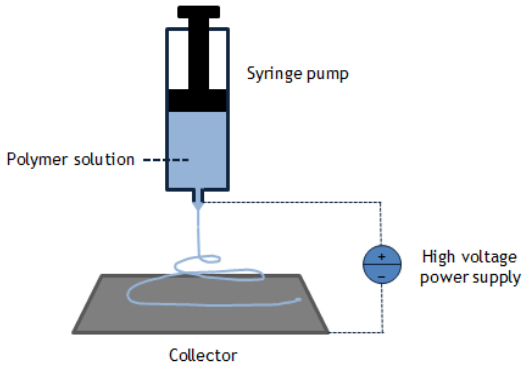

Fig. 1.9: Diagram of an electrospinning set-up.

1.4.2. Solvent-free preparation techniques

1.4.2.1. Melt molding

Melt molding is used for polymers, being a suitable processing alternative for those insoluble in organic solvents, such as poly(glycolic acid), and consists of submitting them to high temperatures and then pouring the melted material in a mold to obtain the desired morphology. This technique allows the incorporation of additives such as ceramics or bioactive compounds, which are homogeneously dispersed in the polymeric matrix, and has the advantage of enabling a complete control on the morphology of the scaffold by changing the shape of the mold. Melt molding is sometimes coupled with particle leaching by adding a porogen to the melt that will be removed once the polymer solidifies (Fig. 1.10). Nevertheless, the high temperatures can degrade the compounds, and mold residues may have to be removed from the graft before further use *(Allaf 2018)*. In the case of melt molding combined with particle leaching methods, there is also the risk of partly removing bioactive

compounds loaded into the matrix, as previously remarked *(Walker and Santoro 2017)*.

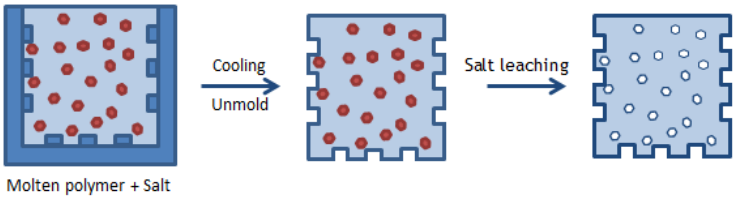

Fig. 1.10: Diagram of melt molding-salt leaching.

1.4.2.2. Fused deposition modeling (FDM)

FDM is a 3D printing method applied to thermoresponsive polymers. This technique heats the polymer above the glass transition temperature and extrudes it through a nozzle to build computer-designed patterns layer by layer (Fig. 1.11). FDM avoids the use of organic solvents that are employed in other 3D printing techniques to solubilize polymers, and allows the combination of different polymers or polymer-ceramic blends. Layer thickness, speed of deposition, xyz resolution of movement, or the nozzle design are parameters that can be used to tune surface roughness and resolution. Moreover, FDM usually requires building supports that have to be removed to obtain the desired architecture *(Do et al. 2015, Mohamed et al. 2015)*.

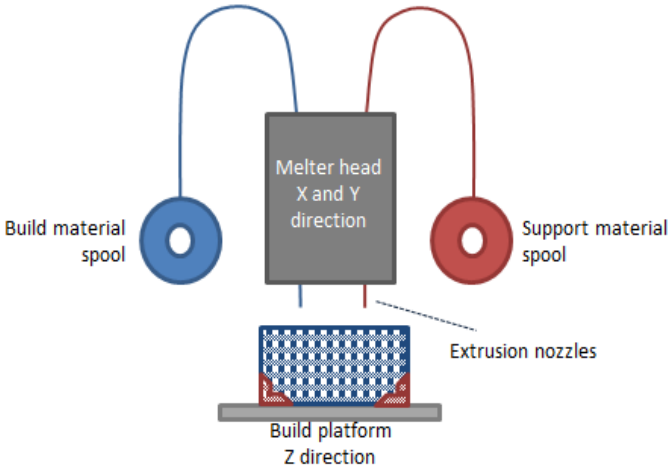

Fig. 1.11: Diagram of fused deposition modeling.

1.4.2.3. Gas foaming

The principle of this technique is the generation of pores in a polymeric matrix through a nucleation-growth mechanism of gas bubbles that results in a macroporous material. The solvent-free version of this technique consists of three steps: 1) Dispersion of a porogen in a polymeric matrix. The porogen can be either a chemical blowing agent, that will decompose into an inert gas by a chemical reaction (sodium bicarbonate) or by thermal degradation (ammonium carbonate), or a physical blowing agent, such as an inert gas (nitrogen, argon or carbon dioxide) insufflated, or a volatile liquid (pentane) absorbed in the polymer. 2) Pore formation through the porogen removal. Gas bubbles are generated in this step following a nucleation-growth mechanism that results in pore formation after gas release. 3) Rapid solidification of the polymeric matrix. The temperature is rapidly lowered to allow the vitrification of the material *(Annabi et al. 2010, Dehghani and Annabi 2011).*

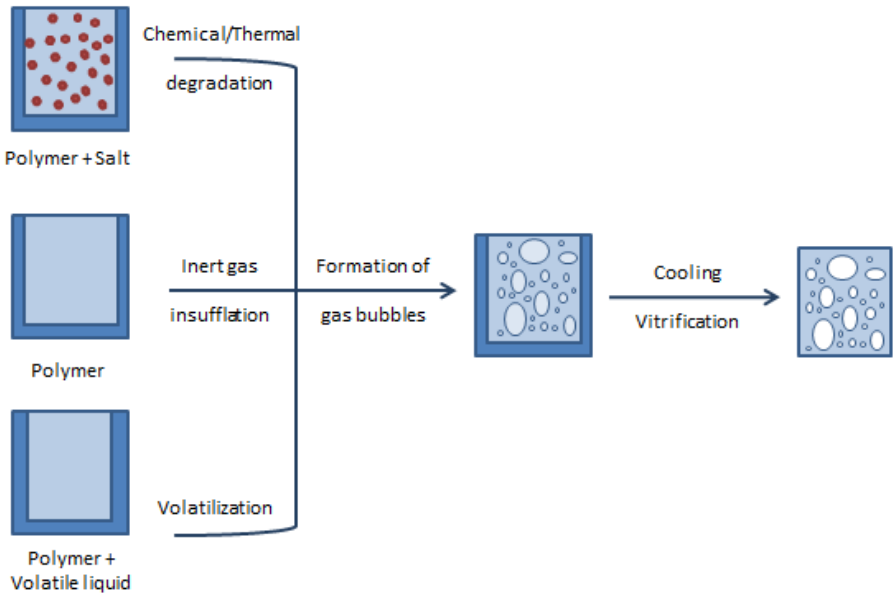

Fig. 1.12: Diagram of gas foaming.

The structures obtained through this technique are expanded polymeric foams with closed-cell or open-cell frames commonly used in the building sector. However, gas foaming can be adapted for regenerative medicine purposes by choosing biocompatible materials with non-toxic degradation products to create open-cell structures with suitable pore sizes and interconnectivity for cell penetration and growth *(Dehghani and Annabi 2011)*. The limitations of this technology lay in the control of the pore size, pore interconnectivity and spatial homogeneity of the material, depending on the rheological properties of the liquefied polymer during foaming. Moreover, long processing times for complete porogen removal may occur in the case of using chemical-blowing agents.

1.4.2.4. Compressed CO_2 and supercritical CO_2-assisted foaming and sintering

A fluid is at supercritical conditions when submitted to pressures and temperatures above its critical point (Fig. 1.13). Supercritical carbon dioxide ($scCO_2$) is the most widely used supercritical fluid due to the relatively mild conditions of its critical point of CO_2 (31.1 ºC and 73.8 bar), low toxicity and price. Physicochemical properties (density, viscosity and diffusivity) of CO_2 at near-critical or supercritical conditions are intermediate between those of gas and liquid state and can be tuned by changing the conditions of pressure and temperature.

The use of near critical or supercritical CO_2 ($scCO_2$) for the fabrication of scaffolds arises as an alternative green-processing method to operating with organic solvents or under high temperatures. The principle behind this processing strategy is that CO_2 can dissolve in high amounts into certain polymers (PCL, PLGA) under near-critical and supercritical conditions, resulting in a plasticizing effect able to reduce the melting and/or glass transition points of the polymers (Fig. 1.14).

Sintering is a solvent-free method that classically employs high temperatures to melt the surface of particles to merge them by formation of necks between particles to obtain a porous matrix (Fig. 1.15a). This technique can be modified by exploiting the plasticizing

effect of compressed CO_2 to achieve the same results under mild conditions that do not cause degradation of materials *(García-González et al. 2015)*. On the other hand, supercritical foaming method consists of putting a foamable polymeric material in contact

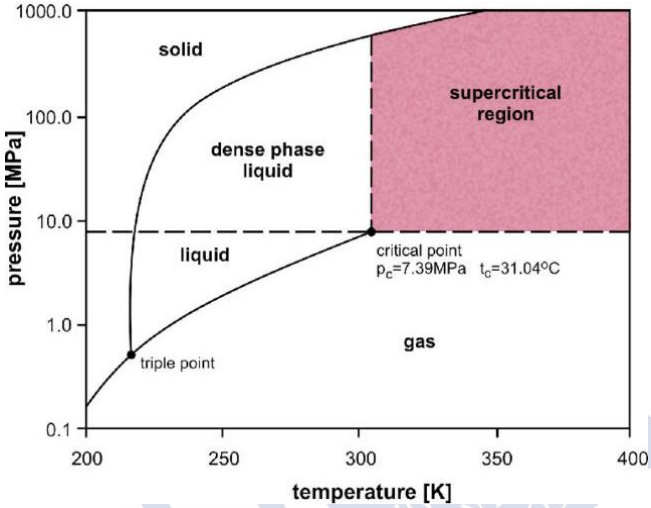

Fig. 1.13: Phase diagram for CO_2. Adapted from Witkowski et al. (2013) with permission of Elsevier.

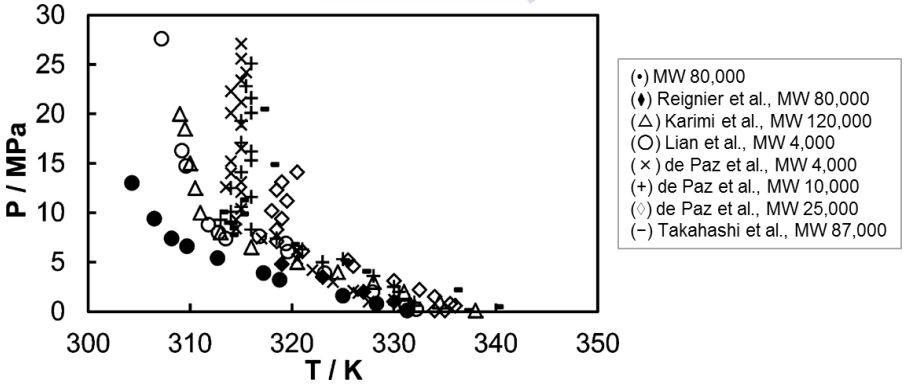

Fig. 1.14: Solid–liquid transition for poly(ε-caprolactone)–CO_2 system. Comparison between experimental and literature data. Reproduced from Markocic et al. (2013) with permission of ACS Publications.

with supercritical CO_2 so that the CO_2 dissolves into it —*soaking stage*—, obtaining a polymer in a molten or in a rubbery state, and then decreasing the pressure to induce a phase separation —*depressurization stage*— that will originate bubbles within the matrix (1.15b). The pore sizes and porosities of the resulting scaffolds are dependent of the processing conditions (mainly pressure, temperature and depressurization rate). Namely, the depressurization rate is related to the formation of nucleation sites. A fast pressure drop will cause a higher supersaturation and lead to higher nucleation rates leading to small pores and less homogenous structures. Conversely, reducing the venting rate allows the growth of the pores and even their coalescence, so the final structure has larger pores and higher pore interconnectivity.

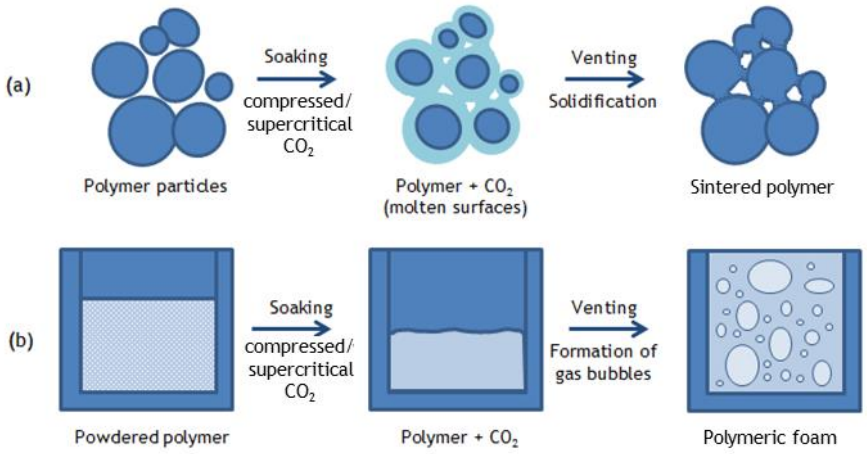

Fig. 1.15: Diagram of near-critical and supercritical CO_2 (a) sintering and (b) foaming.

In the supercritical foaming method, the avoidance of organic solvents or high temperatures to obtain a polymer with a porous structure suppresses the need of posterior purification processes and thermal degradation, leading to drug-incorporation yields of *ca.* 100 %. Besides, the morphological properties of the resulting scaffolds regarding porosity and pore size can be easily tuned controlling the conditions of soaking and depressurization conditions and durations.

The most suitable materials for supercritical foaming are synthetic polymers, such as PCL and PLGA, which are highly biocompatible and have good mechanical properties for bone regeneration. However, the pores obtained usually show poor interconnection rates and smooth surfaces that hinder cell penetration and attachment *(Ge et al. 2013)*. The use of organic solvents (acetone), biofunctional plasticizers (eugenol) or mesoporous silica were proposed as admixtures during the supercritical foaming of polyesters to improve these properties *(Kiran 2010, de Matos et al. 2013, Salerno et al. 2017)*. However, those options pose problems of cytotoxicity, limited range of processability and reduction in mechanical properties. Alternative processing options are thus prospected to improve the pore interconnectivity and surface roughness of scaffolds obtained by supercritical foaming.

Aerogels are defined as:

> "Solid, lightweight and coherent open porous networks of loosely packed, bonded particles or nanoscale fibers, obtained from a gel following the removal of the pore fluid without significant structural modification" *(García-González et al. 2019)*.

In this PhD Thesis, the use of aerogel particles from natural polymers was evaluated as alternative ingredients to be incorporated in the scaffold formulations to be obtained by supercritical foaming.

1.5. REFERENCES

A. Abellán García, A. Ayala García, J. Pérez Díaz and R. Pujol Rodríguez (2018). *Un perfil de las personas mayores en España, 2018. Indicadores estadísticos básicos* **17**. Madrid, Spain. CSIC - Instituto de Economía, Geografía y Demografía (IEGD).

R. Abou-Khalil, F. Yang, M. Mortreux, S. Lieu, Y.-Y. Yu, M. Wurmser, C. Pereira, F. Relaix, T. Miclau, R. S. Marcucio and C. Colnot (2014). "Delayed bone regeneration is linked to chronic inflammation in murine muscular dystrophy." *Journal of Bone and Mineral Research* **29**(2): 304-315.

A. H. Alghadir, S. A. Gabr and E. Al-Eisa (2015). "Physical activity and lifestyle effects on bone mineral density among young adults: sociodemographic and biochemical analysis." *Journal of Physical Therapy Science* **27**(7): 2261-2270.

R. M. Allaf (2018). 4 - Melt-molding technologies for 3D scaffold engineering. *Functional 3D Tissue Engineering Scaffolds*. Y. Deng and J. Kuiper. Duxford, UK, Woodhead Publishing**:** 75-100.

N. Annabi, J. W. Nichol, X. Zhong, C. Ji, S. Koshy, A. Khademhosseini and F. Dehghani (2010). "Controlling the porosity and microarchitecture of hydrogels for tissue engineering." *Tissue engineering. Part B, Reviews* **16**(4): 371-383.

A. Autissier, C. L. Visage, C. Pouzet, F. Chaubet and D. Letourneur (2010). "Fabrication of porous polysaccharide-based scaffolds using a combined freeze-drying/cross-linking process." *Acta Biomaterialia* **6**(9): 3640-3648.

A. L. Boskey and R. Coleman (2010). "Aging and bone." *Journal of Dental Research* **89**(12): 1333-1348.

V. Campana, G. Milano, E. Pagano, M. Barba, C. Cicione, G. Salonna, W. Lattanzi and G. Logroscino (2014). "Bone substitutes in orthopaedic surgery: from basic science to clinical practice." *Journal of Materials Science. Materials in Medicine* **25**(10): 2445-2461.

P. M. Crapo, T. W. Gilbert and S. F. Badylak (2011). "An overview of tissue and whole organ decellularization processes." *Biomaterials* **32**(12): 3233-3243.

F. Chai, G. Raoul, A. Wiss, J. Ferri and H. F. Hildebrand (2011). "Les biomatériaux de substitution osseuse : classification et intérêt." *Revue de Stomatologie et de Chirurgie Maxillo-faciale* **112**(4): 212-221.

M. B. C. de Matos, A. P. Piedade, C. Alvarez-Lorenzo, A. Concheiro, M. E. M. Braga and H. C. de Sousa (2013). "Dexamethasone-loaded poly(ε-caprolactone)/silica nanoparticles composites prepared by supercritical CO_2 foaming/mixing and deposition." *International Journal of Pharmaceutics* **456**(2): 269-281.

F. Dehghani and N. Annabi (2011). "Engineering porous scaffolds using gas-based techniques." *Current Opinion in Biotechnology* **22**(5): 661-666.

A.-V. Do, B. Khorsand, S. M. Geary and A. K. Salem (2015). "3D Printing of Scaffolds for Tissue Regeneration Applications." *Advanced Healthcare Materials* **4**(12): 1742-1762.

M. Doblaré, J. M. García and M. J. Gómez (2004). "Modelling bone tissue fracture and healing: a review." *Engineering Fracture Mechanics* **71**(13): 1809-1840.

T. A. Einhorn and L. C. Gerstenfeld (2015). "Fracture healing: mechanisms and interventions." *Nature Reviews. Rheumatology* **11**(1): 45-54.

I. El Bialy, W. Jiskoot and M. Reza Nejadnik (2017). "Formulation, Delivery and Stability of Bone Morphogenetic Proteins for Effective Bone Regeneration." *Pharmaceutical Research* **34**(6): 1152-1170.

G. Fernandez de Grado, L. Keller, Y. Idoux-Gillet, Q. Wagner, A.-M. Musset, N. Benkirane-Jessel, F. Bornert and D. Offner (2018). "Bone substitutes: a review of their characteristics, clinical use, and perspectives for large bone defects management." *Journal of Tissue Engineering* **9**: 2041731418776819-2041731418776819.

M. A. Flierl, W. R. Smith, C. Mauffrey, K. Irgit, A. E. Williams, E. Ross, G. Peacher, D. J. Hak and P. F. Stahel (2013). "Outcomes and complication rates of different bone grafting modalities in long bone fracture nonunions: a retrospective cohort study in 182 patients." *Journal of Orthopaedic Surgery and Research* **8**(1): 33.

R. Florencio-Silva, G. R. d. S. Sasso, E. Sasso-Cerri, M. J. Simões and P. S. Cerri (2015). "Biology of Bone Tissue: Structure, Function, and Factors That Influence Bone Cells." *BioMed Research International* **2015**: 17.

C. A. García-González, T. Budtova, L. Durães, C. Erkey, P. Del Gaudio, P. Gurikov, M. Koebel, F. Liebner, M. Neagu and I. Smirnova (2019). "An Opinion Paper on Aerogels for Biomedical and Environmental Applications." *Molecules* **24**(9): 1815.

C. A. García-González, A. Concheiro and C. Alvarez-Lorenzo (2015). "Processing of Materials for Regenerative Medicine Using Supercritical Fluid Technology." *Bioconjugate Chemistry* **26**(7): 1159-1171.

J. Ge, M. Li, Q. Zhang, C. Z Yang, P. Wooley, X. Chen and S.-Y. Yang (2013). "Silica Aerogel Improves the Biocompatibility in a Poly- ε -Caprolactone Composite Used as a Tissue Engineering Scaffold." *International Journal of Polymer Science* **2013**: 7.

P. Gentile, V. Chiono, I. Carmagnola and P. V. Hatton (2014). "An overview of poly(lactic-co-glycolic) acid (PLGA)-based biomaterials for bone tissue engineering." *International Journal of Molecular Sciences* **15**(3): 3640-3659.

T. Ghassemi, A. Shahroodi, M. H. Ebrahimzadeh, A. Mousavian, J. Movaffagh and A. Moradi (2018). "Current Concepts in Scaffolding for Bone Tissue Engineering." *The Archives of Bone and Joint Surgery* **6**(2): 90-99.

T. W. Gilbert, T. L. Sellaro and S. F. Badylak (2006). "Decellularization of tissues and organs." *Biomaterials* **27**(19): 3675-3683.

J. Henkel, M. A. Woodruff, D. R. Epari, R. Steck, V. Glatt, I. C. Dickinson, P. F. M. Choong, M. A. Schuetz and D. W. Hutmacher (2013). "Bone Regeneration Based on Tissue Engineering Conceptions — A 21st Century Perspective." *Bone Research* **1**: 216.

A. W. James, G. LaChaud, J. Shen, G. Asatrian, V. Nguyen, X. Zhang, K. Ting and C. Soo (2016). "A Review of the Clinical Side Effects of Bone Morphogenetic Protein-2." *Tissue engineering. Part B, Reviews* **22**(4): 284-297.

E. Kiran (2010). "Foaming strategies for bioabsorbable polymers in supercritical fluid mixtures. Part II. Foaming of poly(ε-caprolactone-co-lactide) in carbon dioxide and carbon dioxide+acetone fluid mixtures and formation of tubular foams via solution extrusion." *The Journal of Supercritical Fluids* **54**(3): 308-319.

B. S. Klosterhoff, S. Nagaraja, J. J. Dedania, R. E. Guldberg and N. J. Willett (2017). Chapter 5 - Material and Mechanobiological Considerations for Bone Regeneration. *Materials and Devices for Bone Disorders*. S. Bose and A. Bandyopadhyay, Academic Press**:** 197-264.

C. Koski, B. Onuike, A. Bandyopadhyay and S. Bose (2018). "Starch-hydroxyapatite composite bone scaffold fabrication utilizing a slurry extrusion-based solid freeform fabricator." *Additive Manufacturing* **24**: 47-59.

J. W. Lee, G. Ahn, J. Y. Kim and D.-W. Cho (2010). "Evaluating cell proliferation based on internal pore size and 3D scaffold architecture fabricated using solid freeform fabrication technology." *Journal of Materials Science: Materials in Medicine* **21**(12): 3195-3205.

F. Loi, L. A. Córdova, J. Pajarinen, T. H. Lin, Z. Yao and S. B. Goodman (2016). "Inflammation, fracture and bone repair." *Bone* **86**: 119-130.

T. Lu, Y. Li and T. Chen (2013). "Techniques for fabrication and construction of three-dimensional scaffolds for tissue engineering." *International Journal of Nanomedicine* **8**: 337-350.

E. Malikmammadov, T. E. Tanir, A. Kiziltay, V. Hasirci and N. Hasirci (2018). "PCL and PCL-based materials in biomedical applications." *Journal of Biomaterials Science, Polymer Edition* **29**(7-9): 863-893.

R. Marsell and T. A. Einhorn (2011). "The biology of fracture healing." *Injury* **42**(6): 551-555.

J. Melke, S. Midha, S. Ghosh, K. Ito and S. Hofmann (2016). "Silk fibroin as biomaterial for bone tissue engineering." *Acta Biomaterialia* **31**: 1-16.

O. A. Mohamed, S. H. Masood and J. L. Bhowmik (2015). "Optimization of fused deposition modeling process parameters: a review of current research and future prospects." *Advances in Manufacturing* **3**(1): 42-53.

H. Nyangoga, E. Aguado, E. Goyenvalle, M. F. Baslé and D. Chappard (2010). "A non-steroidal anti-inflammatory drug (ketoprofen) does not delay beta-TCP bone graft healing." *Acta biomaterialia* **6**(8): 3310-3317.

G. Osterhoff, E. F. Morgan, S. J. Shefelbine, L. Karim, L. M. McNamara and P. Augat (2016). "Bone mechanical properties and changes with osteoporosis." *Injury* **47**: S11-S20.

L. S. Pryor, E. Gage, C.-J. Langevin, F. Herrera, A. D. Breithaupt, C. R. Gordon, A. M. Afifi, J. E. Zins, H. Meltzer, A. Gosman, S. R. Cohen and R. Holmes (2009). "Review of bone substitutes." *Craniomaxillofacial Trauma & Reconstruction* **2**(3): 151-160.

M. R. Roslan, N. F. M. Nasir, E. M. Cheng and N. A. M. Amin (2016). *Tissue engineering scaffold based on starch: A review*. 2016 International Conference on Electrical, Electronics, and Optimization Techniques (ICEEOT).

A. Salerno, S. Dieguez, L. Diaz-Gomez, J. L. Gómez-Amoza, B. Magarinos, A. Concheiro, C. Domingo, C. Alvarez-Lorenzo and C. A. García-González (2017). "Synthetic scaffolds with full pore interconnectivity for bone regeneration prepared by supercritical foaming using advanced biofunctional plasticizers." *Biofabrication* **9**(3): 035002.

E. H. Schemitsch (2017). "Size Matters: Defining Critical in Bone Defect Size!" *Journal of Orthopaedic Trauma* **31**: S20-S22.

G. A. Silva, O. P. Coutinho, P. Ducheyne, I. M. Shapiro and R. L. Reis (2007). "The effect of starch and starch-bioactive glass composite microparticles on the adhesion and expression of the osteoblastic phenotype of a bone cell line." *Biomaterials* **28**(2): 326-334.

G. J. Tortora and B. Derrickson (2012). *Principles of anatomy and physiology*. Hoboken, NJ, John Wiley & Sons.

G. Turnbull, J. Clarke, F. Picard, P. Riches, L. Jia, F. Han, B. Li and W. Shu (2018). "3D bioactive composite scaffolds for bone tissue engineering." *Bioactive Materials* **3**(3): 278-314.

N. M. Vacanti, H. Cheng, P. S. Hill, J. D. T. Guerreiro, T. T. Dang, M. Ma, S. Watson, N. S. Hwang, R. Langer and D. G. Anderson (2012). "Localized delivery of dexamethasone from electrospun fibers reduces the foreign body response." *Biomacromolecules* **13**(10): 3031-3038.

M. A. Velasco, C. A. Narváez-Tovar and D. A. Garzón-Alvarado (2015). "Design, materials, and mechanobiology of biodegradable scaffolds for bone tissue engineering." *BioMed research international* **2015**: 729076-729076.

P. Von Walter (1821). "Wiedereinheilung der bei der Trapanation ausgebohrten Knochenscheibe." *Journal der Chirurgie und Augenheilkunde* **2**: 571-583.

J. L. Walker and M. Santoro (2017). 9 - Processing and production of bioresorbable polymer scaffolds for tissue engineering. *Bioresorbable Polymers for Biomedical Applications*, Woodhead Publishing**:** 181-203.

J. J. Yoon, J. H. Kim and T. G. Park (2003). "Dexamethasone-releasing biodegradable polymer scaffolds fabricated by a gas-foaming/salt-leaching method." *Biomaterials* **24**(13): 2323-2329.

L.-D. You, S. Weinbaum, S. C. Cowin and M. B. Schaffler (2004). "Ultrastructure of the osteocyte process and its pericellular matrix." *The Anatomical Record Part A: Discoveries in Molecular, Cellular, and Evolutionary Biology* **278A**(2): 505-513.

USC
UNIVERSIDADE
DE SANTIAGO
DE COMPOSTELA

2. OBJECTIVES

As discussed in the Introduction section, proper bone healing is determinant for the patients to maintain their autonomy and quality of life. Bone is the second most transplanted tissue; autologous bone graft is the gold standard due to its inherent osteoinductive and osteoconductive capacity, as much as the lack of immune reactions produced. However, the consequent damage to healthy bone structures of the patient, the low amount that can be obtained and the need for longer or repeated surgeries to obtain and implant the graft are important drawbacks for the use of autologous grafts. Despite their higher availability, allogenic and xenogenic grafts are not deployed of risks, so various approaches have been proposed to meet the ever increasing demand of suitable grafts. The design of synthetic scaffolds is the most promising means to satisfy the requirements of resourceness, compatibility and growth stimulation.

Among the techniques aiming at obtaining synthetic grafts suitable for bone tissue, those that do not use organic solvents should be favored not only to avoid toxicity once the graft is implanted, but also for the sake of environment-friendliness, a factor that is of paramount importance when considering the scale-up to industrial production. In addition, the use of solvents of any nature is less suited when incorporating drugs into the formulation, as they could be partially leached from the matrix. Aside from this, procedures with low operating temperatures are desirable since they allow working with thermolabile materials that could otherwise be degraded. The ideal would be a solvent-free technique, enabling a 100 % drug loading yield, with mild processing conditions and that allows full control on the porosity and pore sizes of the resulting graft.

This PhD Thesis work aims to implement compressed and supercritical CO_2 foaming to obtain drug-loaded biocompatible synthetic scaffolds suitable for bone grafting. The drug-release profiles, internal architecture and mechanical properties of the

scaffolds are studied to assess their suitability for the regeneration of bone tissue, as much as the impact of storage on those features. Accordingly, the Thesis was structured in three sections according to those specific purposes as follows:

I) *Preparation of PCL, PLGA and starch scaffolds loaded with dexamethasone by compressed CO_2 foaming and study of their stability in storage.* The purposes of this section are the fundamental study and optimization of compressed CO_2-assisted foaming technique to prepare polymeric scaffolds loaded with dexamethasone, an steroidal anti-inflammatory drug that also presents osteoinductive activity, evaluating the effect of pre-gelified starch on the drug release profile and assessing the impact of storage on the performance of the scaffolds, since shelf-life of bone grafts determines their resourcefulness. For this, three batches for each of the formulations are prepared. One of the batches is tested right after preparation, regarding their porosity, mechanical properties and drug release profiles and degradation rates in a pH 7.4 phosphate buffered solution (PBS) at 37 ºC. The other two batches were stored at 25 °C and 65 % relative humidity for 1 and 3 months prior to their analysis. The selected storage conditions are the ones that correspond to the climatic conditions for Europe, USA and Japan assigned by the International Council for Harmonisation (ICH). This research was done in collaboration with Prof. Philip Jaeger, from the Hamburg University of Technology, and Dr. Inés Ardao, from BioFarma Research Group at USC.

II) *Design and preparation of starch aerogel microparticles for their incorporation in ketoprofen-loaded PCL scaffolds to function as porogenic agents and drug carriers.* The objective of this section is the preparation of micron-sized starch aerogel particles for their incorporation in PCL scaffolds prepared by supercritical foaming in order to increase their porosity, pore size, pore interconnectivity and surface roughness. These parameters, determinant for a successful cell penetration, attachment and growth, are usually limited in polymeric foamed scaffolds, so the addition of aerogel particles that act as nucleation sites and lower the smoothness of pore walls is an alternative to circumvent those drawbacks without the use of organic

solvents or porogens. Aerogel particles are prepared applying an emulsion-gelation method followed by supercritical drying, a technique that allows the removal of solvents while preventing the microstructure from collapsing. The scaffolds are also loaded with ketoprofen, a NSAID, to mitigate post-surgical pain and prevent an exaggerated inflammatory process. Scaffolds with various compositions are obtained and analyzed regarding the drug release profiles from the matrices, their structure and their mechanical properties. Different formulations are compared to assess the effect of incorporating aerogels and ketoprofen on the features of the scaffolds. This research was done in collaboration with Prof. Hermínio C. de Sousa, Dr. Mara E.M. Braga and Dr. Ana M.A. Dias, from the University of Coimbra.

III) *Design and preparation of silk fibroin aerogel microparticles for their incorporation in PCL scaffolds to function as porogenic agents and* in vitro *and* in vivo *comparison between dexamethasone and dexamethasone 21-phosphate.* One of the main goals in this section is the optimization of the preparation of submicron-sized silk fibroin aerogel particles for their incorporation in the scaffolds as porogens and cell attachment-promoters. Aerogels are prepared through an emulsion-gelation process, in which different emulsifier contents and gelation methods are tested to obtain the best efficiency-time ratio and resource consumption balance, followed by supercritical drying. The second aim is the comparison of dexamethasone in the base state and as salt regarding their effect on the morphology of the scaffolds, their release profiles from the matrix and their suitability for bone regeneration. Both *in vitro* tests and *in vivo* assays in Sprague-Dawley rats are carried in order to define the importance of the drug form in the performance of the graft. This research was developed in collaboration with Prof. Carmen Évora, Prof. Araceli Delgado and Dr. Ricardo Reyes, from the University of La Laguna, and Dr. Antonio A. Lozano Pérez, Dr. Salvador D. Aznar Cervantes and Prof. Jose Luis Cenis from the Instituto Murciano de Investigación y Desarrollo Agrario y Alimentario.

USC
UNIVERSIDADE
DE SANTIAGO
DE COMPOSTELA

3. PREPARATION AND STABILITY OF DEXAMETHASONE-LOADED SCAFFOLDS FOR BONE REGENERATION PROCESSED BY COMPRESSED CO_2 FOAMING[§]

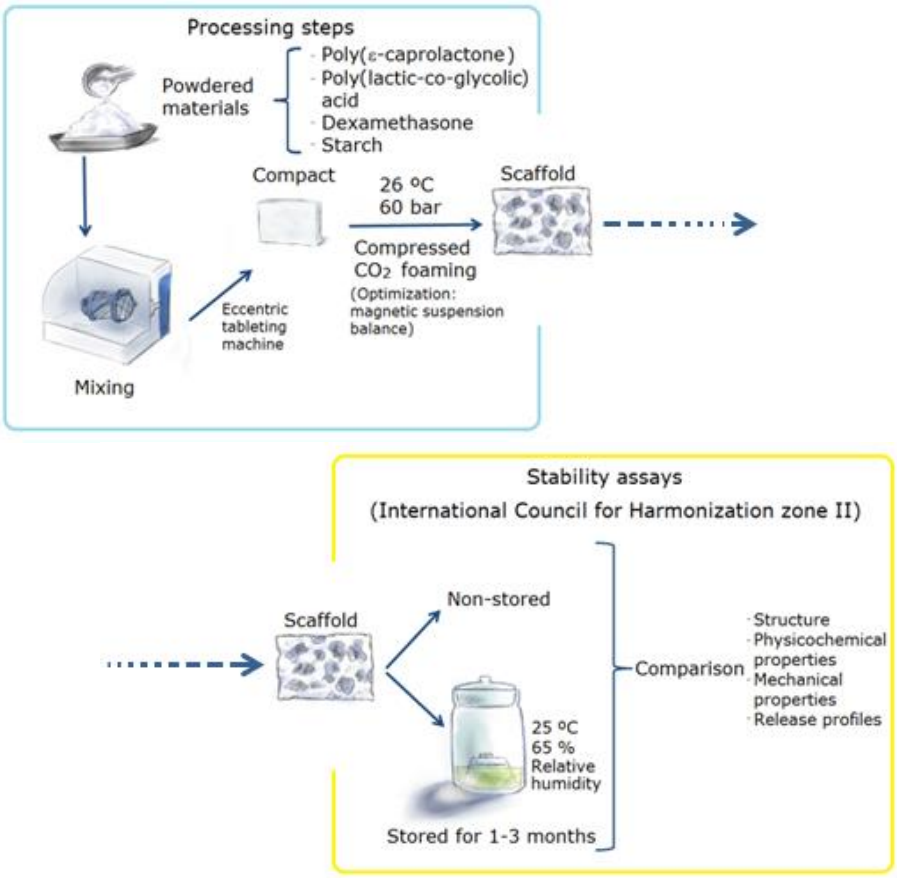

[§]The work described in this chapter has been published in *Goimil et al. J. CO2 Utiliz., 24 (2018) 89-98* and carried out in collaboration with Prof. Philipp Jaeger, from the Hamburg University of Technology, and Dr. Inés Ardao, from BioFarma Research Group at USC.

3.1. INTRODUCTION

Bone tissue usually heals completely after damage without scarring *(Jahagirdar and Scammell 2009)*. Nevertheless, the overall rate of nonunion or delayed union represents 5-10 % of the total fractures and depends on the type of bone injury and the patient condition. In Europe, around one million patients per year undergo a surgical bone reconstruction procedure, with expectations of increasing numbers owing to population ageing, a parameter that compromises bone regeneration *(Gómez-Barrena et al. 2015)*.

Regenerative medicine is a rising discipline aiming to repair, replace or regenerate damaged tissues and organs. A suitable structure should be accordingly provided to cells for their attachment and proliferation, allowing the formation of a functional tissue similar to the one to be reconstructed *(Mao and Mooney 2015)*. In case of bone tissue regeneration, autografts (from the patient), allografts (from donors or corpses) and xenografts (from animals) are natural grafts that can act as mechanical support for tissue growth as well as a source of growth factors that promotes tissue regeneration *(Shibuya and Jupiter 2015)*.

Synthetic porous grafts (scaffolds) are being developed to overcome the problems of availability and post-implantation risks of natural grafts. Compressed CO_2 foaming is regarded as a key green technology for the processing of scaffolds *(García-González et al. 2015)*. This technology is based on the role of CO_2 as a porogen by putting in contact this compressed fluid with the matrix of the scaffold for CO_2 sorption and the subsequent expansion of the scaffold (i.e. foaming) upon CO_2 depressurization through a pore nucleation and growth mechanism *(Fanovich and Jaeger 2012, Salerno et al. 2017)*. This technology is unique for preparing drug-loaded scaffolds in a solvent-free approach whilst avoiding leaching downstream steps *(García-González et al. 2015)*. Problems of cytotoxicity of the scaffolds, thermal degradation of their components and low incorporation yields are thus precluded by using this technique. Moreover, compressed CO_2 can also act as sterilizing agent for the scaffolds *(Spilimbergo and Bertucco 2003)*. Nevertheless, compressed CO_2 foaming was not effective so far in the processing of certain

biopolymers, e.g., PLGA, of low inherent viscosities (<0.5 $dL \cdot g^{-1}$) having attractive degradation profiles for scaffolding purposes *(Sheridan et al. 2000, García González et al. 2015)*. Dramatic foam expansions have been obtained so far with this kind of matrices and a proper process design and optimization is urged to circumvent this limitation of the compressed CO_2 foaming technology.

The *in vivo* performance of the processed scaffolds depends primarily on their structure and composition *(Ho and Hutmacher 2006)*. Porosity must be at least 65 %, ideally around 90 % *(Zhang et al. 2015)*, while pore interconnectivity should be high to enable diffusion of oxygen and nutrients to the cells and removal of metabolites *(Ho and Hutmacher 2006)*. The presence of micro and mesopores in the scaffolds allows the circulation of biological fluids and cell adhesion, while small (5-10 μm) and large macropores (50-200μm) are required to facilitate vessel formation and tissue growth, respectively *(García-González et al. 2015)*. At the same time, the mechanical properties of the scaffold should ideally be suitable to act as a temporary support while the growing tissue is still not able to withstand by itself the intrinsic mechanical demands of bone.

The composition of the scaffold must be precisely selected with a matrix able to provide a degradation rate that suits the growth rate of the bone tissue, and with growth and differentiation agents to promote the proper bone tissue growth. Various biodegradable synthetic polymers, e.g., poly(lactic-co-glycolic) acid –PLGA– and poly(ε-caprolactone) –PCL– *(Zhang et al. 2015, Diaz-Gomez et al. 2016, Diaz-Gomez et al. 2017)*, and natural polymers, e.g., starch, collagen, gelatin, silk, alginate or chitosan *(Duarte et al. 2009, Chimenti et al. 2011, Cuadros et al. 2015, Zhang et al. 2015, Melke et al. 2016)*, are common materials employed as scaffold matrices. Among the growth and differentiation agents, dexamethasone (DX), a drug belonging to the group of glucocorticoids, can induce the differentiation of mesenchymal stem cells (MSC) to osteoblasts *(Yoon et al. 2003)*. DX-loaded scaffolds providing local delivery of the bioactive agent may have the advantage of inducing bone formation whilst avoiding or at least mitigating the undesired collateral effects derived from a systemic administration of glucocorticoids.

Stability under storage is a critical quality attribute to define the performance and the availability of scaffolds. A short shelf-life would hamper the supply of these grafts and raise the cost of the treatment *(Sun and Gouk 2008)*. Nitrogen atmospheres or vacuum conditions are the most common packaging options of the commercial scaffolds. In these cases, the direct exposition to climatic conditions is initially avoided, although it might occur if the packaging is accidentally damaged (e.g., with a microhole) resulting in loss of the inert atmosphere or breaking of vacuum. Systems like knitted polylactide scaffolds and knitted silk fibroin (SERI©) surgical scaffolds have been tested for up to 3 years under room conditions, maintaining their mechanical properties for that period *(Ellä et al. 2011, Jewell et al. 2015)*. Nevertheless, there is still a paucity of information on the effect of storage on the durability of scaffolds with more complex porous structures or loaded with drugs, which might be more sensitive to environmental factors.

In this work, synthetic scaffolds made of mixtures of PCL and PLGA of low inherent viscosity (50:50 w/w) loaded with and without DX were prepared using a novel compressed CO_2-assisted foaming method. The processing method was herein designed and optimized for DX-loaded scaffolds from a previously implemented one *(García González et al. 2015)* so that it could operate in one-pot, during short processing times, without use of organic solvents and under mild temperatures. The role of the incorporation of starch (St) in controlling the DX release profile from the scaffolds was evaluated. Then, the scaffolds (without packaging) were stored in chambers (25 ºC, 65% relative humidity) mimicking the zone II ICH-climatic conditions (Europe, USA and Japan) *(de Matos et al. 2015)* and the stability of the scaffolds in terms of structural, physicochemical and mechanical properties as well as DX release profiles were monitored for 3 months.

3.2. MATERIALS AND METHODS

3.2.1. Materials

PLGA (50:50 lactic:glycolic ratio; M_w 16 kDa; amorphous; T_g=41.4 ºC) was purchased from Purac (Gorinchem, The

Netherlands). PCL (M_w 50 kDa; semicrystalline; T_m=61.6 ºC; ΔH_m=95.9 J/g) was supplied by Polysciences (Warrington, PA, USA). Corn starch (Amylo N-460, 52.6 % amylose content) was bought from Roquette (Lestrem, France). Dexamethasone (DX, 97 % purity) was obtained from Sigma-Aldrich (Saint Louis, MO, USA). Carbon dioxide (99.8 % purity) from Praxair (Madrid, Spain) was used to process the scaffolds. Milli-Q water (resistivity > 18 MΩ·cm; MilliQ, Millipore®, Madrid, Spain), sulfuric acid (95-97 % purity, Merck, Darmstadt, Germany) and acetonitrile (99.9 % purity, Merck, Darmstadt, Germany) were also used.

3.2.2. Preparation of oven-dried starch gels (St_p)

10 g of corn starch were dispersed in 210 g of water under magnetic stirring and then heated for 20 min at 121 ºC (Autoclave Raypa, model AES-12, Terrassa, Spain). Then, the starch dispersion was transferred to a fridge at 4 ºC and maintained for 60 h for retrogradation, and subsequently poured on Petri dishes and put in an oven at 80 ºC for water evaporation. The resulting dry solid films were ground in a ball mill (Mix MM 400, Retsch Inc., Newton, PA, USA) to obtain powdered starch particles of *ca.* 20 μm size.

3.2.3. CO_2 sorption in the scaffold polymers

A gravimetric method was used to monitor carbon dioxide sorption in PLGA and in PCL:PLGA (50:50 w/w) mixtures at elevated pressure. A high-pressure magnetic suspension balance (Rubotherm GmbH, Bochum, Germany) was used to measure the CO_2 uptake by PLGA as a function of time and simultaneously detecting the volume change by a high pressure view cell (Eurotechnica GmbH, Hamburg, Germany), at the operating conditions of 66 bar and 26 ºC (compressed liquid) and 51 bar and 26 ºC (compressed gas) for PLGA and of 60 bar and 26 ºC (compressed gas) for the PCL:PLGA mixture. The polymer was previously filled in the powdered form into a glass vessel, molten at 70 °C, cooled down for solidification and then placed in the magnetic suspension balance (Fig. 3.1). The force resulting from the mass and the buoyancy of the polymer is transmitted to a microbalance at the outside of the autoclave via a

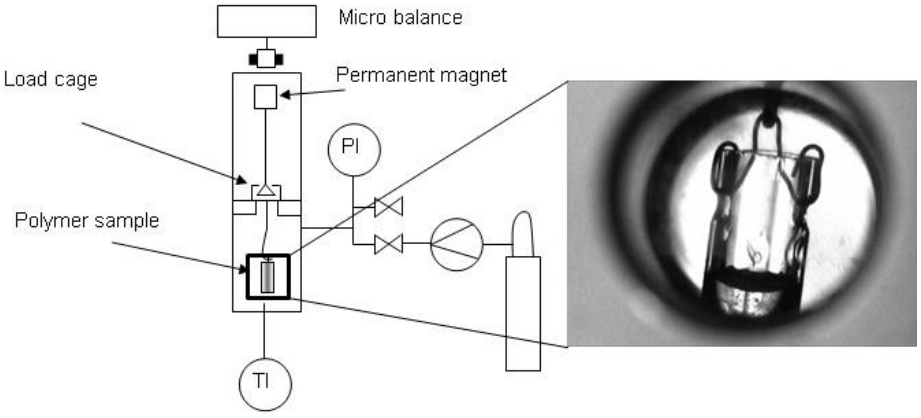

Fig. 3.1: Sketch of the high-pressure magnetic suspension balance used for CO_2 sorption tests in polymers. Inset: Glass vessel containing the polymeric mixture (bottom) inside the balance before the start of the test.

magnetic coupling. From the evolution of the weight as a function of time, the diffusion process could be followed and the CO_2 solubility determined (<5 % deviation) once saturation was achieved *(Crank 1975)*.

3.2.4. Compressed CO_2 foaming of synthetic scaffolds

Polyester-based scaffolds were prepared using a multi-step process sketched in Fig. 3.2. The components of the scaffolds (Table 3.1) were homogenized in a mortar and mixed for 5 min (Mixer Wab, model T2C, Switzerland) and then compressed in an eccentric tableting machine (FE236FC, Korsch, Berlin, Germany) to obtain compacts of 400 mg with prismatic dimensions (14x10x2.6 mm).

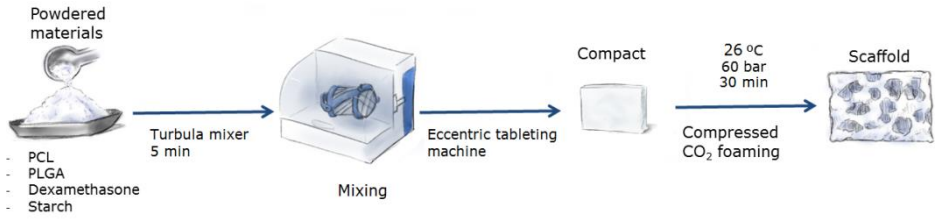

Fig. 3.2: Schematic workflow for the preparation of polyester-based scaffolds using compressed CO_2 technology.

Table 3.1: Composition (in weight percentage) of compressed CO_2-processed scaffolds.

Scaffolds	PLGA:PCL 50:50	DX	St_p
St0-DX0	100	-	-
St0-DX	94.5	5.5	-
St-DX	85	5	10

The compacted materials were processed in a high pressure equipment (Thar Technologies, Pittsburgh, PA, USA) adapted for compressed CO_2 foaming. Briefly, the compacts were placed in a rotating basket (700 rpm) inside the foaming vessel and put in contact with CO_2 at 26 ºC and 60 bar for 30 min. After this soaking period, pressure was lowered from 60 to 30 bar at a flow rate of 10 bar/min, and then pressure was increased again until 60 bar by adding liquid CO_2 at 1 ºC. This process was repeated three times, before proceeding to complete the depressurization period at a flow rate of 10 bar/min. Finally, the external layer of the scaffolds was removed with a scalpel one day after processing and before any further use.

The foaming process was also monitored with a view cell (Eurotechnica, Hamburg, Germany) and recorded with a CCD-camera. Visual behavior of the foaming process of St0-DX0 scaffold was compared to a similar experiment with direct depressurization from 60 bar to atmospheric pressure at 10 bar/min without addition of liquid CO_2, to unveil the relevance of the foaming process strategy used in this work.

3.2.5. Scaffolds characterization

3.2.5.1. Structural, physicochemical and mechanical characterization of scaffolds

Images from the cross-sections of the scaffolds were obtained by scanning electron microscopy (SEM, EVO LS15, Zeiss, Oberkochen, Germany). Overall porosity (ε) was calculated using the following equation:

$$\varepsilon = (1 - \rho_{bulk}/\rho_{skel}) \cdot 100 \qquad (3.1)$$

where ρ_{bulk} is the bulk density estimated from the dimensions and the weight of the scaffolds (after the foaming process), and ρ_{skel} is the skeletal density of the scaffolds measured by helium pycnometry (Quantachrome; Boynton Beach, FL, USA) at 25 ºC and 1.03 bar.

Textural properties of the scaffolds (total pore volume –V_p–, pore size distribution and open porosity –ε_{MIP}–) before and after storage were measured through mercury intrusion porosimetry (MIP) (Autopore IV 9500 model, Micromeritics, Norcross, GA, USA). MIP was operated with a 3 mL-penetrometer for solids and at working pressures ranging from 0.07 to 1724 bar. Thermal properties were analyzed through differential scanning calorimetry (DSC) (TA Instruments Q100; New Castle, DE, USA) using two heating cycles up to 125 ºC with a cooling cycle down to -10 ºC inbetween, at a rate of 10 ºC/min and under a nitrogen atmosphere. Mechanical properties were analyzed at 37 ºC using a Rheolyst AR1000N rheometer (TA Instruments, New Castle, DE, USA) fitted with an environmental test chamber, a solid torsion kit and a data analyser (AR2500). The scaffolds were located between two clamps (8 mm gap) and then subjected to an angular frequency sweep in the 0.05-20 rad/s range

3.2.5.2. Stability under storage

Scaffolds of defined dimensions and weights of the three compositions (Table 3.1) were placed on top of a platform inside sterile hermetic glass vessels, which contained sulfuric acid solution (37 % v/v) in the bottom to maintain the required relative humidity (65 %) at 25 ºC *(Wilson 1921)*. The glass vessels were stored for 1 and 3 months. Once the storage period was over, the scaffolds were collected for further characterization (Section 3.2.5.1).

3.2.5.3. DX release tests

Prismatic pieces (10 mg) of scaffolds were individually transferred to flasks containing 50 mL of PBS pH 7.4. The flasks were kept in an oscillating shaker (JP Selecta, Unitronic 320 OR model, Abrera, Spain) at 37 ºC and 60 rpm for 3 weeks *(Duarte et al. 2009)*. Aliquots of 1 mL were sampled through the release period at selected times and the volume was replaced with fresh PBS medium. DX

release tests were performed in triplicate. The dissolution profile of 1 mg of DX powder in 100 mL of PBS was also recorded in triplicate for the sake of comparison.

DX concentration was quantified by HPLC (Waters; Milford, MA, USA) consisting on a 717 plus Autosampler, a 600 Controller and a 996 Photodiode Array Detector. A C_{18} column (Symmetry© C18, particle size 5 μm, 3.9 mm diameter x 150 mm length) from Waters (Milford, MA, USA) was used at 30 ºC. The mobile phase consisted on a mixture of water:acetonitrile 67:33 (v/v), operating in the isocratic mode, and the flow rate was set at 1 mL/min *(Moya-Ortega et al. 2010)*. The volume injected in the column was 20 μL. DX was quantified using UV/Vis diode-array detector at 242 nm with a retention time of 5.5 min. Samples were filtered prior to analysis using 0.2 μm nylon filters to avoid potential interference due to the presence of particles from the scaffolds. The calibration curve of DX in PBS was done in triplicate in the concentration range 0.025-50 μg/mL (Fig. 3.3).

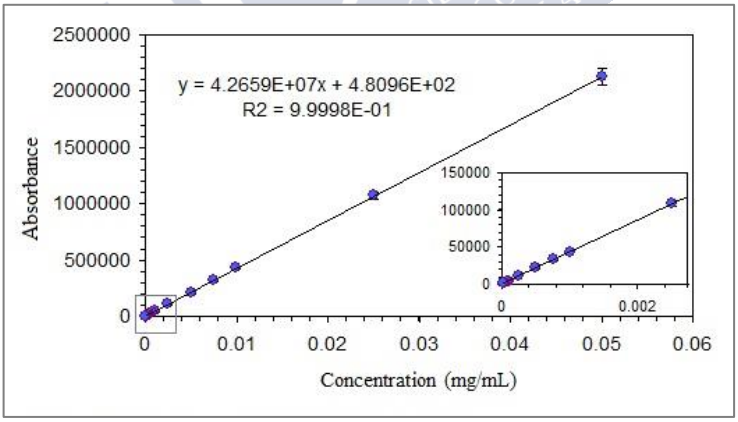

Fig. 3.3: Calibration curve and equation for dissolved DX in PBS pH 7.4 by HPLC at 242 nm.

3.2.5.4. Erosion assay

Fifteen prismatic scaffold pieces (15 mg) of each formulation were suspended in separated Eppendorf tubes containing 1 mL of PBS pH 7.4 and kept in an oscillating bath at 37 ºC and 60 rpm. The

medium was replaced weekly with fresh PBS. At selected time points (3, 7, 14, 21 and 59 days) that were pre-established in accordance to classical bone regeneration cycle times *(Einhorn and Gerstenfeld 2015)*, three pieces (i.e. three replicates) were retrieved from the bath, gently rinsed with Milli-Q water, freeze-dried (Lyophilizer Telstar, model LyoQuest Plus -85ºC/ECO, Terrassa, Spain) and weighed *(de Matos et al. 2015)*. Similarly and in addition to these measurements, the weight loss was also recorded after the release assays (Section 2.5.3).

3.3. RESULTS AND DISCUSSION

3.3.1. Scaffold processing design

Different processing techniques have been reported for the manufacturing of synthetic scaffolds, such as emulsion freeze-drying, phase separation, melt moulding, 3D-printing and salt leaching *(Walker and Santoro 2017)*. Among them, compressed CO_2-based technologies are emerging, advantageous tools for the manufacturing of scaffolds for regenerative medicine *(Quirk et al. 2004, García-González et al. 2009, García-González et al. 2015, Salerno et al. 2017)*. Supercritical and compressed CO_2 foaming are particularly attractive since they allow fast scaffolds processing at mild temperatures. These features are of particular interest if the incorporation of thermolabile bioactive compounds to the scaffolds with high yields is envisaged *(Goimil et al. 2017)*. Namely, DX maintains its bioactivity when kept under temperatures up to 40 ºC, but it is sensitive to intense heat conditions, even for short time periods *(Küpper et al. 2006, Dudley et al. 2012)*. Therefore, the optimization of the processing conditions of compressed CO_2 foaming for each specific polymeric matrix-DX combination is required to avoid DX thermal degradation and to obtain scaffolds with adequate morphology.

For the manufacturing of DX-loaded scaffolds made of PLGA:PCL (50:50 w/w), the operating temperature was set to 26 ºC to avoid bioactivity losses. On the other hand, the concentration of CO_2 absorbed in the polymeric matrix during the soaking period of the foaming process is a critical parameter influencing the mean pore size

and the bulk density of the resulting scaffolds *(García-González et al. 2015)*. The minimum soaking time needed to reach stable CO_2 sorption values at 26 ºC was set based on magnetic suspension balance tests of PCL and PLGA to get reproducible conditions for the scaffold processing. Fig. 3.4 shows the weight change of PLGA exposed to compressed CO_2 as a function of time. The change in mass followed the course of a non-stationary diffusion of the fluid into the polymer until a constant weight was reached. Under compressed liquid conditions (66 bar, 26° C), CO_2 sorption in PLGA increased with time until a plateau (i.e. close to CO_2 saturation) was reached after *ca.* 1 h of exposure. Significant CO_2 sorption (7 wt.% in Fig. 3.4) in PLGA under compressed liquid conditions was thus obtained. Solubility values in the 6.4-15 wt.% range were reported for CO_2 in other polyesters at similar or higher operating pressure and temperature *(Aionicesei et al. 2009, Markočič et al. 2011)*. Conversely, much lower CO_2 sorption in PLGA (*ca.* 1 wt.%) was obtained under the same exposure time when decreasing the pressure to 51 bar (i.e. gaseous CO_2 state). CO_2 saturation of the polymer was not reached in this case but CO_2 sorption in PLGA remained in the 1.0-1.3 wt. % range in the 30-120 min exposure period. The increased CO_2 sorption in PLGA with pressure was also observed with other polyesters (PLLA, PCL) including PLGA of different molecular weight from the one used in this study *(Aionicesei et al. 2009, Fanovich and Jaeger 2012)*. The CO_2 sorption in PLGA is diffusion-controlled and takes place by filling with CO_2 the free volume holes of the polymer created by Brownian motions of the polymeric chains of PLGA *(Markočič et al. 2011)*. The lower diffusivity of gaseous CO_2 within the polymeric matrix explains the slower CO_2 sorption kinetics with respect to liquid CO_2. The lower amount of absorbed CO_2 from the gaseous state leads to a more reduced mobility of the polymeric chains. On the other hand, the CO_2 sorption kinetics in PCL under the same compressed gas conditions (51 bar, 26 ºC) as with PLGA also resulted in a relatively slow kinetics with long saturation periods *(Fanovich and Jaeger 2012)*.

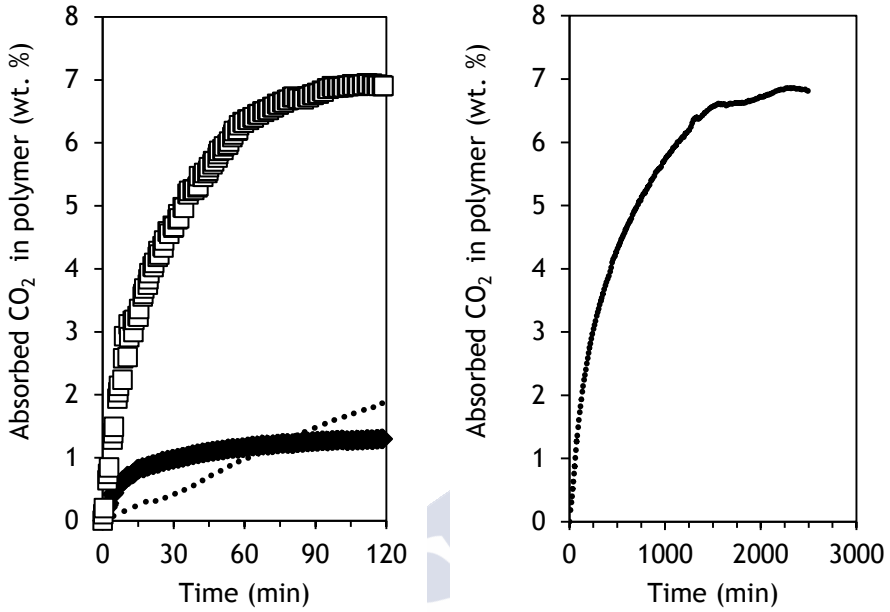

Fig. 3.4: CO_2 sorption kinetics in PLGA at compressed gas (51 bar, 26 °C) (black diamonds) and compressed liquid (66 bar, 26 ºC) (white squares) conditions, and in PLGA:PCL (50:50 w/w) mixtures at the foaming conditions (60 bar, 26 ºC) (dotted line).

The next step for the scaffold processing was to establish a foaming protocol able to provide porous scaffolds from the PCL-PLGA compacts with controlled morphology. Being the operating temperature set to 26 ºC, pressure was accordingly chosen at 60 bar (i.e. compressed gas CO_2 conditions) and operating time at 30 min in an attempt to provide enough CO_2 sorption in the polymer for foaming whilst allowing a controlled volume expansion of the resulting scaffold upon depressurization at 10 bar/min. Under these soaking conditions, PLGA and PCL have intermediate and low CO_2 sorption values, respectively. The content of CO_2 in the mixture at the designated process conditions was of *ca.* 0.5 wt. % after 30 min of contact (Fig. 3.4). Compared to the behavior of pure PLGA, this value is much lower and was related to the lower diffusivity of CO_2 in PCL than in PLGA *(Aionicesei et al. 2008, Fanovich and Jaeger 2012)* as

well as the higher molecular weight and crystallinity of the PCL. The CO_2 content at saturation of the polymeric mixture was relatively high and linked to the presence of PCL, as supported by data from literature *(Fanovich and Jaeger 2012)*. Moreover, CO_2 may also act as sterilizing agent under these foaming conditions *(Spilimbergo and Bertucco 2003, Diaz-Gomez et al. 2016)*. Despite the pressure and temperature conditions used being considered as moderate, the foaming expansion process prevailed over the polymer vitrification and the depressurization step resulted in an overexpressed process with formation of foams of uncontrolled shape and with large bubbles of several millimeters. A modified foaming process consisting of periodic additions of liquid CO_2 (1 ºC) during the depressurization was then developed to reach a controlled foaming process *(García González et al. 2015)*. Additions of liquid CO_2 gradually upon depressurization reduced the temperature in the vessel resulting in a faster vitrification of the polymeric matrix and thus reducing its expansion. Three or more periodic additions of liquid CO_2 were effective in vitrifying the matrix to obtain volume expansions close to the target porosity of 70-75 % and macropore sizes in the order of 100 µm. Three additions of liquid CO_2 were set for ulterior tests for the sake of the economy of the process.

3.3.2. Morphological, thermal, biodegradable and mechanical properties

After using the modified compressed CO_2 processing, scaffolds of white and homogeneous appearance and light-weight (0.24-0.30 g/cm^3) were obtained in all cases. No weight loss was observed in the scaffolds after foaming, thus indicating that none of the admixtures was significantly dissolved in CO_2 and vented upon processing. The low solubility of DX under compressed CO_2 (molar fraction < $3 \cdot 10^{-6}$) even under supercritical conditions and/or high pressures (350 bar)*(Chim et al. 2012)* coupled to the mild pressure and temperature operating conditions used in this work explains the absence of DX losses upon processing. The increase in volume of the scaffolds after the foaming process was of *ca.* 4-fold with respect to the volume of

the unprocessed compact, resulting in overall porosities of 68-75% (Table 3.2).

SEM pictures of St0-DX0 scaffolds unveiled a porous structure with most of the macropores in the 50-200 μm region (Fig. 3.5A&B). The incorporation of DX and mainly of St_p in the scaffolds resulted in the appearance of a second family of macropores of smaller size (*ca.* 10 μm) randomly distributed throughout the scaffolds (Fig. 3.5C-F). The use of these admixtures may result in the presence of secondary nucleation sites during the foaming process responsible for the presence of smaller pores in these scaffolds (St0-DX and St-DX scaffolds) *(de Matos et al. 2013)*. Macropores are still the major contributors on porosity (i.e. in volume) for these scaffolds, but not in population (i.e. in number of pores). The obtained dual porosity is susceptible to promote vascularization (through the small macropores) and to favor cell colonization and tissue growth (through the large macropores) *(Salerno et al. 2012, García-González et al. 2015)*. The observed anisotropic distribution of pores can prevent a fast tissue formation on the external region of the scaffolds that may hinder the access of cells and nutrients towards the inner part resulting in the necrosis of the core *(Silva et al. 2006, Salerno et al. 2012)*. Moreover, the presence of DX also seems to promote the formation of channels formed by macropores interconnected by broad pore throats (arrows in Fig. 3.5C&E). These macrochannels might facilitate the penetration of cells towards the inner part of the scaffolds *(Silva et al. 2006)*. The control on the formation of these macrochannels will be the subject of further optimization through changes in the processing parameters during the compact preparation (e.g., powder granulometry, compression pressure) and the foaming process (e.g., depressurization rate).

The porous structure of the scaffolds was characterized using MIP (Table 3.2). All scaffolds had good pore interconnection as small differences (<5-10 %) were observed between the overall porosity measured by helium pycnometry (ε) and the open porosity obtained by mercury porosimetry (ε_{MIP}) (Table 3.2). The apparent discrepancy of the MIP results with St0-DX0 scaffolds and those observed by SEM

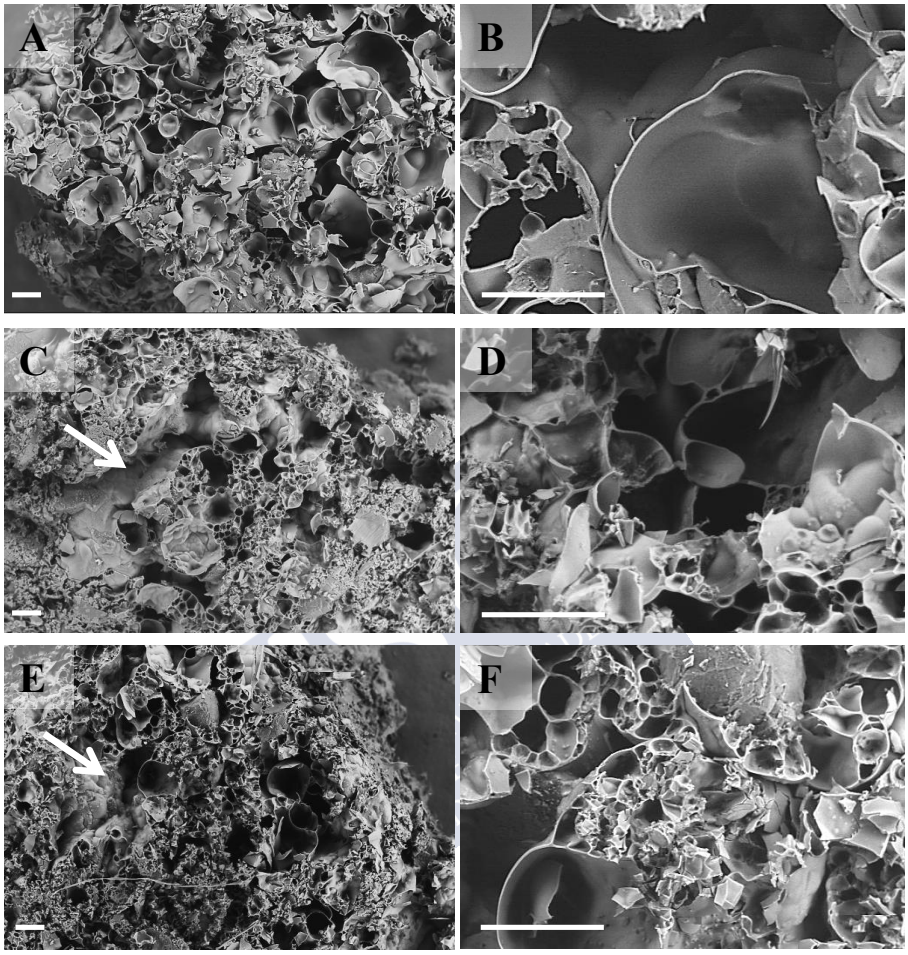

Fig. 3.5: SEM images of (A, B) St0-DX0, (C, D) St0-DX and (E, F) St-DX non-stored scaffolds. The presence of DX and St_p favored the formation of macrochannels (indicated by arrows). Scale bars: 200 μm.

in Fig. 3.5 was related to the limitations of the former technique *(Giesche 2006)*. Indeed, the correlation used in MIP between applied pressure and pore size assumes a cylindrical shape of the pores and that the size of the pore is equal to the broadest entry (throat) to the pore. Moreover, MIP technique is also limited by the connectivity and spatial arrangement of the pores, e.g., large pores surrounded by smaller pores are only filled with mercury at the pressure needed to

fill the latter ones, and the computed size will be the same for all the pores *(Giesche 2006)*. Accordingly, the large pores from St0-DX0 scaffolds might have narrow throat sizes and explain the high contribution of the small pores unveiled by MIP. The presence of DX and St_p in the scaffold formulations (St0-DX and St-DX) changed the pore size distribution. The population of mid- (10-100 μm) and large-sized (>100 μm) pores increased with DX and St_p likely due to the secondary pore nucleation site provided by these admixtures and the observed formation of macrochannels, respectively.

Thermal properties of the polymers were altered when blended and processed under compressed CO_2 conditions (Table 3.3). Under the experimental conditions used for foaming (26 ºC, 60 bar), both PCL and PLGA were above their glass transition values (T_g) according to the view cell experiments (Section 3.1) and, therefore, in the glassy state. This information is crucial since it ensures a certain volume expansion after CO_2 depressurization. After processing, St0-DX0 scaffolds showed two melting thermal events ($T_{m,1}$ and $T_{m,2}$) one

Table 3.2: Porosity and pore size distribution of the scaffolds before and after storage at 25 ºC and 65% relative humidity. Pores were separated according to their pore size into small (<10 μm), mid-sized (10-100 μm) and large pores (>100 μm).

Scaffolds	ε (%)	ε_{MIP} (%)	V_p (cm^3/g)	Volume contribution (%)		
				<10 μm	10-100 μm	>100 μm
St0-DX0						
Non stored	69.1±2.7	65.5	1.78	71.20	24.50	4.30
1 month	67.6±1.6	54.0	1.55	49.31	43.60	7.09
3 months	68.2±3.7	67.2	1.64	50.00	42.34	7.66
St0-DX						
Non stored	71.8±14.2	63.9	2.04	50.08	42.85	7.07
1 month	71.1±9.8	63.6	1.78	52.46	37.82	9.72
3 months	65.3±16.0	61.8	1.49	49.97	43.53	6.50
St-DX						
Non stored	74.7±10.4	65.3	1.99	61.82	31.91	6.27
1 month	68.9±11.1	61.9	1.72	58.10	35.98	5.92
3 months	71.9±10.4	46.3	0.80	50.00	40.48	9.52

shifted towards lower values than the melting point of pure PCL (61.57 ºC) and the other towards higher values and with decreased crystallinity of PCL (ΔH_m=80.44 J/g_{PCL}) because of PCL-PLGA chemical interactions *(Diaz-Gomez et al. 2016)*. Melting of PCL was assumed to take place only partially under the experimental conditions of foaming and PCL fractionation should have occurred. The molten fraction of PCL, corresponding to the lighter fraction of PCL, was responsible for the first thermal event observed ($T_{m,1}$). The T_g of PLGA was overlapped with the first melting point of PCL and could not be individually evaluated. The reduction in the melting point value $T_{m,1}$ with respect to the normal melting point of PCL was ascribed to PCL-PLGA interactions and to the intrinsic lower melting point values of the light fraction from PCL. The increase in the $T_{m,2}$ value was attributed to the average melting point of the heavier fraction of PCL, not molten upon the compressed CO_2 foaming process. The identification of the thermal events and the hypothesis of the partial melting of PCL during the foaming process were confirmed with the second heating cycle of the DSC analysis. PCL completely melted during the first heating cycle (end cycle at 125 ºC) and favored the interaction between PCL and PLGA. A single melting event ($T'_{m,1}$) was then observed during the second heating cycle shifted towards lower values than the normal melting point of PCL, thus indicating a stronger PCL-PLGA interaction and without PCL fractionation.

The effect of the incorporation of admixtures (DX and St) in the scaffolds on the thermal transitions of the synthetic scaffolds was evaluated. DX had a minimum effect on the thermal properties of the scaffolds (St0-DX) with a limited decrease in the polymer crystallinity (ΔH_m=72.19 J/g_{PCL}). Differently, a dramatic depletion in the melting point values ($T_{m,1}$ and $T_{m,2}$) was observed with the incorporation of starch to the formulation (St-DX). The pregelification of the starch used in this work (St_p) favored the PCL-St interaction by hydrogen bonding between the hydroxyl groups of starch and the ester carbonyl groups of PCL and was responsible for these shifts in the melting point values *(Averous et al. 2000, Ali Akbari Ghavimi et al. 2015, Diaz-Gomez et al. 2016).*

Table 3.3: Thermal properties of the processed scaffolds before and after storage tests at 25 ºC and 65 % relative humidity.

Scaffolds	1st heating cycle			2nd heating cycle	
	$T_{m,1}$ (ºC)	$T_{m,2}$ (ºC)	ΔH(J/g)	$T'_{m,1}$ (ºC)	ΔH(J/g)
St0-DX0					
Non stored	48.3	62.1	40.2	56.1	36.4
1 month	42.5	61.0	64.3	54.7	53.6
3 months	38.6	62.8	50.0	54.6	32.9
St0-DX					
Non stored	48.2	61.9	34.1	56.3	37.1
1 month	42.1	60.2	40.7	54.4	34.5
3 months	38.1	62.2	47.8	54.5	31.2
St-DX					
Non stored	43.2	57.4	36.4	53.2	32.0
1 month	42.2	61.2	54.0	54.6	46.4
3 months	34.5	61.7	39.1	54.2	25.0

Biodegradation is a critical design parameter of the scaffolds to suit the bone tissue growth rate *(Woodruff et al. 2012)*. The mixture of PCL with a low molecular weight PLGA was accordingly chosen in this work to tune the erosion rate, since it combines the slow degradation of PCL in the order of months *(Diaz-Gomez et al. 2016)* with the much faster degradation of PLGA in the order of weeks *(Lu et al. 2000)*. The effect of scaffolds composition on the erosion rate was assessed in PBS pH 7.4 medium (Fig. 3.6). The erosion rate was similar for the first 14 days for all the scaffolds formulations with a weight loss of *ca.* 25 wt.% due to the degradation of the polyesters, mainly PLGA. This degradation might be initially promoted owing to the acidic environment provided by the soluble degradation products with limited diffusion through the porous matrix of the scaffolds *(Berkland et al. 2007)*. Upon degradation, the pore sizes of the scaffolds increased and the diffusion of the degradation products to the PBS medium was enhanced, resulting in a less acidic pore microenvironment and a subsequent decrease in the degradation rate of the polymers. The transition towards slower degradation rates took longer for the scaffolds St0-DX and St-DX (*ca.* 21 days). The

incorporation of DX in the formulation accelerated the degradation rate since it contributes to the formation of less crystalline polymeric matrices, to the scaffold weight loss due to the release of DX in the degradation medium (see Section 3.3.4) and to a more open structure as DX progressively dissolves. The presence of starch in the scaffolds (St-DX) gave rise to a morphology of higher open porosity and larger pores favoring the intimate contact of the degradation medium with the scaffold and a less crystalline polymeric matrix *(Cai et al. 2014)*. Additionally, starch would degrade in PBS solution due to its partial dissolution (i.e. leaching) through the breakage of hydrogen bonds of starch molecules. Moreover, the starch used in this work is particularly susceptible to dissolution due to its high amylose content (52.6 % amylose) *(Han and Lim 2004)*. Subsequently, the erosion rate of the scaffolds increased with the presence of starch, as already reported for PCL-starch blends *(Ali Akbari Ghavimi et al. 2015)*.

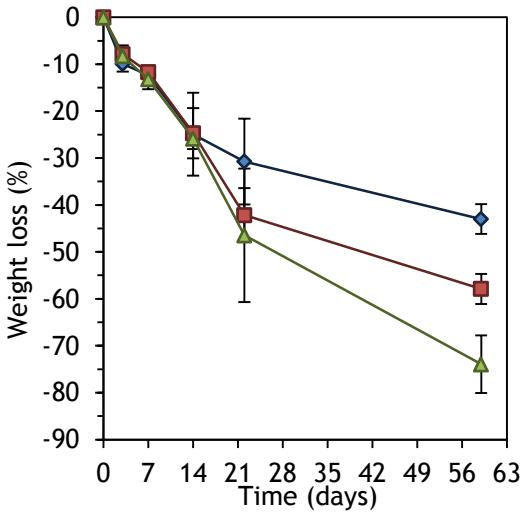

Fig. 3.6: Erosion tests of the processed scaffolds in PBS pH 7.4 medium (37 ºC, 60 rpm): St0-DX0 (in diamonds), St0-DX (squares) and St-DX (triangles).

Bone fractures usually heal within 6 and 8 weeks, but the period to repair bone defects will vary depending on the defect size, and can take from 6 to 12 months to form a mature tissue *(Woodruff et al. 2012)*. Nevertheless, these scaffolds incorporate an osteogenic factor

(DX), which is expected to accelerate the healing process and thus fit the needed degradation rate. In addition, some polymeric scaffolds have shown a faster degradation rate *in vitro* than *in vivo* due to the formation of connective tissue around the structure *(Ellä et al. 2011)*.

Regarding the mechanical properties, viscoelastic behavior was observed for all the scaffolds formulations (Fig. 3.7). The storage (G') and loss (G'') moduli were close to the values of 0.1 and 0.01 GPa, respectively, in the tested range of angular frequencies. These mechanical parameters fall slightly below the values reported in the literature for trabecular and cortical bones of human and animal origin: G'=0.3-10 GPa; G''=0.01-0.60 GPa *(Linde et al. 1988, Yamashita et al. 2001, Buechner and Lakes 2003)*.

3.3.3. Effect of storage

The volume of all scaffolds decreased after the storage period at 25 ºC and 65 % relative humidity (Table 3.4). Loss in weight was negligible. Therefore, densification of the scaffolds and reduction in the overall porosity occurred during the storage period. The densification was more pronounced for the scaffolds containing DX and St_p and had a direct impact on the micromeritic properties as evaluated by MIP analysis (Table 3.2). For St0-DX0 scaffolds, a reduction in the population of small pores (<10 μm) took place upon storage, which was mainly related to the broadening of the pore throat sizes. Moreover, a reduction in the open porosity (ε_{MIP}) was observed due to a certain pore collapse upon storage. The pore size distribution was almost unaltered in the case of St0-DX scaffolds, although a certain shift towards the lowest limit of each pore range took place with longer storage time periods, since a reduction in the overall pore volume (V_p in Table 3.2) and a reduction in the scaffold volume (Table 3.4) were observed.

The most significant change in porous morphology upon storage was observed for the scaffolds containing starch (St-DX). After one month of storage under controlled temperature and humidity conditions, densification occurred with a certain reduction in the overall and open porosities as well as in the total pore volume (Tables 3.2 and 3.4). A dramatic change in the porous structure of St-DX took

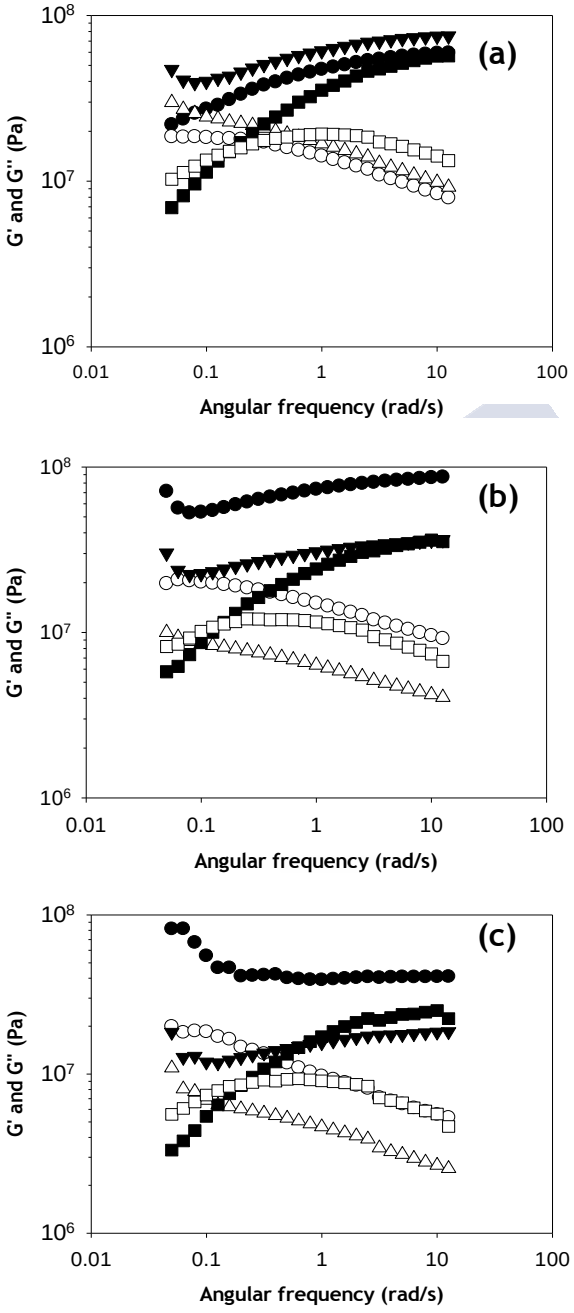

Fig. 3.7: Storage (G'; black symbols) and loss (G''; white symbols) moduli of the scaffolds (a) St0-DX0, (b) St0-DX and (c) St-DX before and after storage at 25 ºC and 65 % relative humidity. Circles, triangles and squares stand for non-stored scaffolds, scaffolds stored for 1 month and scaffolds stored for 3 months, respectively.

Table 3.4: Changes (in percentage) of weight, volume, density and porosity of PCL-PLGA-based scaffolds after being stored for 1 and 3 months at 25 ºC and 65 % relative humidity.

Scaffolds	St0-DX0		St0-DX		St-DX	
Storage period	1 month	3 months	1 month	3months	1 month	3 months
Change in weight (%)	-0.48±0.18	-0.62±0.43	-0.38±0.47	-0.78±0.35	-0.50±0.27	-0.52±0.93
Change in volume (%)	-6.19±7.53	-2.35±4.47	-12.59±10.31	-15.81±9.45	-18.69±12.19	-12.60±5.14
Change in bulk density (%)	6.68±8.94	1.89±4.85	15.15±12.49	19.11±12.68	24.81±19.55	14.19±6.62
Change in overall porosity (%)	-2.69±3.73	-0.90±1.92	-3.76±3.53	-5.67±1.90	-6.11±3.89	-4.87±3.23

place in a more prolonged storage period (three months) with a marked decrease in the open porosity and in the overall pore volume (V_p). The swelling capacity of the amylopectin fraction of the starch in the presence of moisture might explain the observed phenomena of reduction of porosity *(Alcázar-Alay and Meireles 2015)*.

Regarding the thermal transitions of the scaffolds, mid-term storage periods resulted in a noticeable effect on the first melting point ($T_{m,1}$) region of the scaffolds (Table 3.3). This depletion on $T_{m,1}$ values was more significant with longer time periods and was attributed to the overlapping of the first melting of PCL with the glass transition of PLGA coupled to the plasticizing effect of water on PLGA *(Blasi et al. 2005)*. Water vapor would progressively adsorb on PLGA resulting in a decrease in the T_g inferring a reduction in $T_{m,1}$ *(Bouissou et al. 2006)*. This depletion effect due to adsorbed water was also observed for $T'_{m,1}$ during the second DSC-heating cycle for St0-DX0 and St0-DX scaffolds. A reverse trend was observed for St-DX scaffolds where $T'_{m,1}$ increased with time likely due to a higher starch-PCL interaction with the swollen starch.

The erosion rate of the scaffolds in PBS pH 7.4 at 37 ºC varied depending on the previous storage time under 25 ºC and 65 % relative

humidity (Table 3.5). For St0-DX0 scaffolds, the increasing plasticizing effect of the adsorbed moisture on PLGA with time *(Blasi et al. 2005)* resulted in a severe weight loss, notably after 3 months of storage. The presence of DX in the scaffolds (St0-DX) and its release seemed to have a minor effect on the erosion rates when compared to the unloaded scaffolds (St0-DX0), although higher variability in the results was observed. The slower degradation of PCL due to its increased crystallinity over the storage time (Table 3.3) mitigated the higher weight loss that could be expected due to DX release to the PBS medium (Table 3.5). A reverse trend was observed with the incorporation of starch in the formulation (St-DX), with the most pronounced weight loss for non-stored scaffolds, and the lowest value obtained after 3 months of storage. This effect of starch in the scaffold erosion was attributed to the increased starch-PCL interaction of the St-DX scaffold after 3 months of storage if compared to the other two scaffold formulations (Table 3.3).

Table 3.5: Weight loss (in percentage) after 3 weeks in PBS pH 7.4 medium at 37 ºC and 60 rpm of scaffolds previously stored at 25 ºC and 65% relative humidity during different time periods (0, 1 and 3 months).

Scaffolds	Non-stored	1 month-storage	3 month-storage
St0-DX0	-13.38±1.79	-15.28±0.38	-34.40±1.61
St0-DX	-13.76±5.51	-18.53±2.83	-34.70±8.15
St-DX	-22.67±4.17	-18.61±10.24	-23.52±5.58

The viscoelastic properties of the St0-DX0 scaffolds remained unaltered after long storage periods (Fig. 3.7a). Nevertheless, a different mechanical profile after 3 month-storage was observed, since at low angular frequencies G'' predominates over G' in a fluid-like (viscous) behaviour that indicated loss of mechanical stability. Scaffolds containing DX and St_p did not only follow this behaviour but also underwent other noticeable changes. The increase in the DX-polymeric matrix interactions upon storage of St0-DX scaffolds, as previously observed by DSC analysis, might explain the decrease in both the loss and storage moduli (Fig. 3.7b). The use of starch in the scaffold formulations resulted in the largest reduction in the values of

the viscoelastic moduli (Fig. 3.7c). The low interfacial adhesion between PCL and starch had a strong effect on the viscoelastic properties of the scaffolds *(Mehr et al. 2015)*. The loss and storage moduli decreased upon storage likely due to the plasticizing effect of adsorbed water on starch and the increased PCL-St interaction as unveiled by DSC analysis.

3.3.4. Dexamethasone release

The observed release profiles of DX from the scaffolds were composed of three steps (Fig. 3.8): (i) burst of DX during the first 2-3 hours; (ii) slow release of DMXT in the following days up to 2 weeks; (iii) faster release of the remaining DX payload during the following days.

The dissolution profile of pure DX in PBS pH 7.4 at 37 ºC showed a DX concentration loss as the dissolution time progressed (Fig. 3.9). This decrease was attributed to the degradation of DX in the release medium and followed a zero-order kinetics with a kinetic constant of k_d=2.2 10^{-4} mg/(mL·day). This degradation kinetic profile was similar to that reported in the literature for DX in PBS pH (7-7.4) containing sodium azide at 37 ºC *(Hickey et al. 2002)*. The slightly faster degradation kinetics compared to the literature (k_d=10^{-5} mg/(mL·day)) might be due to a different crystalline form or size of DX or the partial degradation of the bioactive compound by microbiological action *(Hickey et al. 2002, Zhu et al. 2015)*.

The observed release profiles were recalculated taking into account the degradation rate of DX to get the actual release profiles, which led to DX release percentages close to 90-100 wt.% after 3 weeks in PBS. After a certain lag time (t_d in Table 3.6) of less than 10 min needed for the wetting of the scaffold with PBS, a burst release was observed in the first 4 h. Thereafter, a sustained and constant DX release was observed for all of the scaffolds for at least three weeks according to the actual DX release profiles (*cf.* the actual DX release profile from non-stored DX-St scaffolds in Fig. 3.10) and regardless of the storage time period used (not shown). The burst release was related to the release of DX weakly bound to the scaffolds or in the surface of the pores, whereas the erosion of the polymeric matrix controlled the sustained release of DX embedded within the scaffolds.

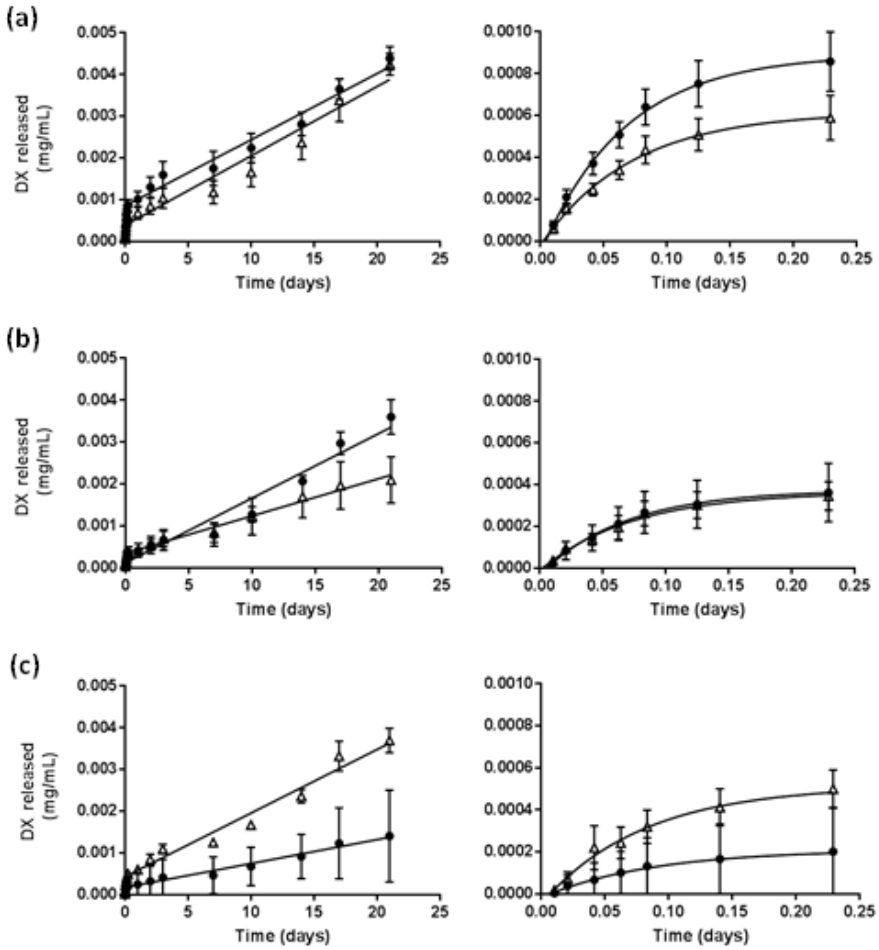

Fig. 3.8: Release profiles of DX in PBS pH 7.4 medium at 37 ºC from (a) non-stored scaffolds, and scaffolds stored for (b) 1 month and (c) 3 months during a release period of 21 days (left) and the first 6 hours (right). Black circles and white triangles represent St0-DX and St-DX scaffolds, respectively. Black lines represent the proposed DX release kinetics.

The actual DX release was hardly affected by the presence of starch. Both scaffold formulations before the storage tests showed similar weight loss rates during the first three weeks (Fig. 3.6). Accordingly the kinetic constants from both formulations were similar (Table 3.6).

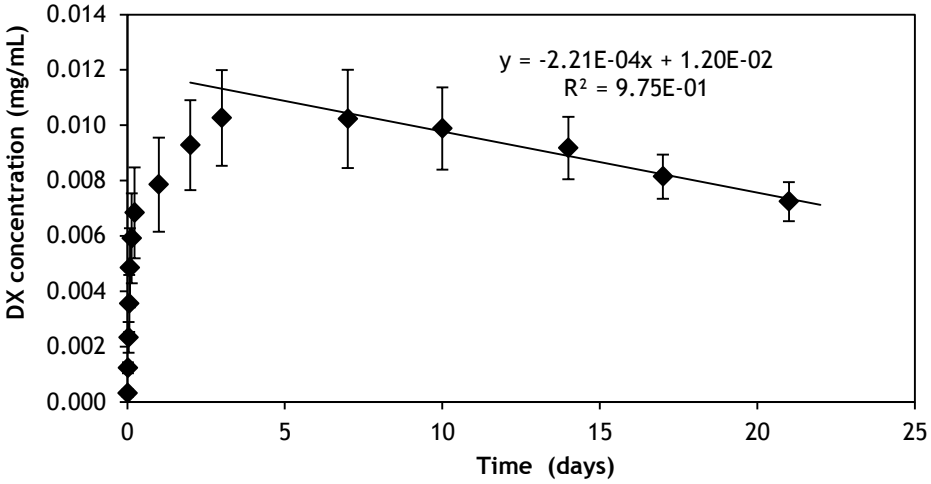

Fig. 3.9: DX degradation profile in the same medium as in the release tests, i.e. PBS pH 7.4 at 37 ºC and 60 rpm.

The burst release represented between 3 and 10 wt.% of the DX payload depending on the scaffold formulation and storage period and fitted the first-order release kinetics (Table 3.6 and Fig. 3.8). The DX release profile (k_1) was similar for this burst stage to the dissolution rate of pure DX in the crystalline form (k_1=13.9 day^{-1}). The DX release during the sustained release period fitted well the zero-order release kinetics for all the scaffold formulations (k_2 in Table 3.6 and Fig. 3.8) indicating that the release was mainly governed by a mechanism of matrix erosion. This linear release rate controlled by erosion is in accordance to the similar pattern previously observed in the erosion tests of the scaffolds, showing a linear weight loss of the matrix over 3 weeks (Fig. 3.6).

DX release rate during the burst release period (k_1) decreased upon storage at 25 ºC and 65 % relative humidity regardless of the scaffold formulation. The observed densification of the scaffolds upon mid-/long-term storage periods hindered the DX dissolution from the scaffolds and reduced its release rate. During the sustained release period, the scaffolds stored for a month under controlled conditions also had a lower release rate than the non-stored ones. For this storage

Table 3.6: Kinetic fitting parameters (the burst release step to the first-order equation (k_1) and the sustained release step to the zero-order equation (k_2)) of the DX release profiles in PBS medium (pH 7.4) at 37 ºC and 60 rpm from scaffolds previously stored at 25 ºC and 65 % relative humidity during different time periods (0, 1 and 3 months). The wellness of the zero-order equation fitting (R^2) or the first-order equation fitting (normalized values of the square of the residuals, r^2) are expressed in parenthesis.

Storage period		St0-DX	St-DX
Non-stored	t_d (day)	0.0044	0.0025
	k_1 (day^{-1})	15.1 ($9.3 \cdot 10^{-10}$)	13.9 ($9.6 \cdot 10^{-10}$)
	$k_2 \cdot 10^4$ (mg/mL·day)	3.8 -0.975	3.87 -0.951
1-month storage	t_d (day)	0.0058	0.0025
	k_1 (day^{-1})	14.8 ($3.3 \cdot 10^{-10}$)	13.6 ($8.2 \cdot 10^{-10}$)
	$k_2 \cdot 10^4$ (mg/mL·day)	3.75 -0.951	3.1 -0.984
3-month storage	t_d (day)	0.0072	0.0070
	k_1 (day^{-1})	11.6 ($2.2 \cdot 10^{-10}$)	12.5 ($2.1 \cdot 10^{-9}$)
	$k_2 \cdot 10^4$ (mg/mL·day)	2.78 -0.977	3.73 -0.97

period, scaffolds without starch (St0-DX scaffolds) showed slightly faster release rate likely due to the more open porosity and the shift of pore size distribution towards larger pores than St-DX scaffolds (Table 3.2). Reversely, after 3 months of storage, the release rate from St0-DX scaffolds was slower than St-DX ones (Table 3.6), despite the former having a more significant matrix degradation after the release period (Table 3.5). The increase under storage in the PCL-starch interaction (Table 3.3) and in the contribution of large macropores

(>100 μm) (Table 3.2) enhanced the water penetration to the polymeric matrix domains containing the DX, thus favoring a higher burst release and a faster DX release with respect to the scaffolds not containing St_p (St0-DX scaffolds).

3.4. CONCLUSIONS

Compressed CO_2 assisted-foaming is a suitable process to obtain DX-loaded synthetic scaffolds avoiding the use of high temperatures and organic solvents while providing high incorporation yields. The combination of polyesters and starch allows the tuning of the erosion profile of the scaffolds but at the expense of causing processability problems when using traditional compressed CO_2 foaming approaches. Periodic additions of liquid CO_2 upon the depressurization step is an innovative processing strategy that overcomes the processability limitations and preserves the physical integrity of the scaffolds. The obtained drug-loaded scaffolds present a dual porosity that might be susceptible to promote vascularization and bone tissue formation. Magnetic suspension balance experiments reveals as a useful tool for the optimization of the foaming process design in terms of solubility and processing time. Direct exposition of scaffolds to the ICH-climatic conditions of Europe, USA and Japan (zone II) for up to three months has a detrimental effect in the scaffolds performance with more dense structures, faster degradation rates and a certain decrease in the viscoelastic properties. The magnitude of these changes depends on the composition of the scaffolds, since DX and starch lead to less crystalline structures and more sensitive to environmental humidity. DX release rate from the scaffolds is mainly governed by the erosion of the matrix. The controlling effect of pregelified starch on DX release may be inhibited if scaffolds are previously stored under controlled humidity for long time periods. Overall, the significance of the storage conditions on the performance of drug-loaded scaffolds was highlighted using scaffolds obtained by an innovative, straightforward and solvent-free processing approach based on the use of CO_2 as foaming agent.

3.5 REFERENCES

E. Aionicesei, M. Škerget and Ž. Knez (2008). "Measurement of CO2 solubility and diffusivity in poly(l-lactide) and poly(d,l-lactide-co-glycolide) by magnetic suspension balance." *The Journal of Supercritical Fluids* **47**(2): 296-301.

E. Aionicesei, M. Škerget and Ž. Knez (2009). "Mathematical modelling of the solubility of supercritical CO_2 in poly(l-lactide) and poly(d,l-lactide-co-glycolide)." *The Journal of Supercritical Fluids* **50**(3): 320-326.

S. C. Alcázar-Alay and M. A. A. Meireles (2015). "Physicochemical properties, modifications and applications of starches from different botanical sources." *Food Science and Technology (Campinas)* **35**: 215-236.

S. Ali Akbari Ghavimi, M. H. Ebrahimzadeh, M. Solati-Hashjin and N. A. Abu Osman (2015). "Polycaprolactone/starch composite: Fabrication, structure, properties, and applications." *Journal of Biomedical Materials Research Part A* **103**(7): 2482-2498.

L. Averous, L. Moro, P. Dole and C. Fringant (2000). "Properties of thermoplastic blends: starch–polycaprolactone." *Polymer* **41**(11): 4157-4167.

C. Berkland, E. Pollauf, C. Raman, R. Silverman, K. Kim and D. W. Pack (2007). "Macromolecule release from monodisperse PLG microspheres: Control of release rates and investigation of release mechanism." *Journal of Pharmaceutical Sciences* **96**(5): 1176-1191.

P. Blasi, S. S. D'Souza, F. Selmin and P. P. DeLuca (2005). "Plasticizing effect of water on poly(lactide-co-glycolide)." *Journal of Controlled Release* **108**(1): 1-9.

C. Bouissou, J. J. Rouse, R. Price and C. F. van der Walle (2006). "The Influence of Surfactant on PLGA Microsphere Glass Transition and Water Sorption: Remodeling the Surface Morphology to Attenuate the Burst Release." *Pharmaceutical Research* **23**(6): 1295-1305.

P. M. Buechner and R. S. Lakes (2003). "Size effects in the elasticity and viscoelasticity of bone." *Biomechanics and Modeling in Mechanobiology* **1**(4): 295-301.

J. Cai, Z. Xiong, M. Zhou, J. Tan, F. Zeng, MeihuMa, S. Lin and H. Xiong (2014). "Thermal properties and crystallization behavior of thermoplastic starch/poly(ε-caprolactone) composites." *Carbohydrate Polymers* **102**: 746-754.

J. Crank (1975). The Mathematics of Difussion. O. U. Press. New York**:** 44-89.

T. R. Cuadros, A. A. Erices and J. M. Aguilera (2015). "Porous matrix of calcium alginate/gelatin with enhanced properties as scaffold for cell culture." *Journal of the mechanical behavior of biomedical materials* **46**: 331-342.

R. B. Chim, M. B. C. de Matos, M. E. M. Braga, A. M. A. Dias and H. C. de Sousa (2012). "Solubility of Dexamethasone in Supercritical Carbon Dioxide." *Journal of Chemical & Engineering Data* **57**(12): 3756-3760.

I. Chimenti, G. Rizzitelli, R. Gaetani, F. Angelini, V. Ionta, E. Forte, G. Frati, O. Schussler, A. Barbetta, E. Messina, M. Dentini and A. Giacomello (2011). "Human cardiosphere-seeded gelatin and collagen scaffolds as cardiogenic engineered bioconstructs." *Biomaterials* **32**(35): 9271-9281.

M. B. C. de Matos, A. P. Piedade, C. Alvarez-Lorenzo, A. Concheiro, M. E. M. Braga and H. C. de Sousa (2013). "Dexamethasone-loaded poly(ε-caprolactone)/silica nanoparticles composites prepared by supercritical CO_2 foaming/mixing and deposition." *International Journal of Pharmaceutics* **456**(2): 269-281.

M. B. C. de Matos, A. M. Puga, C. Alvarez-Lorenzo, A. Concheiro, M. E. M. Braga and H. C. de Sousa (2015). "Osteogenic poly(ϵ-caprolactone)/poloxamine homogeneous blends prepared by supercritical foaming." *International Journal of Pharmaceutics* **479**(1): 11-22.

L. Diaz-Gomez, A. Concheiro, C. Alvarez-Lorenzo and C. A. García-González (2016). "Growth factors delivery from hybrid PCL-starch

scaffolds processed using supercritical fluid technology." *Carbohydrate Polymers* **142**: 282-292.

L. Diaz-Gomez, C. A. García-González, J. Wang, F. Yang, S. Aznar-Cervantes, J. L. Cenis, R. Reyes, A. Delgado, C. Évora, A. Concheiro and C. Alvarez-Lorenzo (2017). "Biodegradable PCL/fibroin/hydroxyapatite porous scaffolds prepared by supercritical foaming for bone regeneration." *International Journal of Pharmaceutics* **527**(1): 115-125.

L. Diaz-Gomez, F. Yang, J. A. Jansen, A. Concheiro, C. Alvarez-Lorenzo and C. A. García-González (2016). "Low viscosity-PLGA scaffolds by compressed CO_2 foaming for growth factor delivery." *RSC Advances* **6**(74): 70510-70519.

A. R. C. Duarte, J. F. Mano and R. L. Reis (2009). "Dexamethasone-loaded scaffolds prepared by supercritical-assisted phase inversion." *Acta Biomaterialia* **5**(6): 2054-2062.

A. R. C. Duarte, J. F. Mano and R. L. Reis (2009). "Preparation of starch-based scaffolds for tissue engineering by supercritical immersion precipitation." *The Journal of Supercritical Fluids* **49**(2): 279-285.

R. Dudley, B. McDowell, C. Mahl and A. B. Sarkar (2012). "Influence of temperature on the thirty-day chemical stability of extemporaneously prepared dexamethasone paste." *International Journal of Pharmaceutical Compounding* **16**(3): 258-261.

T. A. Einhorn and L. C. Gerstenfeld (2015). "Fracture healing: mechanisms and interventions." *Nature Reviews Rheumatology* **11**(1): 45-54.

V. Ellä, T. Annala, S. Länsman, M. Nurminen and M. Kellomäki (2011). "Knitted polylactide 96/4 L/D structures and scaffolds for tissue engineering: Shelf life, in vitro and in vivo studies." *Biomatter* **1**(1): 102-113.

M. A. Fanovich and P. Jaeger (2012). "Sorption and diffusion of compressed carbon dioxide in polycaprolactone for the development of porous scaffolds." *Materials Science and Engineering: C* **32**(4): 961-968.

C. A. García-González, A. Concheiro and C. Alvarez-Lorenzo (2015). "Processing of Materials for Regenerative Medicine Using Supercritical Fluid Technology." *Bioconjugate Chemistry* **26**(7): 1159-1171.

C. A. García-González, A. Vega-González, A. M. López-Periago, P. Subra-Paternault and C. Domingo (2009). "Composite fibrous biomaterials for tissue engineering obtained using a supercritical CO_2 antisolvent process." *Acta Biomaterialia* **5**(4): 1094-1103.

C. A. García González, L. Diaz-Gomez, C. Alvarez Lorenzo and A. Concheiro Nine (2015). System for administering biologically active substances produced by foaming techniques using compressed gases or supercritical fluids. Spanish. **WO 2017013288 A1**.

H. Giesche (2006). "Mercury Porosimetry: A General (Practical) Overview." *Particle & Particle Systems Characterization* **23**(1): 9-19.

L. Goimil, M. E. M. Braga, A. M. A. Dias, J. L. Gómez-Amoza, A. Concheiro, C. Alvarez-Lorenzo, H. C. de Sousa and C. A. García-González (2017). "Supercritical processing of starch aerogels and aerogel-loaded poly(ε-caprolactone) scaffolds for sustained release of ketoprofen for bone regeneration." *Journal of CO_2 Utilization* **18**: 237-249.

E. Gómez-Barrena, P. Rosset, D. Lozano, J. Stanovici, C. Ermthaller and F. Gerbhard (2015). "Bone fracture healing: Cell therapy in delayed unions and nonunions." *Bone* **70**: 93-101.

J. A. Han and S. T. Lim (2004). "Structural changes in corn starches during alkaline dissolution by vortexing." *Carbohydrate Polymers* **55**(2): 193-199.

T. Hickey, D. Kreutzer, D. J. Burgess and F. Moussy (2002). "Dexamethasone/PLGA microspheres for continuous delivery of an anti-inflammatory drug for implantable medical devices." *Biomaterials* **23**(7): 1649-1656.

S. T. Ho and D. W. Hutmacher (2006). "A comparison of micro CT with other techniques used in the characterization of scaffolds." *Biomaterials* **27**(8): 1362-1376.

R. Jahagirdar and B. E. Scammell (2009). "Principles of fracture healing and disorders of bone union." *Surgery (Oxford)* **27**(2): 63-69.

M. Jewell, W. Daunch, B. Bengtson and E. Mortarino (2015). "The development of SERI® Surgical Scaffold, an engineered biological scaffold." *Annals of the New York Academy of Sciences* **1358**(1): 44-55.

T. E. A. H. Küpper, S. Bettina, R. Burkhard, A.-V. Hemmerling, S. Volker and S. Juergen (2006). "Drugs and Drug Administration in Extreme Environments." *Journal of Travel Medicine* **13**(1): 35-47.

F. Linde, C. B. Gothgen, I. Hvid and B. Pongsoipetch (1988). "Mechanical properties of trabecular bone by a non-destructive compression testing approach." *Engineering in Medicine* **17**(1): 23-29.

L. Lu, S. J. Peter, M. D. Lyman, H.-L. Lai, S. M. Leite, J. A. Tamada, S. Uyama, J. P. Vacanti, L. Robert and A. G. Mikos (2000). "In vitro and in vivo degradation of porous poly(dl-lactic-co-glycolic acid) foams." *Biomaterials* **21**(18): 1837-1845.

A. S. Mao and D. J. Mooney (2015). "Regenerative medicine: Current therapies and future directions." *Proceedings of the National Academy of Sciences of the United States of America* **112**(47): 14452-14459.

E. Markočič, M. Škerget and Ž. Knez (2011). "Solubility and diffusivity of CO_2 in poly(l-lactide)–hydroxyapatite and poly(d,l-lactide-co-glycolide)–hydroxyapatite composite biomaterials." *The Journal of Supercritical Fluids* **55**(3): 1046-1051.

N. G. Mehr, X. Li, G. Chen, B. D. Favis and C. D. Hoemann (2015). "Pore size and LbL chitosan coating influence mesenchymal stem cell in vitro fibrosis and biomineralization in 3D porous poly(epsilon-caprolactone) scaffolds." *Journal of Biomedical Materials Research Part A* **103**(7): 2449-2459.

J. Melke, S. Midha, S. Ghosh, K. Ito and S. Hofmann (2016). "Silk fibroin as biomaterial for bone tissue engineering." *Acta Biomaterialia* **31**: 1-16.

M. D. Moya-Ortega, C. Alvarez-Lorenzo, H. H. Sigurdsson, A. Concheiro and T. Loftsson (2010). "γ-Cyclodextrin hydrogels and

semi-interpenetrating networks for sustained delivery of dexamethasone." *Carbohydrate Polymers* **80**(3): 900-907.

R. A. Quirk, R. M. France, K. M. Shakesheff and S. M. Howdle (2004). "Supercritical fluid technologies and tissue engineering scaffolds." *Current Opinion in Solid State and Materials Science* **8**(3): 313-321.

A. Salerno, S. Dieguez, L. Diaz-Gomez, J. L. Gómez-Amoza, B. Magarinos, A. Concheiro, C. Domingo, C. Alvarez-Lorenzo and C. A. García-González (2017). "Synthetic scaffolds with full pore interconnectivity for bone regeneration prepared by supercritical foaming using advanced biofunctional plasticizers." *Biofabrication* **9**(3): 035002.

A. Salerno, S. Zeppetelli, E. Di Maio, S. Iannace and P. A. Netti (2012). "Architecture and properties of bi-modal porous scaffolds for bone regeneration prepared via supercritical CO 2 foaming and porogen leaching combined process." *Journal of Supercritical Fluids* **67**: 114-122.

M. H. Sheridan, L. D. Shea, M. C. Peters and D. J. Mooney (2000). "Bioabsorbable polymer scaffolds for tissue engineering capable of sustained growth factor delivery." *Journal of Controlled Release* **64**(1–3): 91-102.

N. Shibuya and D. C. Jupiter (2015). "Bone Graft Substitute: Allograft and Xenograft." *Clinics in Podiatric Medicine and Surgery* **32**(1): 21-34.

M. M. C. G. Silva, L. A. Cyster, J. J. A. Barry, X. B. Yang, R. O. C. Oreffo, D. M. Grant, C. A. Scotchford, S. M. Howdle, K. M. Shakesheff and F. R. A. J. Rose (2006). "The effect of anisotropic architecture on cell and tissue infiltration into tissue engineering scaffolds." *Biomaterials* **27**(35): 5909-5917.

S. Spilimbergo and A. Bertucco (2003). "Non-thermal bacterial inactivation with dense CO_2." *Biotechnology and Bioengineering* **84**(6): 627-638.

W. Q. Sun and S.-S. Gouk (2008). "Aging of a Regenerative Biologic Scaffold (AlloDerm Native Tissue Matrix) During Storage at Elevated

Humidity and Temperature." *Tissue Engineering Part C: Methods* **15**(1): 23-31.

J. L. Walker and M. Santoro (2017). 9 - Processing and production of bioresorbable polymer scaffolds for tissue engineering. *Bioresorbable Polymers for Biomedical Applications*, Woodhead Publishing**:** 181-203.

R. E. Wilson (1921). "Humidity Control by Means of Sulfuric Acid Solutions, with Critical Compilation of Vapor Pressure Data." *Journal of Industrial & Engineering Chemistry* **13**(4): 326-331.

M. A. Woodruff, C. Lange, J. Reichert, A. Berner, F. Chen, P. Fratzl, J.-T. Schantz and D. W. Hutmacher (2012). "Bone tissue engineering: from bench to bedside." *Materials Today* **15**(10): 430-435.

J. Yamashita, B. R. Furman, H. R. Rawls, X. Wang and C. M. Agrawal (2001). "The use of dynamic mechanical analysis to assess the viscoelastic properties of human cortical bone." *Journal of Biomedical Materials Research* **58**(1): 47-53.

J. J. Yoon, J. H. Kim and T. G. Park (2003). "Dexamethasone-releasing biodegradable polymer scaffolds fabricated by a gas-foaming/salt-leaching method." *Biomaterials* **24**(13): 2323-2329.

J. Zhang, A. Zhou, A. Deng, Y. Yang, L. Gao, Z. Zhong and S. Yang (2015). "Pore architecture and cell viability on freeze dried 3D recombinant human collagen-peptide (RHC)-chitosan scaffolds." *Materials Science and Engineering C: Materials for Biological Applications* **49**: 174-182.

L. Zhu, Z. Yang, Q. Yang, Z. Tu, L. Ma, Z. Shi and X. Li (2015). "Degradation of dexamethasone by acclimated strain of Pseudomonas Alcaligenes." *International Journal of Clinical and Experimental Medicine* **8**(7): 10971-10978.

USC
UNIVERSIDADE
DE SANTIAGO
DE COMPOSTELA

4. SUPERCRITICAL PROCESSING OF STARCH AEROGELS AND AEROGEL-LOADED PCL SCAFFOLDS FOR SUSTAINED RELEASE OF KETOPROFEN FOR BONE REGENERATION[§]

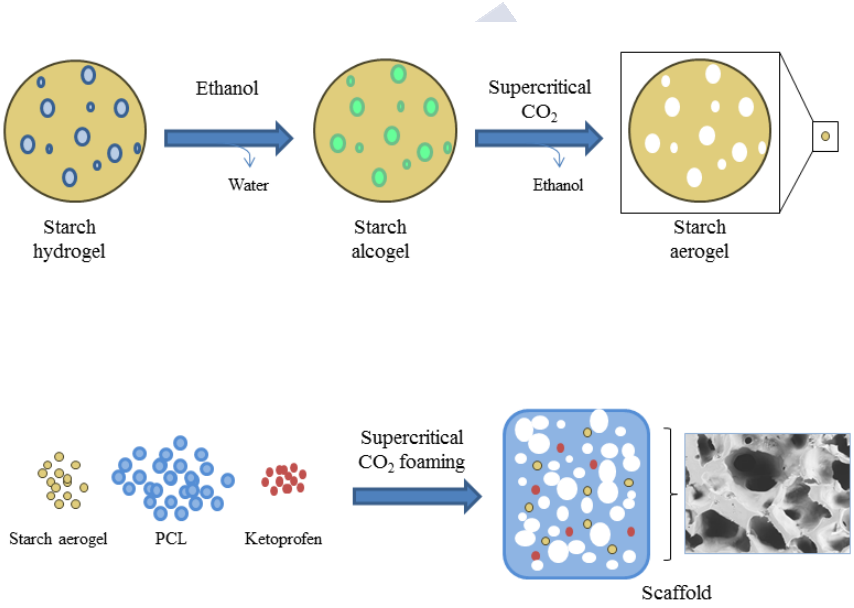

[§]The work described in this chapter has been published in *Goimil et al. J. CO2 Utiliz. 18 (2017) 237-249* and carried out in collaboration with the CIEPQPF, Chemical Engineering Department, FCTUC, University of Coimbra and within the frame of a 4-month PhD research stay.

4.1. INTRODUCTION

Synthetic scaffolds are a promising alternative to biological grafts to promote bone repair in those situations where the natural self-regeneration is compromised. These synthetic constructs should give response to the typical problems associated with safety issues and to the scarcity of biological grafts with respect to the current increasing demand. Moreover, advanced synthetic scaffolds should have a superior performance to provide an accurate porous 3D-structure that guides and promotes tissue growth, enables the diffusion of nutrients and oxygen supplies and cell waste disposal, and acts as a provisional mechanical support *(García-González et al. 2015)*. Finally, bone repair materials should also have a performance aligned with the current social changes associated with the increase in life expectancy of population and with the world commitment of keeping older people autonomy and enhancing their quality of life in the so-called "active ageing" *(Wold Health Organization (WHO) 2002)*.

Bioactive compounds can be incorporated in scaffolds for their local administration to promote bone healing efficiency by tackling several types of post-surgery complications due to infections and other biological processes that can impair the proper tissue regeneration *(Romagnoli et al. 2013)*. Namely, it is necessary to reduce the time taken to solve severe foreign-body inflammatory responses *(Vacanti et al. 2012)*. Otherwise, poor osteointegration of the scaffold due to fibrous encapsulation and granuloma formation can occur *(Sridharan et al. 2015, Przekora and Ginalska 2016)*. Ketoprofen is a nonsteroideal anti-inflammatory drug (NSAID) that is orally administered during the post-operative period to relief pain and to reduce inflammation. The mode of action of ketoprofen is the non-selective inhibition of cyclooxygenases (COX-1 and COX-2), enzymes involved in the production of prostaglandins *(Wibberley et al. 2006, Pountos et al. 2012)*. Ketoprofen does not inhibit bone healing process according to *in vivo* animal studies with goats and rabbits where no effects on MSCs proliferation and osteogenesis were observed after subcutaneous administration of daily doses of ketoprofen (*ca.* 2 mg/kg) at least for several weeks *(van der Heide et al. 2008, Nyangoga et al. 2010)*.

Several processing strategies are reported in the literature to incorporate bioactive compounds in bone scaffolds and to tune their release kinetics patterns to provide a local administration *(Tezcaner and Keskin 2011)*. However, common scaffold processing techniques like solvent casting/particle leaching, phase separation or rapid prototyping have limited versatility to prepare drug-loaded scaffolds. These techniques usually need the use of either organic solvents, or high operating temperatures, or multi-step processing with leaching or purification steps, which may originate problems of cytotoxicity, premature drug degradation, low drug loading yields, reproducibility concerns or long processing times among others. Supercritical foaming of polymeric scaffolds emerges as the only one-step straightforward alternative able to overcome most of the above-mentioned drawbacks. This technique exploits the plasticizing and melting effects of supercritical carbon dioxide ($scCO_2$) on some biodegradable thermoplastic polymers such as poly-α-hydroxyesters (e.g. PLA, PLGA, PCL) to produce highly porous synthetic bone scaffolds in a simple, economical and reproducible procedure *(Diaz-Gomez et al. 2016)*. Nevertheless, the supercritical CO_2 foaming process has some limited control on the production of materials presenting well-defined pore size distributions and pore interconnectivities and, consequently, on the release of drug-loaded scaffolds.

Mesoporous silica particles incorporated in foamed polyester-based scaffolds have been shown to favour heterogeneous pore nucleation, to improve the mechanical properties and to refine the pore size distribution *(de Matos et al. 2013)*. Also, inorganic aerogel particles tested for similar purposes were able to preserve the porous structure of the wet gel in the dry form *(García-González et al. 2012)*. Silica aerogel particles were observed to promote the survival and growth of fibroblastic and osteoblastic cells if incorporated in PCL-scaffolds obtained by solvent casting *(Ge et al. 2013)*. Nevertheless, the incorporation of silica in scaffold formulations is still a concern since rigorous downstream processes are required to remove remnants of toxic silica precursors and the full biodegradability, bioerosion and excretion profiles of silica aerogels are still not fully confirmed. The

use of polysaccharide aerogels as a safer, biodegradable and even cheaper alternative mesoporous material to be incorporated in synthetic grafts seems promising *(García-González et al. 2011)* and it is prospected in this work.

Purely organic aerogel scaffolds can present high mesoporosity and good cytocompatibility, *(Pircher et al. 2014, Salerno and Domingo 2014, Martins et al. 2015)* but weak mechanical properties for hard-tissue repair and limited control of macroporosity. Mechanical reinforcement of aerogels implies post-processing steps *(Pircher et al. 2014)*. Techniques explored to confer macroporosity to aerogel scaffolds give restricted results concerning the overall macroporosity values and the control of the macropores sizes *(Salerno and Domingo 2014, Martins et al. 2015, Stergar and Maver 2016)*. Differently, the combination of micron-sized polymeric aerogel particles with biodegradable polyesters using the supercritical CO_2 foaming technique to prepare scaffolds would assemble and combine the high porosity and mesopore volume of aerogels, the good mechanical properties of polyesters and the capacity of tuning macropores sizes and densities of the $scCO_2$ foaming method.

Starch aerogel powders emerge as an interesting admixture of polymeric-based scaffolds due to the intrinsic biocompatibility and biodegradability of starch and to the excellent textural properties of aerogels *(Maleki et al. 2016)*. Moreover, starch is an abundant and relatively cheap polysaccharide of particular interest for regenerative medicine purposes *(Elvira et al. 2002, Silva et al. 2007)*. Starch is able to interact with polyesters changing its crystallinity depending on the starch gelification method used *(Diaz-Gomez et al. 2016)*. Starch aerogels have been prepared from different sources (corn, pea, tapioca, potato), formats (monoliths, beads, particles) and using different gelation mechanisms (thermal, inclusion complexing, microwaves) *(Mehling et al. 2009, García-González et al. 2011, García-González et al. 2012, García-González and Smirnova 2013, Kenar et al. 2014, Milovanovic et al. 2015, Muñoz García et al. 2015)*. Namely, aerogel particles reported in the literature have particle sizes in the order of hundreds of microns or larger for starch and of tens of microns or higher for other polysaccharides *(Alnaief et*

al. 2011, García-González et al. 2015). Nevertheless, starch aerogels in the size range of few microns would be ambitioned for several pharmaceutical and biomedical applications and, namely, for their incorporation in composite scaffolds presenting uniform physicochemical and mechanical properties.

The aim of this work was to prepare starch aerogel microspheres and to evaluate their potential roles once incorporated in ketoprofen-loaded PCL-based scaffolds on the control of the pore structure of the material and of the ketoprofen release over time. One-micron sized starch aerogel microspheres were developed by emulsion-gelation under ultrasound sonication followed by supercritical drying, for the first time. Ketoprofen was loaded in the starch aerogel particles by a supercritical CO_2 impregnation method or directly incorporated in the scaffold by a supercritical CO_2 foaming process for the sake of comparison. The resulting scaffolds were evaluated regarding their morphological, mechanical and physicochemical properties, as well as to their ketoprofen-release profiles.

4.2. MATERIALS AND METHODS

4.2.1. Materials

PCL (PCL_{raw}, 50 kDa, T_m=61.4 ºC, 66.7 % crystallinity) was purchased from Polysciences (Warrington, PA, USA) in the powdered form. Corn starch in the native form (St_{raw}, amylo N-460; 52.6 % amylose content, 12.9 % loss on drying, conform to USP and EP Pharmacopeias) was obtained from Roquette (Lestrem, France), and carbon dioxide (99.9 % purity) was supplied by Praxair, Inc. (Madrid, Spain). Ketoprofen (K, T_m= 95.8 ºC, 99.7 % purity) was provided by Acofarma (Terrassa, Spain). Polyglycerol polyricinoleate (PGPR) was obtained from Palsgaard (Juelsminde, Denmark). Paraffin oil was provided by Panreac (Castellar del Vallès, Spain). Ethanol (99.8 % purity) was obtained from Omnilab (Bremen, Germany) and diethyl ether (98 % purity) from Labkem (Mataró, Spain).

4.2.2. Starch aerogel preparation

Starch gels in the form of microspheres were obtained by the emulsion-gelation method *(García-González et al. 2012).* Briefly, a

water-in-oil emulsion (w/o) was prepared from a mixture of paraffin oil and a starch aqueous solution 15 % (w/w) in a 3:1 oil-to-water weight ratio. 3 % (w/w) of PGPR with respect to the aqueous phase was added to the oil phase as an emulsifier. The mixture obtained (240 g) was autoclaved (Raypa Steam Sterilizer, Terrassa, Spain) at 121°C and 1.1 bar for 20 min. After sterilization and partial cooling (95 °C), the mixture was homogenized using an ultrasound probe (450D, Branson Digital Sonifier, Nuevo Laredo, Mexico), using an amplitude of 50 % for 2 min, then cooled down for the thermal gelation of starch, and kept for 48 h at 4 °C for starch retrogradation. A dispersion of starch hydrogel particles in paraffin was thus obtained. The dispersion was centrifuged (5804 R, Eppendorf, Hamburg, Germany) at 5000 rpm for 15 min to separate the hydrogel particles from the oil phase. Starch hydrogel microspheres were then directly transferred to absolute ethanol for solvent exchange, which was replaced daily for two days until complete removal of water to get an alcogel (St_{gel}). This straight solvent exchange into ethanol (with two solvent exchanges) corresponds to an optimized procedure minimizing processing steps whilst preserving the textural properties of the resulting aerogel. In certain cases ($St_{gel\text{-}DEE}$), an additional solvent exchange with diethyl ether was carried out before the double solvent exchange to ethanol.

Starch aerogel microspheres (StA and $StA_{\text{-}DEE}$) were obtained by supercritical drying of the starch alcogels (St_{gel} and $St_{gel\text{-}DEE}$, respectively). Briefly, starch alcogels soaked in ethanol were dried under a CO_2 flow of 6 g/min during 3.5 h in a 100-mL autoclave (Thar Technologies, Pittsburgh, PA, USA). This drying processing time corresponds to the optimum duration to reach complete solvent removal with a minimum impact on the textural properties of the starch aerogel backbone *(García-González et al. 2012)*. The operating temperature and pressure conditions were 40 °C and 120 bar, respectively. A depressurization time of 70 min at a constant flow rate of 1 g CO_2/min was used to reach atmospheric pressure. Starch aerogel powders were collected from the autoclave for further use and analysis.

4.2.3. Supercritical impregnation/deposition of ketoprofen in starch aerogels

Selected starch aerogel samples were impregnated with ketoprofen using a $scCO_2$-assisted impregnation/deposition method following a similar procedure previously reported in the literature *(García-González et al. 2015)*. Briefly, starch aerogel powders (0.5 g) and ketoprofen (0.5 g) were filled in two separate paper filter cartridges and loaded in a 100-mL stainless steel autoclave (Thar Technologies, Pittsburgh, PA, USA). There was no physical contact between aerogels and ketoprofen prior to the supercritical process. Impregnation/deposition conditions were set to 40 ºC and 150 bar under a $scCO_2$ atmosphere for 11 h and in the batch mode. Then, the system was depressurized during 90 min at a constant flow rate of 0.9 g/min and the ketoprofen-loaded aerogels (StA_K) were collected and stored. Ketoprofen content in the aerogel was quantified by extraction with ethanol and subsequent measurements by UV-Vis spectrophotometry (λ = 255 nm) in accordance to the literature *(García-González et al. 2015)*.

4.2.4. Porous PCL-starch aerogels composites scaffolds preparation

Weighed amounts (1.3 g as total weight) of powdered mixture formulations of different compositions (Table 4.1) were physically mixed and placed in Teflon cylindrical moulds (internal diameter: 17 mm; length: 24.6 mm) (Brand GmbH, Wertheim, Germany). The moulds were then inserted in a high-pressure stainless steel autoclave (Thar Technologies, Pittsburgh, PA, USA) and exposed to $scCO_2$ at 37 ºC and 140 bar, for 60 min in a static mode. Then, the autoclave was depressurized to ambient pressure at a venting rate of 1.8 g/min. Obtained scaffolds were recovered and stored overnight (under room conditions to allow complete CO_2 desorption) and then weighed. A scalpel was used to remove the solid skins on the scaffold outer surfaces and to shape the scaffolds before further characterization.

Table 4.1: Scaffolds compositions (expressed in weight percentage) in terms of poly(ε-caprolactone) (PCL), ketoprofen (K), starch (St) in the native form (St_{raw}), unloaded aerogel (StA) and ketoprofen-loaded (StA_K) aerogels.

Scaffold	PCL, wt. %	St, wt. %	K, wt. %
PCL	100	-	-
PCL-St_{raw}	90	10 (St_{raw})	-
PCL-StA	90	10 (StA)	-
PCL-K	95	-	5
PCL-St_{raw}-K	85	10 (St_{raw})	5
PCL-StA-K	85	10 (StA)	5
PCL-StA_K-K	85	10 (StA_K)	5

4.2.5. Structural, physicochemical and mechanical characterization of starch aerogels and scaffolds

Micrographs of prepared starch aerogels and scaffolds were recorded by scanning electron microscopy (SEM, EVO LS15, Zeiss, Oberkochen, Germany; and FESEM ULTRA PLUS, Zeiss, Oberkochen, Germany). Aerogel samples were iridium-sputtered prior to imaging in order to minimize charging and to improve the image quality (contrast). Scaffolds were previously cut with a surgical blade in the form of slices and then analyzed without any further pretreatment. Cross section of the aerogel microspheres were carried out using the site specific Focused Ion Beam technique (Dual Beam Helios Nanolab 600, FEI, Hillsboro, OR, USA) combined with image capture by SEM microscopy. An automated FIB-SEM slice-and-view method was performed to mill with Ga^+ ions at a current of 26 pA at 30 kV and to collect images at predetermined time intervals and selected images were captured. Scaffolds were also characterized by digital imaging using a CCD Microscope Camera (DFC7000 T, Leica, Wetzlar, Germany) operating at room temperature.

Particle size distribution of starch alcogel microparticles suspended in ethanol was studied by dynamic light scattering analysis with a Zetasizer Nano ZS (Malvern Instruments; Malvern, UK), equipped with a He/Ne 633 nm laser and after a 5 min-sonication of the dispersion.

Textural properties of the starch aerogels were determined by low-temperature N_2 adsorption–desorption analysis (ASAP 2000 Micromeritics Inc.; Norcross, GA, USA). Before measurements, samples were dried under vacuum (<1 mPa) at 80 ºC, and for 24 h. Specific surface areas (A_{BET}) of starch aerogels were determined applying the BET (Brunauer–Emmett–Teller) method. Specific pore volumes ($V_{p,BJH}$) and mean pore diameter ($d_{p,BJH}$) were estimated using the BJH (Barrett–Joyner–Halenda) method. Textural properties of the scaffolds were also determined by low-temperature N_2 adsorption–desorption analysis (samples were previously dried under vacuum (<1 mPa) at room temperature for 24 h before measurements). Scaffolds were also analyzed by mercury-intrusion porosimetry (MIP, Micromeritics Autopore IV 9500; Norcross, GA, USA). Pore size distributions, total pore volumes ($V_{p,BJH}$, $V_{p,MIP}$), specific surface areas (A_{BET}, A_{MIP}), mean pore diameters ($d_{p,BJH}$, $d_{p,MIP}$) and open porosities (ε_{MIP}) were determined accordingly.

A 3D network model of the macroporous structure of the scaffold was obtained from the MIP cumulative curves using PoreXpert v.1.6.567 software (PoreXpert Ltd, Plymouth, UK). This software generates a three-dimensional void structure presenting percolation characteristics as close as possible to those of the material experimentally characterized by MIP. Modeling assumes that the material consists of interconnected unit cells of 1000 pores (of arbitrary cubic shape) arranged in a regular three-dimensional 10×10×10 array, and connected by up to 3000 throats (of arbitrary cylindrical shape) *(Johnson et al. 2003, Nogueiras-Nieto et al. 2011)*. A Boltzmann-annealed simplex algorithm was used to estimate and to simultaneously optimize the connectivity (mean number of throats per pore), pore skew, throat skew and correlation level from the mercury intrusion porosimetry cumulative curves. Water permeability (25 ºC, 1.03 bar) was modeled assuming that Poiseuille flow (water) occurred in the z-direction according to Eq. (4.1) *(Johnson et al. 2003)*:

$$k = \frac{\Pi}{8}\omega_{cell}(Farcs)\frac{l_{cell}}{A_{cell}} \qquad (4.1)$$

where l_{cell} and A_{cell} represent the length and the cross-sectional area of the unit cell, respectively and ω_{cell}(Farcs) is an averaging operator over the whole unit cell operating on the flow capacities of the pore throat-pore arcs parallels to the z-axis. PoreXpert calculates the term ω_{cell}(Farcs) by means of the Dinic network analysis algorithm *(Ahuja et al. 1997)*. Water uptake in 50 ms within the scaffold were determined using the Bosanquet equation *(Gomez-Carracedo et al. 2010)*. Mesenchymal stem cells (MSCs) infiltration in the scaffolds was simulated using the filtration module from the software and assuming a cell size of 26.5±5.0 µm, an average value for human MSCs *(Ge et al. 2014)*. PoreXpert simulates straining of particles as they flow through the unit cell from the top to the bottom. The filtration algorithm is based on the permeability algorithm determining the preferential flow routes. When a particle blocks a throat the preferential flow routes are recalculated. The filtration algorithm will continue until all particles have been filtered or flowed through the structure or the permeability of the unit cell has reached zero because the unit cell filter has become clogged.

The skeletal density (ρ_{skel}) of the prepared scaffolds, starch aerogels and raw materials were measured using a helium-pycnometer (Quantachrome; Boynton Beach, FL, USA), operating at 25 ºC and 1.03 bar. Values were determined from five replicates (standard deviation <1%).

Flowability properties of starch aerogel particles were studied using the angle of repose and compressibility techniques. For the angle of repose measurements, the fixed funnel method was used by pouring the powder through the funnel until the resulting cone reached the base of the funnel (height: 1.50 cm). The compressibility of the powders of a known weight and previously sieved with a 0.5-mm sieve was measured using a 100 mL-cylindrical vessel (internal diameter: 3.64 cm). Powders were vibrated in a home-made apparatus at 30 strokes per minute during 15 min. The initial (V_0) and final (V_f) volumes of the samples were recorded before and after vibration, respectively. The compressibility (in percentage) was calculated using Eq. (4.2). The bulk (ρ_{bulk}) density was calculated from the initial and final weight/volume ratios, respectively.

$$Compressibility\ (\%) = \left(\frac{V_0 - V_f}{V_0}\right) \cdot 100 \quad (4.2)$$

The bulk density (ρ_{bulk}) of the prepared scaffolds was determined by measuring the dimensions and the weight of the samples after supercritical processing. The resulting overall porosity (ε) was estimated for both aerogel powder and scaffolds following Eq. (4.3).

$$\varepsilon = \left(1 - \frac{\rho_{bulk}}{\rho_{skel}}\right) \cdot 100 \quad (4.3)$$

The instantaneous water uptake of scaffold pieces of known weight (30-40 mg) was experimentally measured just after wetting them in distilled water (immersion period <1 s) and whipping with filter paper. The water uptake was expressed in volume percentage of pores filled with water using Eq. (4.4)

$$Water\ uptake = \left(\frac{w_{wet}}{w_{dry}} - 1\right)\left(\frac{\rho_{bulk} \cdot 100}{\rho_{H2O} \cdot \varepsilon}\right) \cdot 100 \quad (4.4)$$

where w_{dry} and w_{wet} denote the weight of the scaffolds as prepared and after water immersion, respectively, and ρ_{H2O} is the density of water.

The storage (G') and loss (G'') moduli were measured, in duplicate, in scaffold pieces (18 x16 x 4 mm) at 37ºC using a Rheolyst AR 1000 N rheometer (TA Instruments, New Castle, DE, USA) fitted with an environmental test chamber, a solid torsion kit, and a data analyser (AR2500). The samples were fixed between two clamps with a gap of 8 mm and an angular frequency sweep between 5 and 50 rad s^{-1} at 0.5 % strain was applied.

Differential scanning calorimetry analyses (DSC-Q100, TA Instruments; New Castle, DE, USA) were conducted for the prepared scaffolds under a nitrogen atmosphere (50 mL/min) in the r.t.-200 ºC range under a heating rate of 10 ºC/min. Crystallinity degree of PCL contained in the scaffolds (in percentage) was calculated as follows:

$$Crystallinity = \frac{\Delta H_m}{x \cdot \Delta H^0_{m,PCL}} \cdot 100 \quad (4.5)$$

where x denotes the fraction (in weight) of PCL in the sample; ΔH_m, the melting enthalpy of the sample in J/g; and $\Delta H^0_{m,PCL}$, the melting enthalpy of 100 % crystalline PCL (142 J/g) *(Tsuji and Ikada 1998)*.

4.2.6. Ketoprofen release studies

Scaffold samples of 10 mg were suspended in 50 mL of PBS pH 7.4. The dissolution profile of 1 mg of ketoprofen dissolved in 100 mL of PBS was determined as reference for the release profiles. Experiments were performed under sink conditions (solubility of ketoprofen in PBS pH 7.4 = 2.2 mg/mL) *(Mukae et al. 1990)*. Flasks were put in an oscillating bath (Unitronic 320 OR, JP Selecta, Barcelona, Spain) at 37 ºC and 60 rpm for 3 weeks. Aliquots of 1 mL were sampled through that period at selected times, and withdrawn volumes were replaced with fresh medium. Ketoprofen concentration was measured by UV-Vis spectrophotometry (8453, Agilent, Santa Clara, CA, USA) at λ = 260 nm. Samples were filtered prior to analysis using 0.2 μm nylon filters to avoid potential interference due to the presence of particles from the scaffolds. Calibration curve was obtained from triplicate dilution series of ketoprofen in PBS, ranging from 0.001 to 0.025 mg/mL, attaining a R^2=0.9994.

Modeling of the ketoprofen release was carried out by fitting the obtained release data to the Korsmeyer-Peppas equation (Eq. (4.6)) *(Siepmann and Peppas 2011)* and using GraphPad Prism version 6.04 for Windows (GraphPad Software, La Jolla, CA, USA) software:

$$F = k \cdot t^n \qquad (4.6)$$

where F is the fraction of drug released at a time t, k is a constant related to the macromolecular polymeric network structure, and n is the diffusional exponent *(Peppas 1985, Siepmann and Peppas 2011)*.

4.2.7. Statistical analysis

All results were expressed as mean ± standard deviation. 1-way ANOVA and Tukey's multiple comparisons tests were used to evaluate the effect of starch aerogel content on the scaffolds on the bulk density and the overall porosity of the scaffolds (Statgraphics Centurion XVI, StatPoint Technologies Inc., Warrenton, VA, USA).

4.3. RESULTS AND DISCUSSION

4.3.1. Starch aerogel microspheres processing

Starch aerogel microspheres with a unimodal particle size distribution of mean size of *ca.* 1.2 μm were obtained by applying the

emulsion-gelation method followed by supercritical CO_2 drying (Fig. 4.1). After supercritical drying, the particle size of these aerogel particles was considered as suitable for their incorporation in the PCL-based scaffolds without interfering in the isocratic properties of the resulting material. Remnants of the native starch granules were not observed by SEM, confirming the effectiveness of the gelation process.

Previous attempts to get polysaccharide aerogel spheres using different processing techniques (prilling, microfluidics) resulted in particle diameters from hundreds of microns to some milimeters *(De Cicco et al. 2016, Zhou et al. 2016)*. Particularly, previous results on polysaccharide aerogel spheres obtained by emulsion-gelation methods resulted in particle sizes in the range of tens to hundreds of microns *(Alnaief et al. 2011, García-González et al. 2012, García-González et al. 2015)*. In this work, the aerogel particle size threshold of ten microns has been trespassed by combining the proper choice of the emulsifier source (polyglycerol polyricinoleate) and content (3% (w/w)) and a vigorous agitation method (ultrasound probe). In addition, a relatively low polydispersity index (PdI) was also achieved.

SEM pictures with higher magnifications confirmed the good sphericity of the particles as well as the presence of porosity in the

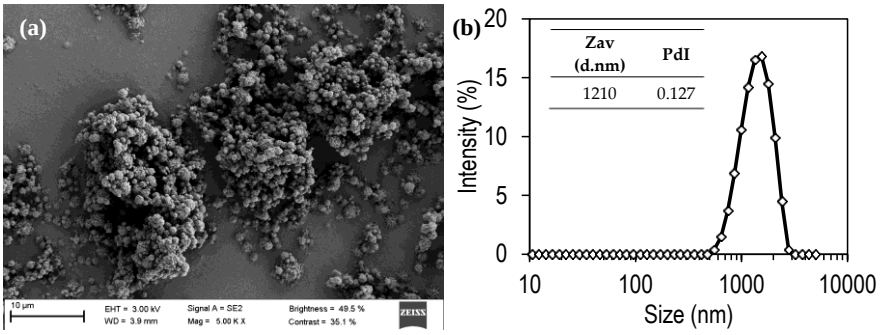

Fig. 4.1: Particle size evaluation of starch aerogel microspheres (StA): (a) SEM image of starch aerogels and (b) and particle size distribution of the starch gel particles. Inset: representative parameters from the dynamic light scattering analysis.

material (Fig. 4.2). StA sample showed a porous and wrinkle surface partially coated with fused particles. This coating is likely due to the presence of the emulsifier (PGPR) in the samples. To confirm this hypothesis, starch gels were washed with diethylether (a solvent for PGPR and a non-solvent for starch) prior to drying. A porous structure formed by a mesh of strands arising from the starch components rearrangement upon gelation was unveiled after this treatment (StA_{-DEE} sample). FIB-SEM technique allowed obtaining a cross-section of the aerogel microspheres (Fig. 4.3). The mesoporous inner structure of both aerogel particles was thus confirmed.

The analysis of the textural properties of starch aerogels (StA) confirmed the presence of a mesoporous structure having average pore diameters between 24 and 25 nm, and with relatively high BET-surface areas (93 m^2/g), BJH-pore volume (0.69 cm^3/g) and porosities (87.7±0.2 %). These values were similar to those reported in literature

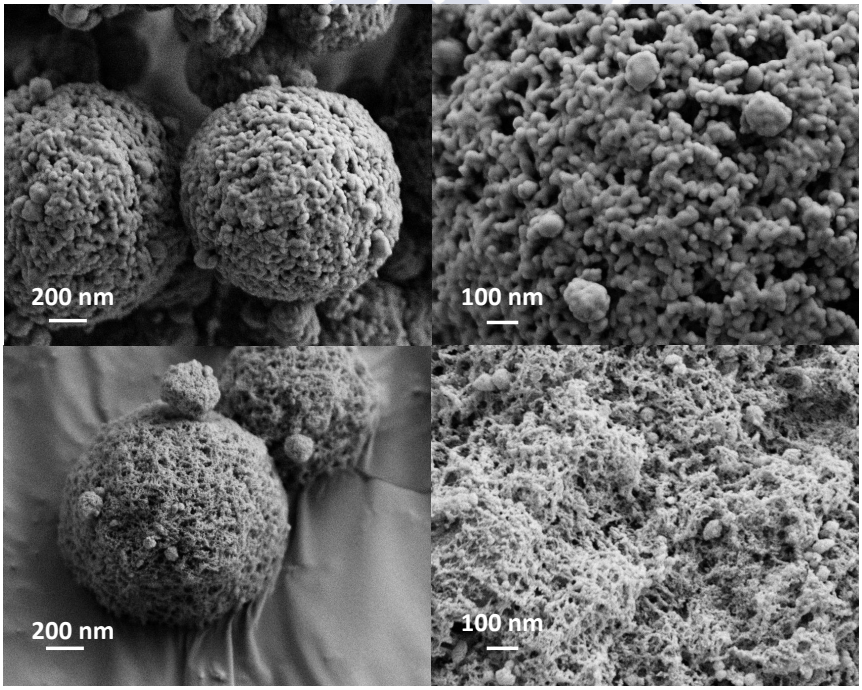

Fig. 4.2: Morphology (left) and textural appearance (right) of starch aerogel microspheres obtained without (StA, top) and with (StA_{-DEE}, bottom) emulsifier removal treatment.

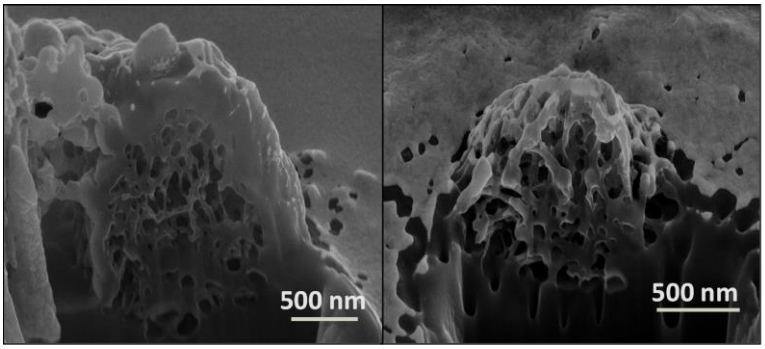

Fig. 4.3: FIB-SEM images of the inner structure of starch aerogel microspheres obtained without (StA, left) and with (StA_{-DEE}, right) emulsifier removal treatment.

for larger starch aerogel particles *(García-González et al. 2012)*. The surfactant removal treatment resulted in an aerogel (StA_{-DEE}) with one-fold increase in BET-surface area (188 m^2/g) and BJH-pore volume (1.25 cm^3/g) with respect to the untreated sample. These higher values are comparable to those reported for starch aerogels in the form of monoliths obtained by standard gelation methods *(García-González et al. 2012, García-González and Smirnova 2013)*. BJH-mean pore diameters of the starch aerogels was of *ca.* 24 nm for both treatments showing that the diethylether was successful in removing the emulsifier whilst preserving the mesoporous structure. C-constant values obtained from the BET equation, which are related with the adsorbate/adsorbent interaction energies and thus associated with material hydrophilicity, *(Marcinko et al. 2003, García-González et al. 2009)* showed that untreated starch aerogel had an intermediate C-value of 36. This C-value is likely due to the combined effects of the relative contributions of the outer surface presence of fatty acids (from the PGPR) and of the inner surface presence of hydroxyl groups (from starch). The absence of PGPR for StA_{-DEE} aerogel microspheres significantly increased the C-value (C=102) due to the improved interactions that can be established between the hydroxyl groups in both inner and outer surfaces of the aerogel and the adsorbed N_2. However, in this work the intermediate hydrophilicity of StA aerogels was preferred for the subsequent incorporation in the scaffolds since it would be expected to favor the interactions of aerogel microspheres

Table 4.2a: Composition, morphological and textural properties of supercritically processed aerogels and scaffolds. Mean values and standard deviation (n=3).

Scaffold	ρ_{bulk}, g/cm^3	ρ_{skel}, g/cm^3	ε, %	A_{BET}, m^2/g	$V_{p,BJH}$, cm^3/g	$d_{p,BJH}$, nm	A_{MIP}, m^2/g	$V_{p,MIP}$, cm^3/g	$d_{p,MIP}$, µm	ε_{MIP}, %
PCL	0.482± 0.027	1.106± 0.012	56.4± 2.4	-	-	-	5.61	0.64	0.46	42.05
PCL-St$_{raw}$	0.517± 0.111	1.146± 0.008	54.9± 9.6	-	-	-	3.66	0.49	0.46	35.22
PCL-StA	0.386± 0.078	1.142± 0.012	66.2± 6.8	1.3	0.0017	15.1	5.76	0.55	0.38	38.98
PCL-K	0.511± 0.082	1.098± 0.004	53.5± 7.4	1.2	0.0006	3.3	5.98	0.40	0.27	30.93
PCL-St$_{raw}$-K	0.461± 0.091	1.155± 0.013	60.1± 7.9	1.4	0.0009	3.8	3.99	0.46	0.46	33.93
PCL-StA-K	0.345± 0.049	1.147± 0.005	69.9± 4.3	1.6	0.0040	14.1	5.48	0.41	0.30	31.68
PCL-StA$_K$-K	0.329± 0.079	1.111± 0.012	70.4± 7.1	1.7	0.0054	14.9	1.55	0.72	1.87	44.81

Table 4.2b: Composition, morphological and textural properties of supercritically processed aerogels and scaffolds. Mean values and standard deviation (*n*=3).

Scaffold	*Pore median*, µm	*Interconnectivity*, %	*Water uptake (<1s)*[a], % vol.	*Water uptake (50ms)*[b], % vol.	k_w, mD	*Cell infiltration*, %
PCL	74.1	92.5	8.33± 1.41	94.35	616.66	83
PCL-St_{raw}	75.0	92.2	3.71± 2.36	94.21	421.77	77
PCL-StA	85.1	90.7	9.17± 3.75	94.62	4902.43	87
PCL-K	84.2	65.2	5.82± 2.45	86.62	2439.63	94
PCL-St_{raw}-K	67.2	82.2	17.03± 8.97	81.51	67.54	83
PCL-StA-K	94.8	74.8	46.95± 9.59	91.85	7469.82	92
PCL-StA_K-K	99.0	93.0	25.52± 2.78	98.72	5866.79	84

[a]*In vitro* value; [b]*In silico* value

with both the hydrophobic PCL-based matrix scaffold and the aqueous body fluids.

The obtained favourable flow properties of starch aerogel powders allow their volumetric dosing and mixing with the other components to prepare scaffolds by supercritical foaming. Starch aerogels presented an angle of repose of 29.0±1.9º, which is comparable to those reported for reference materials with good flowability like spray-dried lactose (31-33º) *(DFE pharma 2013, Huang et al. 2013).* In addition, the angle of repose was improved with respect to native starch St_{raw} (36.9±2.1º). Finally, the reduced particle sizes and high porosities/surface areas of the prepared starch aerogel powders tend to be more cohesive than for larger and denser particles. Accordingly, the compressibility obtained for starch aerogel powder was 32.2±0.2 %, while for native starch was 30.5±0.5 %.

4.3.2. Scaffolds development and morphological characterization

Lightweight PCL-based cylindrical scaffolds were obtained using the supercritical foaming process (Fig. 4.4 and 4.5 and Table 4.2). Obtained pure PCL porous materials had an external nonporous layer of some few microns and a macroporous inner structure of 200-300 μm pore size (Fig. 4.5a) partially interconnected through throats of two different families, one below 1 μm and other above 50 μm (Fig. 4.6a).

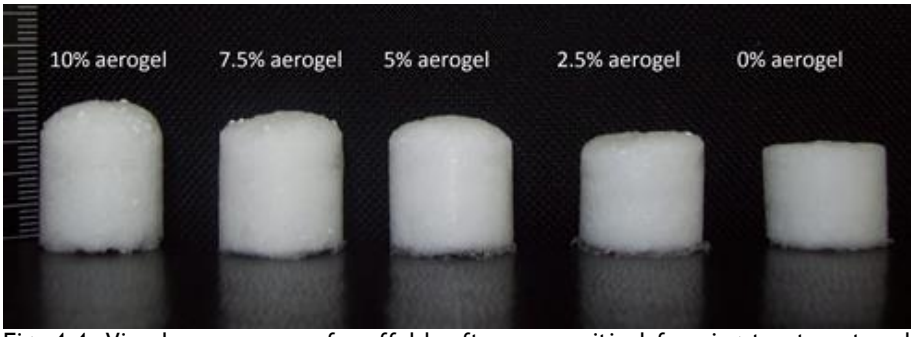

Fig. 4.4: Visual appearance of scaffolds after supercritical foaming treatment and removal from the cylindrical mould. From right to left, PCL scaffolds with increasing content in starch aerogel (StA).

Starch was added in the formulation of PCL-based scaffolds to tune the porous morphology and the release profile of bioactive agents. The incorporation of corn starch in its native form (PCL-St_{raw}) was not successful since the resulting porous material presented a poor PCL-starch miscibility and spatial distribution, as observed in the inset of Fig. 4.4b, as well as a higher densification and reduced porosity with respect to pure PCL scaffolds (Table 4.2). A similar densification of PCL scaffolds was also reported with the use of oven-dried starch gels (i.e., xerogels)*(Diaz-Gomez et al. 2016)*.

The incorporation of starch in the form of aerogel microparticles to the formulation gave rise to scaffolds having increased porosities and decreased bulk densities proportional to the starch aerogel content in the scaffold (Fig. 4.7). Namely, an increase in porosity and a decrease of bulk density of up to *ca.* 20% was observed for PCL-StA scaffolds when compared with the purely PCL scaffold. A visual change of the scaffold consisting on the presence of a dome-like top ending of the PCL-StA scaffolds was also noticed, instead of a flat surface as observed for PCL scaffolds (Fig. 4.4). Additionally, an increase in the pore size (300-600 μm) and in pore interconnectivity through larger pores seems to take place for PCL-StA scaffolds (Fig. 4.5c,left). The aerogel particles seem to be mainly located nearby pore surfaces giving rise to an evident increase in surface roughness of the pores (Fig. 4.5c right). This preferential location of aerogel particles nearby pore surface seems to indicate that porous microspheres may be playing a decisive role in the generation of pores in PCL. In the supercritical foaming process, pores are essentially generated upon depressurization due to the supersaturation in CO_2 (nucleation), and grow due to the diffusion of CO_2 out from the matrix *(García-González et al. 2015)*. The role of nanometric and micrometric inclusions as secondary pore generation sites in scaffolds obtained by supercritical foaming has been already reported for other matrices incorporating highly porous inorganic particles inducing an increased and dual porosity *(Collins et al. 2008, de Matos et al. 2013)*. However, the role of aerogels in the scaffolds on pore generation goes beyond a secondary pore nucleation site behaviour as reported before, since a high interconnectivity of pores through large throats was also

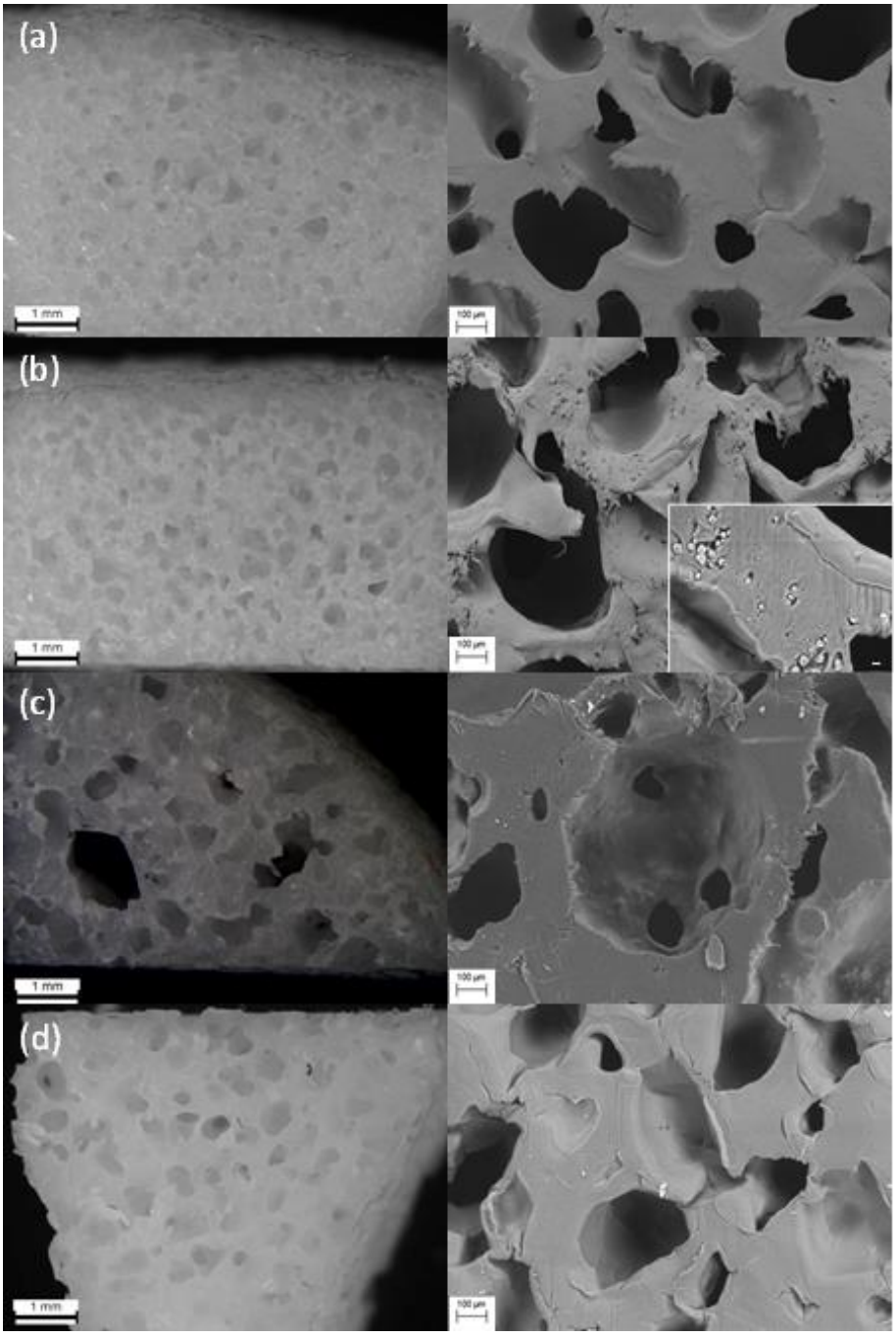
(a)
1 mm
100 µm
(b)
1 mm
100 µm
(c)
1 mm
100 µm
(d)
1 mm
100 µm

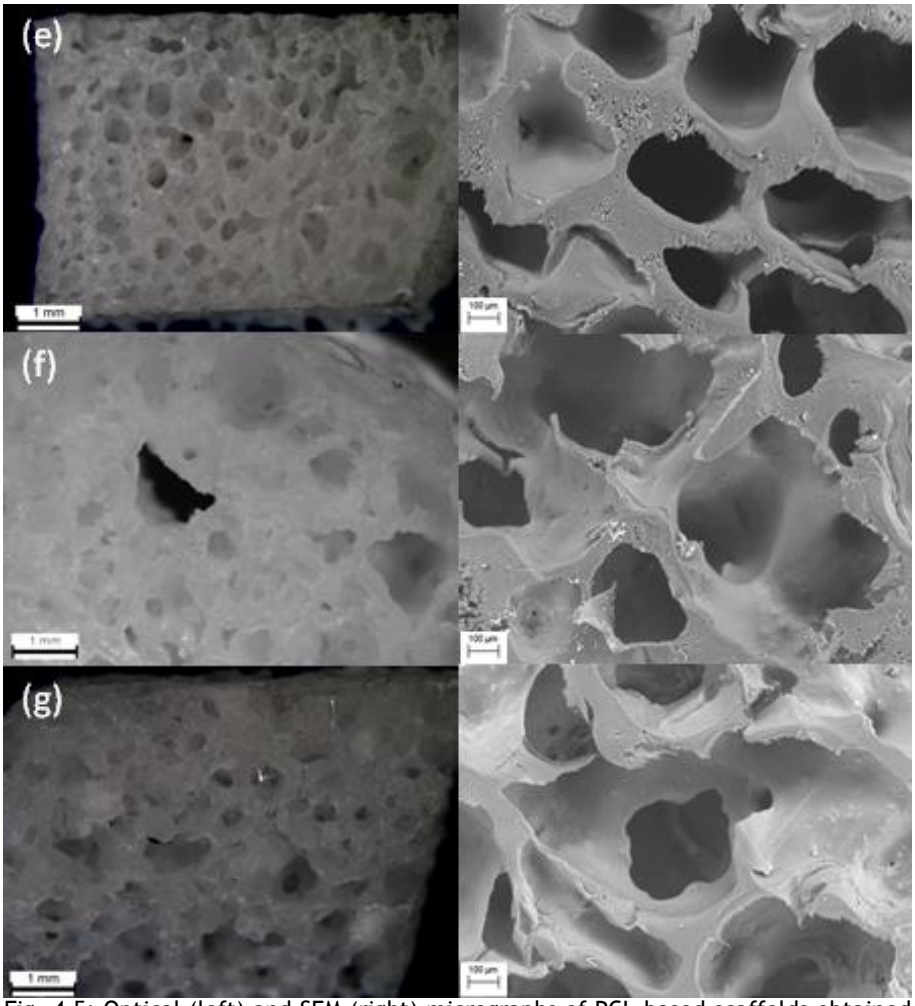

Fig. 4.5: Optical (left) and SEM (right) micrographs of PCL-based scaffolds obtained using supercritical: (a) PCL, (b) PCL-St_{raw}, (c) PCL-StA, (d) PCL-K, (e) PCL-K-St_{raw}, (f) PCL-K-StA and (g) PCL-K-StA_K. Scale bars: (left) 1mm, (right) 100 μm and (inset) 10 μm.

observed here for the first time (Fig. 4.6a). The inherent porosity of aerogels would allow secondary CO_2 release pathways out from the scaffold matrix during the depressurization process and might likely favour the connection between pores (i.e. interconnectivity).

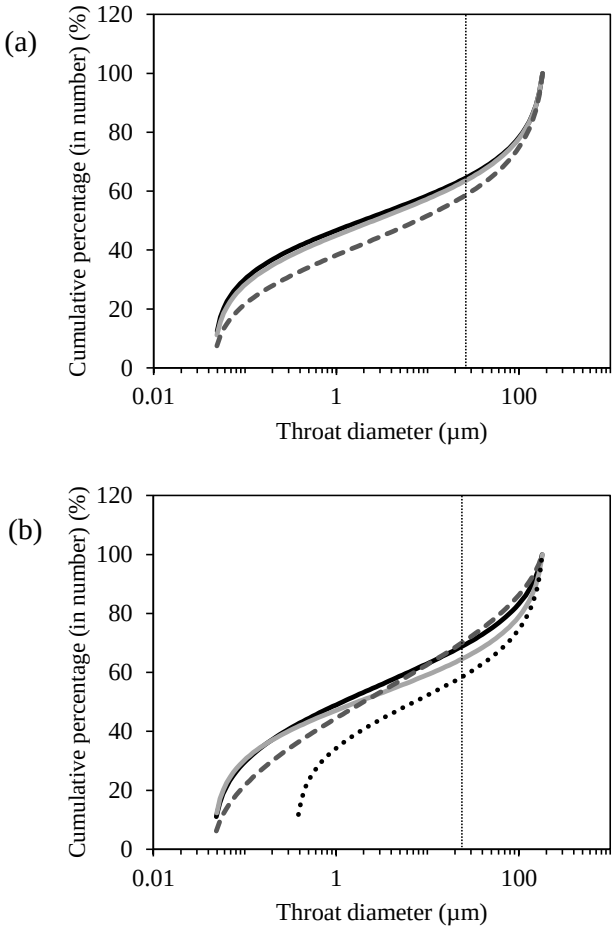

Fig. 4.6: Pore interconnectivity evaluation through throat size distribution analysis of scaffolds (a) without and (b) with ketoprofen payload. Dotted vertical line corresponds to mean MSCs size. Legend: PCL(-K) (black lines), PCL-St_{raw}(-K) (grey lines), PCL-StA(-K) (dashed lines), PCL-$StA_{,K}$-K (dotted line).

The incorporation of ketoprofen in the scaffolds had a significant influence in the scaffold morphology. A densification of the scaffold and a reduced porosity were observed for PCL-K scaffold by SEM (Fig. 4.5d and Table 4.2). The specific surface area of the scaffolds (A_{MIP}) resulted almost unaltered with the incorporation of ketoprofen, whereas the specific pore volume ($V_{p,MIP}$) was reduced as a

consequence of the reduction of the mean pore size ($d_{p,MIP}$). In contrast, the pore median of PCL-K scaffold increased highlighting a morphology formed by large pores with less interconnection and through smaller throats than for the pure PCL scaffold (Table 4.2 and Figs. 4.5d and 4.6).

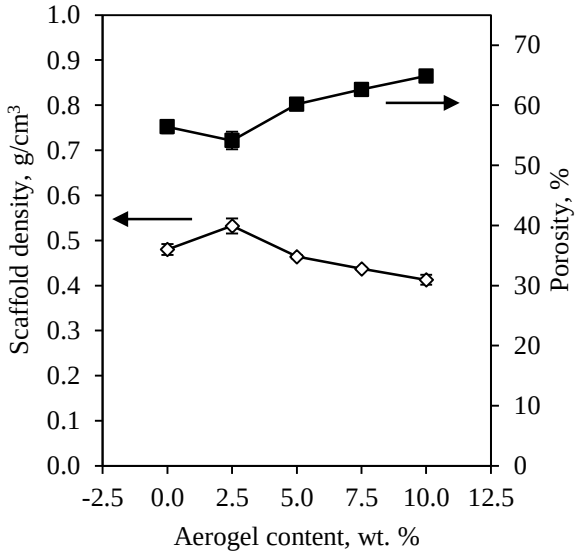

Fig. 4.7: Effect of starch aerogel content in PCL-based scaffolds on the bulk density and porosity of the scaffolds. Statistical comparison regarding scaffold density: 1-way ANOVA test ($F_{4,5d.f.}$=35.37; α<0.01); Tukey's multiple comparisons test: .Statistical comparison regarding scaffold porosity: 1-way ANOVA ($F_{4,5d.f.}$=45.03; α<0.01); Tukey's multiple comparisons test: Notation: the groups connected by an underline are not significantly different.

A reverse trend was observed with the incorporation of ketoprofen in starch-containing scaffolds (PCL-St_{raw}-K and PCL-StA-K) (Fig. 4.5e,f). The bulk density of the scaffolds decreased as a consequence of ketoprofen addition and a slight increase in scaffold porosity was observed. In general, there is a divergence between the overall porosity (ε) and the open porosity obtained by the MIP technique (ε_{MIP}), notably for the starch aerogel containing samples. These differences in the porosity values can be attributed to the presence of closed pores and to the mesoporosity arising from

aerogels, which is out of the pore range of measurement of MIP technique. A refinement in the textural properties was observed in both cases with reduced $V_{p,MIP}$ and $d_{p,MIP}$. Pore interconnectivity and throat size was reduced for the scaffolds loaded with ketoprofen, but still being significantly higher for starch aerogel-containing scaffold (PCL-StA-K) (Fig. 4.6b).

The use of starch aerogel previously loaded with ketoprofen through supercritical impregnation in the scaffold formulation (PCL-StA_K-K) resulted in the lightest and more porous material of all the studied materials. StA_K aerogel was the result of a previous optimization of the supercritical impregnation process of starch aerogel microspheres with ketoprofen using different processing times up to reaching a plateau in the drug content (8 wt.%). StA_K corresponds to starch aerogel microspheres impregnated with less than a monolayer coverage of ketoprofen *(García-González et al. 2015)* in the amorphous form. The incorporation of StA_K in the scaffold had a significant effect on the material properties resulting in an increased mean and median pore sizes. This scaffold showed very high pore interconnectivity with a significant contribution of throat sizes above the MSCs size (Fig. 4.6b). The three scaffolds containing starch aerogel (PCL-StA, PCL-StA-K, PCL-StA_K-K) were the ones with the highest porosities and pore medians, thus supporting the key role of this mesoporous admixture in the pore nucleation and growth mechanism upon supercritical foaming.

Regarding the mechanical properties, the storage and loss moduli of PCL scaffolds at 37ºC were above 10^8 and 10^7 Pa, respectively (Fig. 4.8a). The incorporation of starch or ketoprofen in the PCL-based scaffold had a modest impact in both values (Fig. 4.8a,b). However, the incorporation of starch and ketoprofen together in the PCL-scaffolds resulted in a decrease in values of both moduli, being the combination of starch aerogel and ketoprofen (PCL-StA-K) the less detrimental one. Nevertheless, the storage moduli obtained for all the scaffolds fall between the values reported for trabecular and cortical bones from humans and animals (0.3-10 GPa) *(Linde et al. 1988, Yamashita et al. 2001, Buechner and Lakes 2003)*. The loss moduli were also suitable for bone scaffolding purposes, since the loss

tangent or torsional damping (tan δ=G''/G') obtained for all the samples was in the 0.03-0.06 range, values aligned with the results reported for human and bovine bone *(Buechner and Lakes 2003)*. Finally, the increase in starch aerogel content from 2.5 to 10.0 wt.% in the PCL-based scaffolds had no significant impact on the resulting viscoelastic properties (Fig. 4.8b).

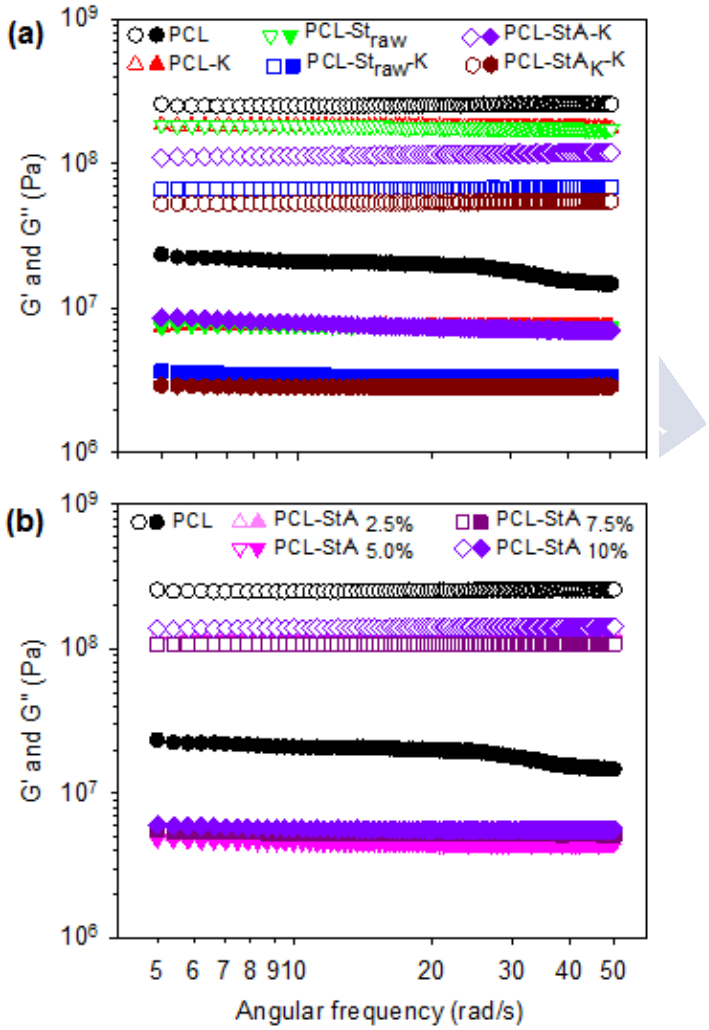

Fig. 4.8: Storage (G'; blank symbols) and loss (G''; solid symbols) moduli of PCL-based scaffolds. (a) Effect of the components of the formulation; and (b) effect of starch aerogel content in PCL-based scaffolds.

4.3.3. Physicochemical characterization of PCL-based scaffolds

Thermal behaviour of PCL was significantly influenced by the supercritical processing method used and by the presence of admixtures (St_{raw}, StA, StA_K, K) in the formulation of the scaffold, according to the DSC results in Table 4.3. Regarding the supercritical foaming method, two different steps are taking place during the process: the exposure to CO_2 at selected pressure and temperature, and the depressurization steps. During the step of exposure to CO_2, CO_2 is in contact with the scaffold formulation and the melting of the PCL is taking place leading to a fluid-liquid mixture. Then, a sudden solidification of the sample (solid-fluid phase separation) is taking place during the depressurization step of the supercritical foaming process due to the dramatic difference in the plasticizing effect of PCL with CO_2 within a certain pressure range (70-90 bar) *(De Paz et al. 2010, Markočič et al. 2013).* Accordingly, crystallinity of the PCL decreased after the supercritical treatment (PCL scaffold) due to the formation of amorphous domains surrounding the PCL crystals upon depressurization. The melting point (T_m) of PCL increased by 2.3 ºC after the foaming process due to a crystallite rearrangement and, particularly, due to the slow depressurization step (1.8 g/min) favouring the growth of the lamellar thickness of the PCL crystals.

The presence of starch in the scaffold composition had an influence in the thermal behaviour of the scaffolds. The crystallinity of the scaffolds increased by *ca.* 10% regardless of the starch format used in the formulation (St_{raw}, StA or StA_K). During the scaffolds foaming processing, starch would likely act as a secondary nucleation site during the PCL crystallization upon depressurization *(de Matos et al. 2013, Diaz-Gomez et al. 2016).* Interestingly, the behaviour of the PCL melting point differed between the formulations containing either native or aerogel formats. PCL-St_{raw} scaffolds had melting point values similar to those of PCL scaffolds, whereas PCL-StA scaffolds had reduced melting point values. Starch aerogel-PCL chemical interactions can take place between the highly accessible hydroxyl groups from the starch aerogel open surface and the PCL, as already reported for other combinations of PCL with hydroxyl-containing

compounds *(Ruseckaite and Jiménez 2003)*. Moreover, the high specific surface area of starch aerogel powders likely favors the formation of more nucleation sites when the plasticizing effect of CO_2 suddenly depletes during the depressurization step. Consequently, the melting point reduction observed with the addition of starch aerogels can be explained by the PCL-crystal nucleation process prevailing over crystal growth leading to the formation of smaller crystals.

Crystallinity and melting point of PCL-scaffolds were significantly reduced with the incorporation of ketoprofen in the formulation (PCL-K scaffolds). PCL and ketoprofen (logP>3) are medium polar compounds and the observed shifts in the thermal events were related to a chemical interaction between the biopolymer and the drug through electron donor-electron acceptor interactions *(Marcinkowski et al. 2015)*. Melting point of ketoprofen was not observed in the DSC thermograms suggesting that the drug was either molecularly dispersed or in the amorphous form in the PCL-matrix *(Guzmán et al. 1996)*.

The use of starch in combination with ketoprofen as admixtures of the PCL-based formulations (PCL-St_{raw}-K and PCL-StA-K) increased the melting point and the crystallinity of the resulting scaffolds with respect to PCL-K scaffold. The preferential interaction of ketoprofen with starch between the hydroxyl groups of the polysaccharide and the carbonyl and carboxyl groups from the drug if compared with PCL, explains the observed change in PCL-melting

Table 4.3: Thermal properties of PCL-based scaffolds processed under supercritical foaming conditions

Material/scaffold	T_m (°C)	ΔH_m (J/g)	Crystallinity (%)
PCL	63.7±1.9	84.5±0.8	59.5±0.6
PCL-St_{raw}	64.6±0.8	89.4±2.9	70.0±2.3
PCL-StA	62.1±0.4	88.9±1.4	69.5±1.1
PCL-K	61.2±1.0	83.1±0.9	61.6±0.7
PCL-St_{raw}-K	62.0±0.4	87.1±3.7	72.2±3.1
PCL-StA-K	62.3±0.8	82.5±2.3	68.3±1.9
PCL-StA_K-K	60.6±0.3	83.8±0.3	69.4±0.2

point value *(Lozano and Martínez 2006, García-González et al. 2012, García-González et al. 2015)*. The increased crystallinity was related to the presence of the starch in the formulation as explained before. Both behaviours are refrained by the DSC results from PCL-StA_K-K scaffold formed by PCL, ketoprofen and ketoprofen-saturated starch aerogel microspheres. In this case, crystallinity is high due to the presence of the starch aerogels, whereas T_m value is similar to that of PCL-K scaffold because ketoprofen is in excess with respect to starch in the formulation thus promoting the interaction with PCL.

4.3.4. Permeability and human MSCs infiltration modeling of the scaffolds

Scaffolds used for bone regeneration need porous structures with different pore ranges that are able to allow the transport of fluids containing nutrients, metabolites and wastes as well as the accessibility of cells within the material for bone ingrowth and neovascularization *(García-González et al. 2015)*. The study of the water uptake and permeability through the scaffold and the percolation capacity of particles of defined sizes (namely similar to those of MSCs) give essential information for the *in silico* screening of the performance of scaffolds. Results are presented in Table 4.2.

According to the *in silico* values, all prepared PCL-based scaffolds presented a fast water uptake with more than 80% of the open pore volume filled with the liquid in less than 50 ms after being immersed in pure water. Experimental values for water uptake differed from the modelled values. Values were in general lower than the modelled values due to the experimental procedure, where samples were weighed just after whipping with filter paper. The *in silico* water uptake values were obtained considering the same hydrophilicity for all the samples and this neglect might explain the differences obtained between *in vitro* and *in silico* values. Two distinct groups of scaffold were unveiled regarding *in vitro* values of instantaneous water uptake: those containing ketoprofen and starch aerogel (PCL-StA-K and PCL-StA_K-K) and the rest of the studied scaffolds. The interaction of ketoprofen with starch (*cf.* Section 4.3.3) seems to influence the amount of polysaccharide particles in the graft directly exposed to the

surface of the pore walls, thus improving the hydrophilicity of the scaffolds.

The differences in composition, pore morphology (pore and throat sizes) and interconnectivity observed for the different PCL-based scaffolds studied (*cf.* Sections 4.3.2 and 4.3.3) strongly influenced the permeability of aqueous solutions and the MSCs percolation through the 3D-porous network of the scaffolds. Despite all scaffolds may present high pore interconnectivity values, the throat size distribution and the throat-to-pore ratio in scaffolds are additional key parameters varying the fluid flow properties and the MSCs percolation through the material.

The high contribution of throats in the 1-10 μm region for the PCL and PCL-St_{raw} scaffolds resulted in a low water permeability and a limited infiltration capacity of simulated MSCs within the scaffold. The loading of the scaffolds with ketoprofen slightly improved both properties. The use of starch aerogel microspheres in the formulations significantly altered the throat size distribution leading to enhanced water permeability (5-10 times higher) and MSCs infiltration capacity (up to 13 %). Water permeability values of starch aerogel containing scaffolds fell close to the lower limit of the permeability range reported for cancellous bone (10^4-10^8 mD) *(Syahrom et al. 2013)*. Hence, the incorporation of starch aerogel micropheres to the PCL-based scaffolds inferred the most promising 3D-porous architecture for bone tissue ingrowth.

4.3.5. Ketoprofen release from PCL scaffolds

The choice of the scaffold formulation, the modulation of the scaffold porosity, the drug loading strategy and the drug loading amount are factors significantly influencing the drug release profile from bone scaffolds *(Tezcaner and Keskin 2011)*. In this work, a porous scaffolds consisting on a hydrophobic porous matrix (PCL) with highly porous hydrophilic components (starch particles) and having high chemical affinity through hydrogen bonding *(Lozano and Martínez 2006, Messner et al. 2012)* for ketoprofen was accordingly chosen to sustain the release during days (Fig. 4.9). As a result, all prepared scaffolds presented slower ketoprofen release profiles than

that corresponding to the dissolution profile of the crystalline drug. An initial burst occurred during the first hours, and then sustained release was recorded for several days. This time-dependent ketoprofen release profile seems suitable to provide a prompt anti-inflammatory response in the initial stages (burst step) and also long-term action (sustained release step) during the bone healing process *(Prabaharan et al. 2007, Raafat and Abd-Allah 2018).*

The use of starch aerogels as an admixture of the scaffold composition had a relevant role in the tuning of the ketoprofen release profile. Scaffolds containing starch aerogels (PCL-StA-K and PCL-StA_K-K) had a faster initial release (within 30 min) if compared with scaffolds not containing starch (PCL-K, 1 h) or with unprocessed starch (PCL-St_{raw}-K, 2 h). Then, PCL-StA-K and PCL-StA_K-K have sustained releases with more than 90% of the payload within 3 days, whereas the ketoprofen release took longer times for the rest of the scaffolds. The higher accessibility of water to the scaffolds containing starch aerogel microspheres unveiled by the water permeability study (Table 4.4) is likely responsible for the observed accelerated release profile, especially during the burst stage. The preferential location of starch aerogel microspheres in the pore surface coupled to the affinity of ketoprofen for the hydroxyl groups from starch would explain the accelerated but sustained release profile of ketoprofen from the scaffolds. Drug release profiles from the scaffolds were fitted to the Korsmeyer-Peppas equation (Table 4.4) showing *n* values below threshold of 0.45 in all cases. According to these results, the drug release falls into a complex diffusion-controlled mechanism comprising a combination of diffusion through the matrix and through the pores filled with the solution from the release medium *(Peppas 1985, Diaz-Gomez et al. 2016).*

Table 4.4: Kinetic fitting parameters of the ketoprofen release profiles from drug-loaded scaffolds in PBS solution (pH 7.4) according to Eq. (4.6).

Scaffold	k, h^{-n}	n	R^2
PCL-K	0.224±0.038	0.304±0.049	0.884
PCL-St_{raw}-K	0.294±0.016	0.261±0.016	0.969
PCL-StA-K	0.244±0.035	0.320±0.041	0.923
PCL-StA_K-K	0.299±0.041	0.304±0.040	0.920

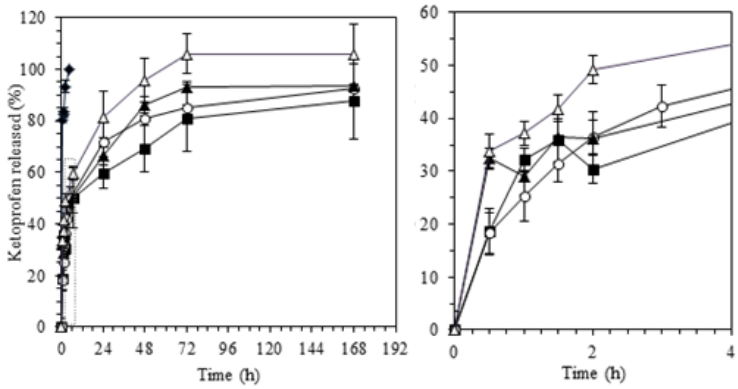

Fig. 4.9: Ketoprofen released from PCL-based scaffolds in PBS solution (pH 7.4) during 7 days. Ketoprofen dissolution profile (black diamonds) is provided for the sake of comparison. Legend: PCL-K (black squares), PCL-St_{raw}-K (white circles), PCL-StA-K (black triangles) and PCL-StA_K-K (white triangles).

4.4. CONCLUSIONS

Biodegradable mesoporous particles from polysaccharides of a size as small as one micron are processed in this work for the first time. This format encompasses the outstanding textural properties of aerogels (high specific surface areas and pore volumes) and the excellent solid physical mixing capacity of microparticles. The incorporation of starch aerogel microspheres in highly porous PCL scaffolds processed by supercritical CO_2 foaming significantly improved the potential uses of these biomaterials for bone regeneration applications, notably regarding pore throat size, water permeability and MSCs infiltration capacity. These PCL-based scaffolds also provided good mechanical properties and an *in vitro* sustained release of an anti-inflammatory drug (ketoprofen) during several days. *In vivo* ketoprofen release tests need to be carried out to confirm this two-stage release pattern under physiological conditions. The mild operating conditions used for the processing of the scaffolds (40 ºC, 150 bar) open up the possibility to incorporate other bioactive compounds (e.g., growth factors) for sustained release to facilitate other bone healing biological processes or to be used as subcutaneous implants or medical devices for drug release.

4.5 REFERENCES

R. K. Ahuja, M. Kodialam, A. K. Mishra and J. B. Orlin (1997). "Computational investigations of maximum flow algorithms." *European Journal of Operational Research* **97**(3): 509-542.

M. Alnaief, M. A. Alzaitoun, C. A. García-González and I. Smirnova (2011). "Preparation of biodegradable nanoporous microspherical aerogel based on alginate." *Carbohydrate Polymers* **84**(3): 1011-1018.

P. M. Buechner and R. S. Lakes (2003). "Size effects in the elasticity and viscoelasticity of bone." *Biomech Model Mechanobiol* **1**(4): 295-301.

N. J. Collins, G. A. Leeke, R. H. Bridson, F. Hassan and L. M. Grover (2008). "The influence of silica on pore diameter and distribution in PLA scaffolds produced using supercritical CO_2." *Journal of Materials Science: Materials in Medicine* **19**(4): 1497-1502.

F. De Cicco, P. Russo, E. Reverchon, C. A. García-González, R. P. Aquino and P. Del Gaudio (2016). "Prilling and supercritical drying: A successful duo to produce core-shell polysaccharide aerogel beads for wound healing." *Carbohydrate Polymers* **147**: 482-489.

M. B. C. de Matos, A. P. Piedade, C. Alvarez-Lorenzo, A. Concheiro, M. E. M. Braga and H. C. de Sousa (2013). "Dexamethasone-loaded poly(ε-caprolactone)/silica nanoparticles composites prepared by supercritical CO_2 foaming/mixing and deposition." *International Journal of Pharmaceutics* **456**(2): 269-281.

E. De Paz, A. Martín, S. Rodríguez-Rojo, J. Herreras and M. J. Cocero (2010). "Determination of phase equilibrium (solid-liquid-gas) in poly-(ε-caprolactone)-carbon dioxide systems." *Journal of Chemical and Engineering Data* **55**(8): 2781-2785.

DFE pharma. (2013). "Directly compressible lactose." Retrieved 06/07/2016, 2016, from https://www.dfepharma.com.

L. Diaz-Gomez, A. Concheiro, C. Alvarez-Lorenzo and C. A. García-González (2016). "Growth factors delivery from hybrid PCL-starch scaffolds processed using supercritical fluid technology." *Carbohydrate Polymers* **142**: 282-292.

C. Elvira, J. F. Mano, J. San Román and R. L. Reis (2002). "Starch-based biodegradable hydrogels with potential biomedical applications as drug delivery systems." *Biomaterials* **23**(9): 1955-1966.

C. A. García-González, M. Alnaief and I. Smirnova (2011). "Polysaccharide-based aerogels - Promising biodegradable carriers for drug delivery systems." *Carbohydrate Polymers* **86**(4): 1425-1438.

C. A. García-González, M. C. Camino-Rey, M. Alnaief, C. Zetzl and I. Smirnova (2012). "Supercritical drying of aerogels using CO_2: Effect of extraction time on the end material textural properties." *Journal of Supercritical Fluids* **66**: 297-306.

C. A. García-González, E. Carenza, M. Zeng, I. Smirnova and A. Roig (2012). "Design of biocompatible magnetic pectin aerogel monoliths and microspheres." *RSC Advances* **2**(26): 9816-9823.

C. A. García-González, A. Concheiro and C. Alvarez-Lorenzo (2015). "Processing of materials for regenerative medicine using supercritical fluid technology." *Bioconjugate Chemistry* **26**(7): 1159-1171.

C. A. García-González, J. Fraile, A. López-Periago, J. Saurina and C. Domingo (2009). "Measurements and Correlation of Octyltriethoxysilane Solubility in Supercritical CO2 and Assembly of Functional Silane Monolayers on the Surface of Nanometric Particles." *Industrial & Engineering Chemistry Research* **48**(22): 9952-9960.

C. A. García-González, M. Jin, J. Gerth, C. Alvarez-Lorenzo and I. Smirnova (2015). "Polysaccharide-based aerogel microspheres for oral drug delivery." *Carbohydrate Polymers* **117**: 797-806.

C. A. García-González and I. Smirnova (2013). "Use of supercritical fluid technology for the production of tailor-made aerogel particles for delivery systems." *Journal of Supercritical Fluids* **79**: 152-158.

C. A. García-González, J. J. Uy, M. Alnaief and I. Smirnova (2012). "Preparation of tailor-made starch-based aerogel microspheres by the emulsion-gelation method." *Carbohydrate Polymers* **88**(4): 1378-1386.

J. Ge, L. Guo, S. Wang, Y. Zhang, T. Cai, R. C. H. Zhao and Y. Wu (2014). "The Size of Mesenchymal Stem Cells is a Significant Cause of Vascular Obstructions and Stroke." *Stem Cell Reviews and Reports* **10**(2): 295-303.

J. Ge, M. Li, Q. Zhang, C. Z. Yang, P. H. Wooley, X. Chen and S. Y. Yang (2013). "Silica aerogel improves the biocompatibility in a poly-ε-caprolactone composite used as a tissue engineering scaffold." *International Journal of Polymer Science* **2013**.

A. Gomez-Carracedo, R. Martinez-Pacheco, A. Concheiro and J. L. Gomez-Amoza (2010). "Modelling of porosity and waterfronts in cellulosic pellets for understanding drug release behavior." *International Journal of Pharmaceutics* **388**(1–2): 101-106.

M. Guzmán, J. Molpeceres, F. García and M. R. Aberturas (1996). "Preparation, characterization and in vitro drug release of poly-ε-caprolactone and hydroxypropyl methylcellulose phthalate ketoprofen loaded microspheres." *Journal of Microencapsulation* **13**(1): 25-39.

W. Huang, Y. Shi, C. Wang, K. Yu, F. Sun and Y. Li (2013). "Using spray-dried lactose monohydrate in wet granulation method for a low-dose oral formulation of a paliperidone derivative." *Powder Technology* **246**: 379-394.

A. Johnson, I. M. Roy, G. P. Matthews and D. Patel (2003). "An improved simulation of void structure, water retention and hydraulic conductivity in soil with the Pore-Cor three-dimensional network." *European Journal of Soil Science* **54**(3): 477-490.

J. A. Kenar, F. J. Eller, F. C. Felker, M. A. Jackson and G. F. Fanta (2014). "Starch aerogel beads obtained from inclusion complexes prepared from high amylose starch and sodium palmitate." *Green Chemistry* **16**(4): 1921-1930.

F. Linde, C. B. Gothgen, I. Hvid and B. Pongsoipetch (1988). "Mechanical properties of trabecular bone by a non-destructive compression testing approach." *Engineering in Medicine* **17**(1): 23-29.

H. R. Lozano and F. Martínez (2006). "Thermodynamics of partitioning and solvation of ketoprofen in some organic solvent/buffer and liposome systems." *Brazilian Journal of Pharmaceutical Sciences* **42**(4): 601-613.

H. Maleki, L. Durães, C. A. García-González, P. del Gaudio, A. Portugal and M. Mahmoudi (2016). "Synthesis and biomedical applications of aerogels: Possibilities and challenges." *Advances in Colloid and Interface Science* **236**: 1-27.

S. Marcinko, R. Helmy and A. Y. Fadeev (2003). "Adsorption properties of SAMs supported on TiO_2 and ZrO_2." *Langmuir* **19**(7): 2752-2755.

Ł. Marcinkowski, A. Kloskowski, A. Spietelun and J. Namieśnik (2015). "Evaluation of polycaprolactone as a new sorbent coating for determination of polar organic compounds in water samples using membrane–SPME." *Analytical and Bioanalytical Chemistry* **407**(4): 1205-1215.

E. Markočič, M. Škerget and Z. Knez (2013). "Effect of temperature and pressure on the behavior of poly(ε- caprolactone) in the presence of supercritical carbon dioxide." *Industrial and Engineering Chemistry Research* **52**(44): 15594-15601.

M. Martins, A. A. Barros, S. Quraishi, P. Gurikov, S. P. Raman, I. Smirnova, A. R. C. Duarte and R. L. Reis (2015). "Preparation of macroporous alginate-based aerogels for biomedical applications." *Journal of Supercritical Fluids* **106**: 152-159.

T. Mehling, I. Smirnova, U. Guenther and R. H. H. Neubert (2009). "Polysaccharide-based aerogels as drug carriers." *Journal of Non-Crystalline Solids* **355**(50-51): 2472-2479.

M. Messner, O. Häusler and T. Loftsson (2012). *Solution enhancement of drug substances using soluble amylose*. Proceedings of PBP 8th World Meeting on Pharmaceutics, Biopharmaceutics and Pharmaceutical Technology, Istanbul (Turkey).

S. Milovanovic, I. Jankovic-Castvan, J. Ivanovic and I. Zizovic (2015). "Effect of starch xero- and aerogels preparation on the supercritical CO_2 impregnation of thymol." *Starch/Staerke* **67**(1-2): 174-182.

K. Mukae, Y. H. Bae, T. Okano and S. W. Kim (1990). "A New Thermo-Sensitive Hydrogel: Poly(ethylene oxide-dimethyl siloxane-ethylene oxide)/Poly(N-isopropyl acrylamide) Interpenetrating Polymer Networks I. Synthesis and Characterization." *Polymer Journal* **22**(3): 206-217.

A. Muñoz García, A. J. Hunt, V. L. Budarin, H. L. Parker, P. S. Shuttleworth, G. J. Ellis and J. H. Clark (2015). "Starch-derived carbonaceous mesoporous materials (Starbon®) for the selective adsorption and recovery of critical metals." *Green Chemistry* **17**(4): 2146-2149.

L. Nogueiras-Nieto, J. L. Gómez-Amoza, M. B. Delgado-Charro and F. J. Otero-Espinar (2011). "Hydration and N-acetyl-l-cysteine alter the microstructure of human nail and bovine hoof: Implications for drug delivery." *Journal of Controlled Release* **156**(3): 337-344.

H. Nyangoga, E. Aguado, E. Goyenvalle, M. F. Baslé and D. Chappard (2010). "A non-steroidal anti-inflammatory drug (ketoprofen) does not delay β-TCP bone graft healing." *Acta Biomaterialia* **6**(8): 3310-3317.

N. A. Peppas (1985). "Analysis of Fickian and non-Fickian drug release from polymers." *Pharmaceutica Acta Helvetiae* **60**(4): 110-111.

N. Pircher, S. Veigel, N. Aigner, J. M. Nedelec, T. Rosenau and F. Liebner (2014). "Reinforcement of bacterial cellulose aerogels with biocompatible polymers." *Carbohydrate Polymers* **111**: 505-513.

I. Pountos, T. Georgouli, G. M. Calori and P. V. Giannoudis (2012). "Do Nonsteroidal Anti-Inflammatory Drugs Affect Bone Healing? A Critical Analysis." *The Scientific World Journal* **2012**: 606404.

M. Prabaharan, M. A. Rodriguez-Perez, J. A. de Saja and J. F. Mano (2007). "Preparation and characterization of poly(L-lactic acid)-chitosan hybrid scaffolds with drug release capability." *Journal of Biomedical Materials Research, Part B: Applied Biomaterials* **81B**(2): 427-434.

A. Przekora and G. Ginalska (2016). "In vitro evaluation of the risk of inflammatory response after chitosan/HA and chitosan/β-1,3-glucan/HA bone scaffold implantation." *Materials Science and Engineering: C* **61**: 355-361.

A. I. Raafat and W. M. Abd-Allah (2018). "In vitro apatite forming ability and ketoprofen release of radiation synthesized (gelatin-polyvinyl alcohol)/bioglass composite scaffolds for bone tissue regeneration." *Polymer Composites* **39**(3): 606-615.

C. Romagnoli, F. D'Asta and M. L. Brandi (2013). "Drug delivery using composite scaffolds in the context of bone tissue engineering." *Clinical Cases in Mineral and Bone Metabolism* **10**(3): 155-161.

R. A. Ruseckaite and A. Jiménez (2003). "Thermal degradation of mixtures of polycaprolactone with cellulose derivatives." *Polymer Degradation and Stability* **81**(2): 353-358.

A. Salerno and C. Domingo (2014). "Making microporous nanometre-scale fibrous PLA aerogels with clean and reliable supercritical CO_2 based approaches." *Microporous and Mesoporous Materials* **184**: 162-168.

J. Siepmann and N. A. Peppas (2011). "Higuchi equation: Derivation, applications, use and misuse." *International Journal of Pharmaceutics* **418**(1): 6-12.

G. A. Silva, O. P. Coutinho, P. Ducheyne, I. M. Shapiro and R. L. Reis (2007). "The effect of starch and starch-bioactive glass composite microparticles on the adhesion and expression of the osteoblastic phenotype of a bone cell line." *Biomaterials* **28**(2): 326-334.

R. Sridharan, A. R. Cameron, D. J. Kelly, C. J. Kearney and F. J. O'Brien (2015). "Biomaterial based modulation of macrophage polarization: a review and suggested design principles." *Materials Today* **18**(6): 313-325.

J. Stergar and U. Maver (2016). "Review of aerogel-based materials in biomedical applications." *Journal of Sol-Gel Science and Technology* **77**(3): 738-752.

A. Syahrom, M. R. Abdul Kadir, J. Abdullah and A. Öchsner (2013). "Permeability studies of artificial and natural cancellous bone structures." *Medical Engineering and Physics* **35**(6): 792-799.

A. Tezcaner and D. Keskin (2011). Bioactive Agent Delivery in Bone Tissue Regeneration. *Active Implants and Scaffolds for Tissue Regeneration*. M. Zilberman. Berlin, Heidelberg, Springer Berlin Heidelberg**:** 193-223.

H. Tsuji and Y. Ikada (1998). "Blends of aliphatic polyesters. II. Hydrolysis of solution-cast blends from poly(L-lactide) and poly (ε-caprolactone) in phosphate-buffered solution." *Journal of Applied Polymer Science* **67**(3): 405-415.

N. M. Vacanti, H. Cheng, P. S. Hill, J. D. T. Guerreiro, T. T. Dang, M. Ma, S. Watson, N. S. Hwang, R. Langer and D. G. Anderson (2012). "Localized delivery of dexamethasone from electrospun fibers reduces the foreign body response." *Biomacromolecules* **13**(10): 3031-3038.

H. J. L. van der Heide, G. Hannink, P. Buma and B. W. Schreurs (2008). "No effect of ketoprofen and meloxicam on bone graft ingrowth: A bone chamber study in goats." *Acta Orthopaedica* **79**(4): 548-554.

A. Wibberley, G. P. McCafferty, C. Evans, R. M. Edwards and J. P. Hieble (2006). "Dual, but not selective, COX-1 and COX-2 inhibitors, attenuate acetic acid-evoked bladder irritation in the anaesthetised female cat." *British Journal of Pharmacology* **148**(2): 154-161.

Wold Health Organization (WHO) (2002). *Active Ageing - A Policy Framework* Geneva, Switzerland, from https://www.who.int/ageing/publications/active_ageing/en/

J. Yamashita, B. R. Furman, H. R. Rawls, X. Wang and C. M. Agrawal (2001). "The use of dynamic mechanical analysis to assess the viscoelastic properties of human cortical bone." *Journal of Biomedical Materials Research* **58**(1): 47-53.

Y. Zhou, H. L. Gao, L. L. Shen, Z. Pan, L. B. Mao, T. Wu, J. C. He, D. H. Zou, Z. Y. Zhang and S. H. Yu (2016). "Chitosan microspheres with an extracellular matrix-mimicking nanofibrous structure as cell-carrier building blocks for bottom-up cartilage tissue engineering." *Nanoscale* **8**(1): 309-317.

USC
UNIVERSIDADE
DE SANTIAGO
DE COMPOSTELA

USC
UNIVERSIDADE
DE SANTIAGO
DE COMPOSTELA

5. $ScCO_2$-FOAMED SILK FIBROIN AEROGEL/PCL SCAFFOLDS CONTAINING DEXAMETHASONE FOR BONE REGENERATION[§]

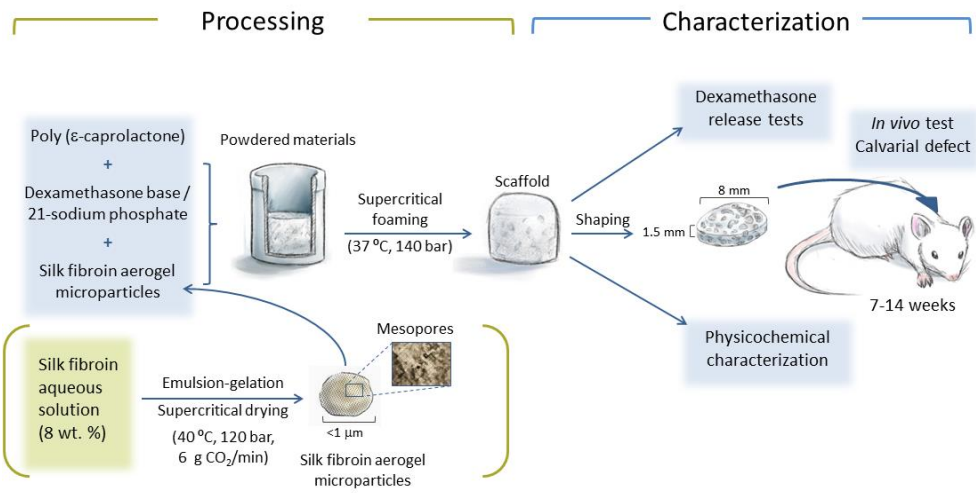

[§]The work described in this chapter has been published in *Goimil et al. J. CO2 Utiliz., 31 (2019) 51-64* and was developed in collaboration with Prof. Carmen Évora, Prof. Araceli Delgado and Dr. Ricardo Reyes, from the University of La Laguna, and Prof. Jose Luis Cenis, Dr. Antonio A. Lozano Pérez and Dr. Salvador D. Aznar Cervantes from the Instituto Murciano de Investigación y Desarrollo Agrario y Alimentario.

5.1. INTRODUCTION

The advent of regenerative medicine discipline boosted the development of engineered bone grafts comprising a polymeric matrix, bioactive agents and even cells *(Bhamidipati et al. 2013, Wang and Yeung 2017)*. The polymeric matrix is designed to provide a provisional mechanical support and to serve as a 3D-template for cell colonization and tissue ingrowth. Bioactive agents should be able to promote cell growth and proliferation as well as differentiation towards the osteogenic lineage. Cells can be either pre-seeded in the grafts using bioreactors before implantation or may colonize the scaffold after the surgical procedure emulating the normal healing process. The proper choice and design of these three elements of the grafts will largely influence the scaffold performance and the osteointegration.

Regarding the polymeric matrix, synthetic polymers provide better reproducibility between batches with respect to natural polymers in terms of molecular weight and purity leading to a more precise control of biodegradation rate to match the biological tissue growth rate *(ur-Rahman and Anjum 2015, Thomas et al. 2018)*. Among them, polyesters, e.g., poly(ε-caprolactone), poly(lactic acid) and poly(lactic-co-glycolic acid), are the most common choice with tunable biodegradation rates in the range from weeks to months, being suitable for their application in bone repair *(Lam et al. 2009, Harwood et al. 2010, Einhorn and Gerstenfeld 2015)*. Namely, these biodegradation rates of polyesters are of interest in bone regeneration of critical size defects. In these cases, tissue regeneration firstly starts in the borders of the defect site and in the tissue-scaffold interface. Then, the tissue regeneration rim will progressively advance until the defect is consolidated, is not critical anymore and can be self-regenerated. Previous studies show that the consolidation of critical size defects in the presence of scaffolds loaded with growth factors (BMP-2) was observed 8 weeks after implantation *(Rodríguez-Évora et al. 2013)*, i.e. a regeneration pace compatible with the biodegradation rate of the polyester matrices.

A wide variety of bioactive agents are being explored as components of these polymer matrices to trigger and modulate cell

adhesion, growth and differentiation *(Perez et al. 2015)*. Although a variety of growth factors have shown to exert very positive effects, limitations related to stability (both during processing and after implantation) together with off-target or undesirable collateral effects (uncontrolled cell growth in surrounding tissues) *(Carbone et al. 2014)* make dexamethasone to still be an advantageous active substance for bone regeneration *(Perez et al. 2015, Zhao et al. 2018)*. This synthetic glucocorticoid induces the osteogenic differentiation in human mesenchymal stem cells *(Nuttelman et al. 2006)* and reduces the foreign body response of synthetic grafts *(Vacanti et al. 2012)* also attenuating inflammatory events that can interfere with the healing process *(Gibon et al. 2017)*.

The incorporation of silk fibroin into bone grafts can also have important bioactive implications by promoting the attachment, growth and colonization of mesenchymal stem cells in the scaffolds *(Kim et al. 2005, Li et al. 2018)*. Besides, silk fibroin shows an interesting combination of mechanical and biodegradation properties, especially under the β-sheet conformation *(Li and Li 2014, Murphy and Romero 2014)*, and is already present in commercial scaffolds for soft tissues (SERI© surgical scaffold) *(Jewell et al. 2015)*. Other scaffolds containing silk fibroin have been studied for bone regeneration, usually in combination with other materials like synthetic polymers *(Melke et al. 2016, Bhattacharjee et al. 2017)*. However, these scaffolds are often prepared using techniques that involve solvents needing to be removed before further use.

The processing strategy for preparing bone scaffolds should provide a proper architecture design to facilitate the neotissue formation as well as to be compatible with the incorporation of bioactive agents at high yields and with retained activity. So far, most processing techniques are characterized by harsh conditions (high temperatures and use of solvents) and multi-step procedures (leaching and downstream processes) that may lead to scaffolds with low incorporation yields and limited performance *(Xin et al. 2018, Ying Deng and Kuiper 2018)*. Supercritical fluid technology based on the use of supercritical carbon dioxide ($scCO_2$) constitutes a processing platform able to overcome the abovementioned limitations in the

preparation of bone scaffolds with advanced properties *(Duarte et al. 2009, Bhamidipati et al. 2013, García-González et al. 2015, Salerno and Pascual 2015).*

Supercritical foaming allows reducing the temperature required for the thermal events (melting point, glass transition) of synthetic polymers up to conditions compatible with temperature-sensitive bioactive agents *(Duarte et al. 2009, Fanovich and Jaeger 2012, de Matos et al. 2013, Salerno and Pascual 2015).* This solvent-free technology exploits the plasticizing effect of compressed CO_2 on polymers to form a porous structure during the controlled removal of CO_2 (i.e. depressurization) *(Bhamidipati et al. 2013, García-González et al. 2015).* Moreover, supercritical foaming is an auspicious strategy to process scaffolds with virtually 100 % yield of incorporation of bioactive agents with retained activity *(Diaz-Gomez et al. 2016).* The mixing of the polymer with bioactive agents is also promoted during the CO_2 soaking period of the foaming process due to the rubbery state of the polymer under these conditions *(de Matos et al. 2013, Fanovich et al. 2013).* However, the supercritical foaming process usually results in scaffolds with high macroporosity but low pore interconnectivity that hinders the access of cells and the transport of nutrients and metabolic wastes throughout the graft *(García-González et al. 2015, Goimil et al. 2017).* The preparation of bioactive agent-loaded scaffolds, by using the supercritical foaming, combined with the incorporation of aerogel microparticles, obtained by supercritical drying, is proposed in the present work to obtain 3D-scaffolds with advanced architectures and performance.

In the regenerative medicine context, silk fibroin in the form of aerogel microparticles, i.e. solid nanostructured materials that preserve the mesoporous structure of the wet gel precursor *(Maleki et al. 2016),* and obtained by supercritical drying of gels might be an advantageous admixture for the processing of scaffolds, which has not been explored so far. The presence of other aerogels in synthetic scaffolds processed by supercritical foaming has been shown to increase the pore sizes and their interconnectivity resulting in enhanced cell infiltration capacity *(Goimil et al. 2017).* Silk aerogels may allow combining the intrinsic bioactive properties of silk fibroin and the

textural properties of aerogels. Silk fibroin aerogel monoliths, prepared by a combination of a sol-gel mechanism followed by supercritical drying *(Mallepally et al. 2014, Marin et al. 2014, Mallepally et al. 2015)*, have shown textural properties dependent on the fibroin molecular weight and the concentration in the aqueous precursor solution *(Mallepally et al. 2015)*. These previously obtained silk fibroin aerogel monoliths were cytocompatible with human foreskin fibroblasts but lacked the macroporosity needed to favor the cell penetration and growth. On the other hand, the supercritical processing of mixtures of polyesters and silk fibroin (as raw material, not as aerogels) have been shown to be feasible at various conditions (140-200 bar, 37-155 ºC) *(Kang et al. 2009, Diaz-Gomez et al. 2017)*. The innovation in the preparation of silk aerogel in the form of particles and their use in the processing of synthetic macroporous scaffolds by supercritical foaming is a feasible solvent-free processing approach with an advanced performance. The particular behavior of these scaffolds stems on the synergistic combination of two CO_2-based technologies that overcomes the individual processing limitations of poor pore interconnectivity (for supercritical foaming) and of lack of macroporosity (for silk aerogel scaffolds) of the scaffolds obtained for both processes separately. Moreover, the integration of the use of CO_2 to promote silk fibroin gelation *(Mallepally et al. 2014)* and to facilitate solid state dispersion *(de Matos et al. 2013)* of the scaffold admixtures was also evaluated.

Thus, in the present work, scaffold formulations containing PCL, silk fibroin aerogel microparticles and dexamethasone were prepared using the supercritical foaming process to contrast two main hypotheses: (i) silk fibroin aerogel microparticles may improve the porous structure of the scaffold facilitating cell infiltration and biological fluid transport; and (ii) the incorporation of dexamethasone as base or as a salt may lead to different drug release profiles and thus to different bone regeneration outcomes. First, SF aerogels were herein developed in the form of submicron-sized particles using supercritical drying. Dexamethasone was added in two different forms: dexamethasone base (DX) and dexamethasone-21-sodium phosphate (DS), which present distinct solubility in aqueous media.

The scaffolds were prepared with various combinations of SF aerogels and DX and DS, and then evaluated in terms of morphology, physicochemical properties, *in silico* capacity for cell infiltration, and tuning of the release profile and subsequent promotion of cell osteodifferentiation. The bone regenerative performance of the scaffolds was assessed in *in vivo* tests using a murine model of critical-size calvarial defect (diameter: 8 mm).

5.2. MATERIALS AND METHODS

5.2.1. Materials

Poly (ε-caprolactone) (PCL_{raw}; 50 kDa) was purchased from Polysciences (Warrington, PA, USA) in the powdered form. Dexamethasone (DX; 99.9 % purity) and dexamethasone-21-phosphate (DS; 99.95 % purity) were from Fagron (Nazareth, Belgium) and Guinama (Valencia, Spain), respectively. Carbon dioxide (99.9 % purity) was supplied by Praxair Inc. (Madrid, Spain). Span 80 (HLB 4.3) was purchased from Sigma-Aldrich (Saint Louis, MO, USA). Paraffin oil and absolute ethanol (Emparta®, 99.5 % purity) were from Panreac (Castellar del Vallès, Spain) and Merck (Darmstadt, Germany), respectively.

5.2.2. Preparation of silk fibroin solution

For the preparation of silk fibroin, cocoons of *Bombyx mori*, obtained from silkworms reared in the sericulture facilities of the IMIDA (Murcia, Spain), were divided into 4 pieces and boiled in 0.02 M Na_2CO_3 for 30 min to remove the glue-like sericin proteins. Then, raw fibroin was rinsed thoroughly with water and dried at room temperature for 3 days. The extracted fibroin was dissolved in 9.3 M LiBr (Acros Organics, Spain) for 3 h at 60 °C to generate a 20 % w/v solution that was dialyzed against distilled water for 3 days (Snakeskin Dialysis Tubing 3.5 kDa MWCO, Thermo Scientific, USA) with 8 water exchanges. The resulting 8% w/v fibroin solution was recovered and filtered.

5.2.3. Preparation of silk aerogel microparticles (SA)

A water-in-oil emulsion was prepared from a mixture of paraffin oil and an aqueous SF solution (8 wt.%) in a 4:1 oil-to-water weight ratio. Span 80 was used as surfactant (3 and 6 wt.% with respect to the aqueous phase for emulsions #1 and #4, respectively) and added to the oil phase. The liquid-liquid mixture was homogenized using an ultrasound probe (450D, Branson Digital Sonifier, Nuevo Laredo, Mexico) with an amplitude of 50 % and for 2 min. The resulting emulsion was then magnetically stirred at 600 rpm for 5 h. As an alternative to the direct stirring of the emulsion, other gelation methods for SF were studied: portions of the 3 wt.% Span 80 emulsion were put either in contact with scCO$_2$ (80 bar, 35 ºC) bubbling (1 g/min) for 30 min (emulsion #2), or ethanol (1:10 ethanol-to-water content) was added prior to the stirring (emulsion #3).

After SF gelation and ageing for 5 h, the dispersed phase of the emulsion turn a gel and a dispersion of gel microparticles in the oil phase was obtained. These oil dispersions (dispersions #1 to #4) were then centrifuged (5804 R, Eppendorf, Hamburg, Germany) at 5,000 rpm for 5 periods of 15 min with the addition of ethanol after each centrifugation period to remove the oil phase and the water of the hydrogel particles to obtain alcogels. For dispersion #4, a fraction (denoted as #4a) was firstly washed with diethyl ether before the ethanol washing steps to ensure a complete removal of the emulsifier. SF aerogel microspheres (aerogels #1 to #4) were obtained by supercritical drying of the alcogels. Briefly, SF alcogels soaked in ethanol were dried under a scCO$_2$ (40 ºC, 120 bar) flow of 6 g/min during 3.5 h in a 100 mL-autoclave (Thar Technologies, Pittsburgh, PA, USA). A depressurization time of 70 min at a constant mass flow rate of 1 g CO$_2$/min was used until atmospheric pressure was reached. SF powders were collected from the autoclave for further use and analysis.

5.2.4. Preparation of scaffolds by supercritical foaming

The scaffold components in the form of dry powders were weighed in the proportions indicated in Table 5.1, physically mixed using a spatula and placed in Teflon cylindrical molds (internal

diameter: 17.0 mm; height: 24.6 mm) (Brand GmbH, Wertheim, Germany). The mixtures were manually compacted using a 17.0 mm-diameter flat aluminum plunger and then placed in a 100 mL-high-pressure stainless steel autoclave (Thar Technologies, Pittsburgh, PA, USA). The supercritical foaming was carried out following a pressurization-soaking-single depressurization stepwise protocol. The autoclave at 37 ºC was pressurized at 5 g/min of CO_2 up to 140 bar (i.e. supercritical conditions) and left under these conditions in the static mode for 1 hour (soaking period). Then, the autoclave was depressurized at a venting rate of 1.8 g/min until atmospheric pressure was reached. The scaffolds were stored overnight at room conditions to allow complete CO_2 desorption, before being weighed and the dimensions measured. The initial and final mass of the scaffolds were compared as a gravimetric method to determine the dexamethasone incorporation yields. The non-porous external layer of *ca.* 10 µm in the scaffolds, which is formed due to the faster diffusion of the CO_2 from the surface of the polymer matrix, was removed with a scalpel prior to further analysis.

Table 5.1: Notation and composition of the scaffolds (in weight percentage) containing poly(ε-caprolactone) (PCL), silk fibroin aerogel #4 (SA) and dexamethasone in the base (DX) and 21-phosphate (DS) forms, and processed by supercritical foaming (37 ºC, 140 bar).

Scaffold	PCL, wt.%	SA, wt.%	DX, wt.%	DS, wt.%
PCL	100	-	-	-
PCL-SA	90	10	-	-
PCL-SA-DX	89.9	10	0.1	-
PCL-SA-DS	89.9	10	-	0.1
PCL-SA-DXDS	89.9	10	0.05	0.05
PCL-SA-5DX	85	10	5	-
PCL-SA-5DS	85	10	-	5
PCL-SA-5DXDS	85	10	2.5	2.5

5.2.5. Structural and physicochemical characterization of the aerogel particles and the scaffolds

Textural properties of the silk aerogel particles were studied by low-temperature N_2 adsorption–desorption analysis (ASAP 2000; Micromeritics Inc.; Norcross, GA, USA). The aerogel powder was previously degassed at 70 ºC and under vacuum (<1 mPa) for 20 h. BET (Brunauer–Emmett–Teller) method was used to estimate the specific surface area (A_{BET}), whereas BJH (Barrett–Joyner–Halenda) method was chosen to calculate the mean pore diameter ($d_{p,BJH}$) and the specific pore volume ($V_{p,BJH}$).

Attenuated Total Reflectance-Fourier Transformed Infrared Spectroscopy (ATR-FTIR) was used to analyze the structural conformation of SF after processing the aerogel particles. Spectra were acquired on a Nicolet iS5 spectrometer, equipped with an iD5 ATR accessory (Thermo Scientific, Madison, WI, USA) controlled with OMNIC v9.3.30 software. Dried aerogels were placed directly onto the diamond window (*ca.* 2 mg) without further manipulation. Samples of silk fibroin nanoparticles *(Lozano‐Pérez et al. 2015)* and a lyophilized film of regenerated SF (after dissolution in LiBr 9.3M and further dialysis) *(Aznar-Cervantes et al. 2013)* were measured as references for the β-sheet structure and for a predominantly random coil and α-helix conformation of SF, respectively. Measurements were made in absorbance mode, in the 550-1800 cm^{-1} spectral range using 64 scans and at a resolution of 4 cm^{-1}. Spectra were focused on the 1800-800 cm^{-1} as the most significant range for SF conformation and N-B strong apodization and mertz phase correction were applied.

The particle size distribution and mean hydrodynamic diameter (Z-average) of the microgel precursor of the optimized silk fibroin aerogel were measured using a Zetasizer Nano ZSP instrument (Malvern Instruments Ltd., Worcestershire, UK) by dynamic light scattering. After high-power ultrasound treatment of the samples (3 min, 30% amplitude) using a Sonifier Branson 450D (Emmerson Ultrasonic Corporation, Danbury, CT, USA), all measurements were performed in purified water at 25 ºC, at 173º angle relative to the source and with a gel concentration of 0.5 mg/mL. Values were

calculated from the measurements performed in triplicate (12 runs per measurement).

Images of the outer morphology of the SF-aerogels and cross sections of the scaffolds were obtained by scanning electron microscopy (SEM, EVO LS15, Zeiss, Oberkochen, Germany). Aerogels were sputtered with a 10 nm-iridium layer prior to imaging with the aim of improving the contrast.

The scaffolds were measured and weighed to calculate their bulk density (ρ_{bulk}), and then their skeletal density (ρ_{skel}) was measured from five replicates by helium pycnometry (Quantachrome; Boynton Beach, FL, USA), operating at 25 ºC and 1.03 bar. The overall porosity (ε) of the scaffolds was calculated as follows:

$$\varepsilon = (1 - \rho_{bulk}/\rho_{skel}) \cdot 100 \qquad (5.1)$$

Mercury-intrusion porosimetry (MIP) analyses were used to determine the pore size distribution, open porosity (ε_{MIP}) and MIP-pore median of the scaffolds using a Micromeritics 9305 pore sizer (Norcross, GA, USA). MIP was operated with a 3 mL penetrometer for solids and using working pressures ranging from 0.07 to 1724 bar. MIP-cumulative curves were used to generate a 3D network model with similar percolation properties as those of the macrostructure of the scaffold using PoreXpert v.1.6.567 (PoreXpert Ltd, Plymouth, UK) software *(García-González et al. 2018)*. The estimation of the pore interconnectivity of the scaffolds from the generated 3D-models was performed using a Boltzmann-annealed simplex algorithm where values are proportional to the number of interconnections (i.e., throats) between pores. The infiltration capacity of mesenchymal stem cells (MSCs) in the scaffolds was simulated using the filtration module from PoreXpert software and assuming an average MSCs size of 26.5±5.0 µm *(Salerno et al. 2017)*. Water permeability (k_w at 25ºC, 1.03 bar) was modeled assuming a Poiseuille flow (water) in the z-direction as follows:

$$k_w = \frac{\pi}{8}\omega_{cell}(Farcs)\frac{l_{cell}}{A_{cell}} \qquad (5.2)$$

being ω_{cell}(Farcs) an averaging operator over the whole unit cell operating on the flow capacities of the pore throat-pore arcs parallels to the z-axis and calculated using the Dinic network analysis

algorithm; and l_{cell} and A_{cell} the length and the cross-sectional area of the unit cell, respectively.

Thermal properties of the scaffolds were evaluated by differential scanning calorimetry (DSC-Q100, TA Instruments; New Castle, DE, USA) performing two heating cycles under a nitrogen atmosphere with temperatures ranging from room temperature to 300 ºC and a cooling cycle down to -10 ºC in-between, using heating and cooling rates of 10 ºC/min. Crystallinity degree of PCL contained in the scaffolds (expressed in percentage) was calculated for each heating cycle using Eq. the following equation:

$$Crystallinity = \frac{\Delta H_m}{x \cdot \Delta H^0_{m,PCL}} \cdot 100 \qquad (5.3)$$

where *x* stands for the fraction (in weight) of PCL in the sample; ΔH_m, the melting enthalpy of the sample in the heating cycle in J/g; and $\Delta H^0_{m,PCL}$, the melting enthalpy of 100 % crystalline PCL (142 J/g) *(Tsuji and Ikada 1998)*.

5.2.6. Dexamethasone release tests

Scaffold pieces (250 mg) of PCL-SA-DX, PCL-SA-DS and PCL-SA-DXDS were immersed in 25 mL of phosphate-buffered solution (PBS) pH 7.4 medium. The flasks were placed in an oscillating shaker (Unitronic 320 OR, JP Selecta, Barcelona, Spain) at 37 ºC and 60 rpm for 3 weeks. Aliquots of 3 mL were sampled through that period at selected times, and the withdrawn volumes were replaced with fresh medium. Concentrations of dexamethasone base were measured by HPLC (Waters, Milford, MA, USA) consisting on a 717 plus Autosampler, a 600 Controller, and a 996 Photodiode Array Detector, equipped with a C18 column (Symmetry© C18, particle size 5 μm, 3.9 mm diameter x 150 mm length) from Waters (Milford, MA, USA), at 30 ºC and λ = 242 nm. Samples were filtered prior to analysis using 0.2 μm nylon filters to avoid potential interferences due to the presence of particles from the scaffolds. Calibration curve was obtained from triplicate dilution series of DX in PBS pH 7.4 in the 0.00005 to 0.0125 mg/mL concentration range ($R^2 > 0.999$).

Concentrations of DS and total dexamethasone were measured by UV–Vis spectrophotometry (8453, Agilent, Santa Clara, CA, USA) at

λ = 242 nm. Calibration curves were obtained from triplicate dilution series in PBS pH 7.4 in the 0.00125 to 0.01 mg/mL concentrations range ($R^2 > 0.99$).

The Higuchi model (Eq. 5.4)

$$D = B \cdot t^{0.5} \quad (5.4)$$

and a modified Higuchi model with an initial burst stage (Eq. 5.5)

$$D = A + B \cdot t^{0.5} \quad (5.5)$$

were fitted to the drug release profiles, D being the amount of dexamethasone released (in percentage with respect to the loaded amount) at time t, A the amount of dexamethasone released (in percentage) during the burst release period, and B the release rate kinetic coefficient (in dose % $h^{-0.5}$). The Akaike criterion was applied to select the best fitting model *(Akaike 1974)*. Kinetics fitting was performed using GraphPad Prism version 6.04 for Windows-GraphPad Software (La Jolla, CA, USA).

5.2.7. *In vivo* studies

Male Sprague-Dawley rats, with weights ranging from 250 to 300 g, were used for the *in vivo* studies. Experiments were previously approved by the local committee for animal studies of the University of La Laguna (Spain) and were carried out in conformity with the European regulation on care and use of animals in experimental procedures.

Surgery was performed under aseptic conditions using isoflurane for general anesthesia. A standardized, critical, circular defect (8 mm diameter) was created on the cranium of the rats to test the bone repair capacity of the scaffolds in a critical defect *(Rodríguez-Évora et al. 2013)*. The scaffolds were cut using a hollow punch with an internal diameter of 8 mm, and the resulting cylinders were sliced (1.5 mm height) to create the implants for *in vivo* tests and sterilized by UV-radiation for 1 h. The bone retrieved was replaced with the implants, the skin was repositioned over the area and stapled. Ketoprofen (3 mg/kg) and buprenorphine (0.05 mg/kg) were subcutaneously administered to lessen postsurgical pain. Upon recovery from the surgery, animals were allowed free activity, food and water uptake.

Five scaffold formulations (PCL, PCL-SA, PCL-SA-DX, PCL-SA-DS and PCL-SA-DXDS) were assessed regarding their bone inductive/regenerative effect, employing 5 groups of 6 rats each that were examined at 7 and 14 weeks after implantation. An additional group of 6 rats with an empty defect was used as surgical control and examined at the same time periods. After each period, 3 rats per group were sacrificed by CO_2 inhalation. The implants were retrieved, fixed (10 % formalin solution) and decalcified in Histofix® decalcifier (Panreac, Spain) and prepared for histological analysis *(Hernández et al. 2012)*. New bone formation and mineralization were identified by hematoxylin-erythrosin and VOF trichrome staining. In VOF staining sections, advanced mineralization areas appear colored in red, while less mineralized areas result in a blue coloration *(Diaz-Gomez et al. 2017)*. All sections per specimen were histomorphometrically evaluated by light microscopy (LEICA DM 4000B) followed by image analysis using the Leica QWin v3Pro software. The area of the tissue within the defect was defined as the region of interest (ROI) to quantify the new bone formation. The original defect area within the ROI was circular (50 mm^2 of area) and with the center being coincident with that of the defect site. New bone formation was accordingly calculated by using Eq. (5.6) and expressed as percentage of repair.

$$\%\, repair = \frac{new\ bone\ area}{original\ defect\ area\ within\ the\ ROI} \cdot 100 \qquad (5.6)$$

The number of ossification foci within the defect area was determined by counting the number of individual regions exhibiting bone extracellular matrix.

Radiography images of the extracted crania were performed with a Philips Optimus X-ray equipment, applying the parameters established in the protocol for the thumb of the human hand (5.2 kV, 1.5 mA/s, and 9.7 mSv and 1 m of distance).

5.2.8. Statistical analysis

An analysis of variance (one-way ANOVA, Tukey's multiple comparison) using a level of significance (p) of 0.05 was used to compare the data of the *in vivo* tests from different experimental

groups and at every individual time point (7 and 14 weeks) with SPSS v21.0 software.

5.3. RESULTS AND DISCUSSION

5.3.1. Silk aerogel particles preparation and optimization

The preparation of SF dry powder in the form of aerogels was herein developed to provide a nanostructured, highly porous and bio-based material with easy handling and dosing to be incorporated as a morphological modifier of the scaffolds in order to confer enhanced pore interconnectivity and surface roughness to the material. Aerogel production is a multi-step process requiring at least a gelation step and a drying step. This last step is commonly carried out by supercritical drying since it is the only one able to preserve the gel structure in the dry form *(García-González et al. 2012, Ulker and Erkey 2014)*. Previously, the gelation of SF in aqueous medium involved the self-assembly of the biopolymer into β-sheet structures *(Matsumoto et al. 2006)*.

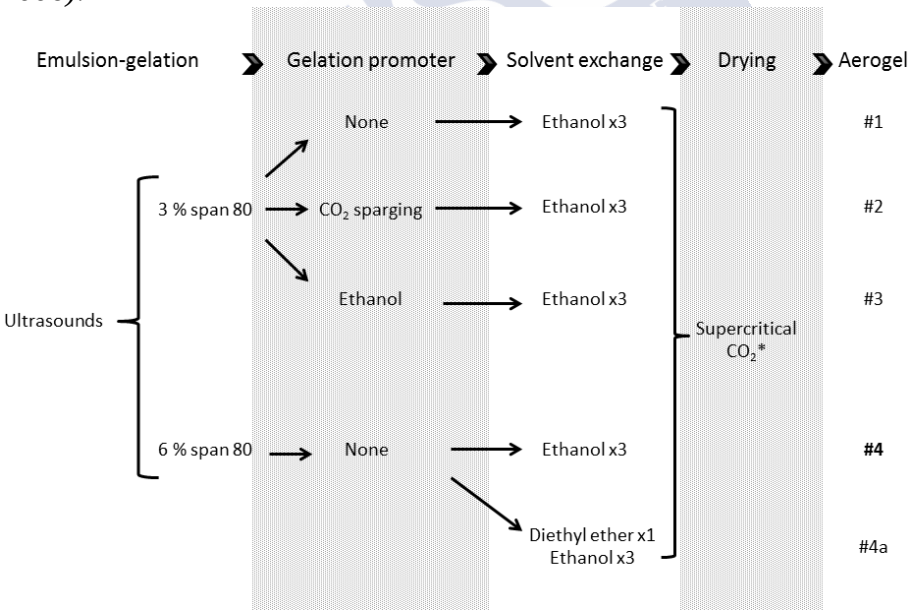

Fig. 5.1: Experimental conditions tested for the processing of SF aerogels. *The operating conditions for supercritical drying were 40 ºC, 120 bar and 6 g CO_2/min.

Different physical (pH, temperature, ionic strength, ultrasound) and chemical (cross-linkers, additives) mechanisms have been reported to induce the sol-gel transition of SF *(Floren et al. 2012, Dubey et al. 2015)*. Among them, ultrasonication has the advantage of rendering SF hydrogels under near neutral pH and room temperature whilst avoiding the use of additives (e.g., salts or chemical cross-linkers) and the derivatization of the SF *(Wang et al. 2008, Samal et al. 2013)*. Ultrasonication accelerates SF gelation by promoting the physical cross-linking of its β-sheets through changes in the hydration of the hydrophobic domains of the biopolymer chains *(Wang et al. 2008)*.

SF microgels were herein developed by water-in-oil emulsification-gelation (Fig. 5.1). Sonication was used for the preparation of the emulsion with the double role of providing mixing power for the emulsification process and of accelerating the SF gelation process. Paraffin oil was used as continuous phase due to its insolubility in water and the very low solubility of water in the oil thus discarding the gelification of SF by the diffusion method *(Baimark et al. 2010)*. After ageing for 5 h to ensure the complete gelation, the oil was removed by centrifugation from the microgels. The gel solvent was exchanged to ethanol, since this solvent is completely miscible with the drying agent ($scCO_2$). After supercritical drying, silk aerogel particles in the 0.3-5 μm range and predominantly spherical were obtained (Fig. 5.2).

The aerogel particles (#1) had internal porosity being partially coated by a layer of surfactant (Span 80) (Fig. 5.2b). The porosity of the SF aerogels was mainly mesoporous according to the obtained type IV-nitrogen adsorption-desorption isotherm and pore size distribution (Fig. 5.3). The obtained textural properties (#1 in Table 5.2) were higher than those reported for silk aerogel monoliths *(Mallepally et al. 2015)*, probably due to the higher SF concentration in the aqueous solution (8 wt.%) used in the present work as well as the different gelation mechanism applied (ultrasonication *vs.* acidification).

.

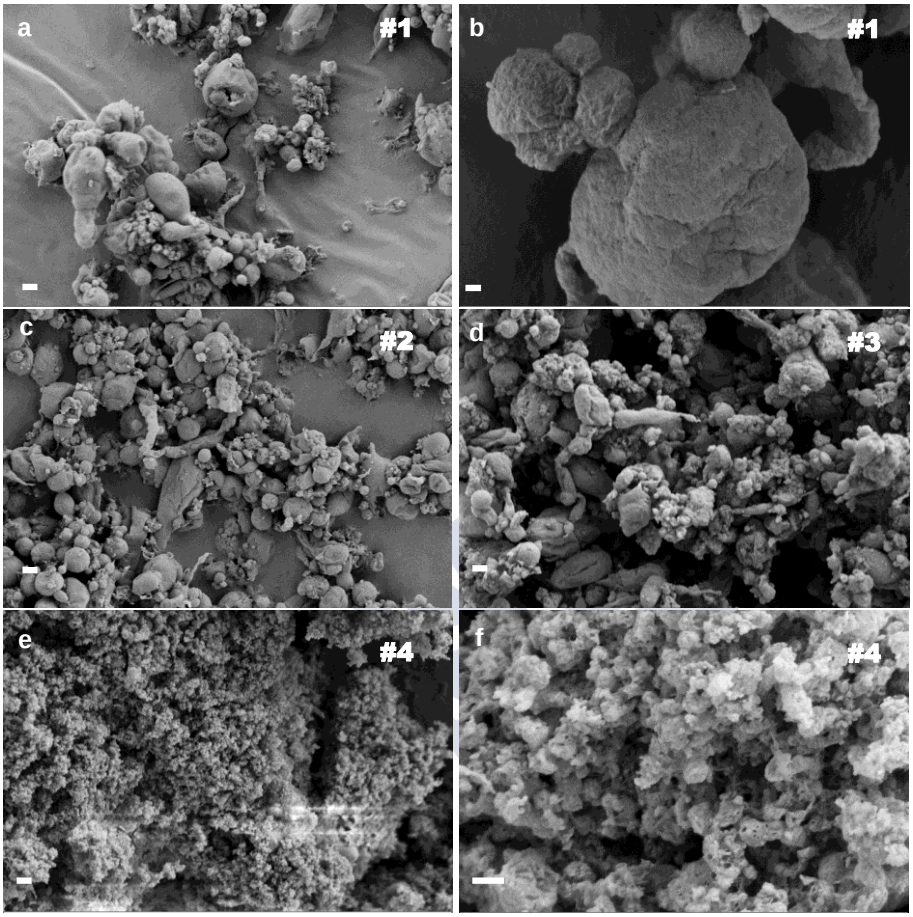

Fig. 5.2: SEM images of SF aerogel microparticles obtained from emulsion-gelification followed by supercritical drying process. Emulsification was carried out using ultrasounds for homogenization and Span 80 as surfactant at different concentrations ((a-d) 3, and (e,f) 6 % w/w). SF gelation was promoted by (a,b,e,f) ultrasonic treatment solely or combined with (c) compressed CO_2 (80 bar, 35ºC) bubbling, and (d) ethanol addition (1:10 ethanol-to-water volume ratio) after the emulsification. Scale bars: (a,c,d,e) 2 μm and (b,f) 200 nm.

The secondary structure in the aerogels was studied since the conformation of the peptide chains in the biopolymer determines the solubility and mechanical properties of the silk fibroin *(Hu et al. 2006)*. Thus, ATR-FTIR spectroscopy was selected to determine the conformation of SF peptide chains in the aerogel particles (Fig. 5.4).

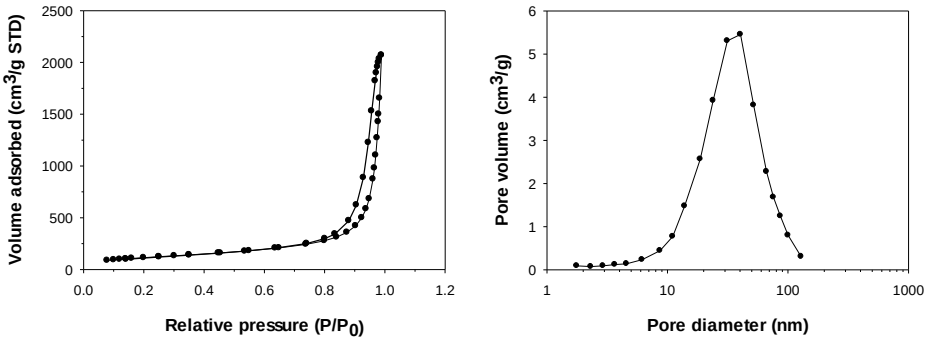

Fig. 5.3: Textural properties of silk aerogel particles #1 by N_2 adsorption-desorption analysis: (a) Type IV adsorption-desorption isotherm, and (b) BJH-pore size distribution

Table 5.2: Textural properties of SF aerogel particles processed under different gelation conditions.

Aerogel	A_{BET}, m^2/g	$V_{p,BJH}$, cm^3/g	$d_{p,BJH}$, nm
#1	429±21	3.21±0.16	24±1
#2	432±22	2.99±0.15	24±2
#3	462±23	3.29±0.16	23±1
#4	336±17	1.87±0.09	18±1
#4a	393±20	2.41±0.12	21±1

The obtained spectrum was compared to references of random coil conformation coupled to α-helix conformation (Fig. 5.4a) and of β-sheet structure (Fig. 5.4b) *(Zhang et al. 2007)*. β-sheet structures from the water insoluble Silk II were characterized by strong bands at 1627 and 1526 cm^{-1} corresponding to amide I and II regions, respectively (Fig. 5.4a). These bands contrast with the characteristic bands of the random coil at 1640 cm^{-1} and the α-helix conformation at 1514 cm^{-1} from amide I and II, respectively *(Wang et al. 2004, Hu et al. 2006, Aznar-Cervantes et al. 2013)*, in the spectrum of the lyophilized SF (Fig. 5.4b). Structural changes took place during the preparation of SF aerogel #1 as reflected in the ATR-FTIR spectrum (Fig. 5.4c). The peak of the amide I region shifted to lower wavenumbers as a consequence of the transformation from the

random coil state in the silk solution to the highly crystalline β-sheet conformation in the particles. Overall, ATR-FTIR results show that the SF aerogel processing allowed the complete transition from random coil to β-sheet conformation of the silk peptides and thus the material is physically stable and water insoluble *(Lozano‐Pérez et al. 2015).*

Ultrasonication-induced gelation was coupled with other gelation promoters to evaluate their combined effect on the resulting aerogel

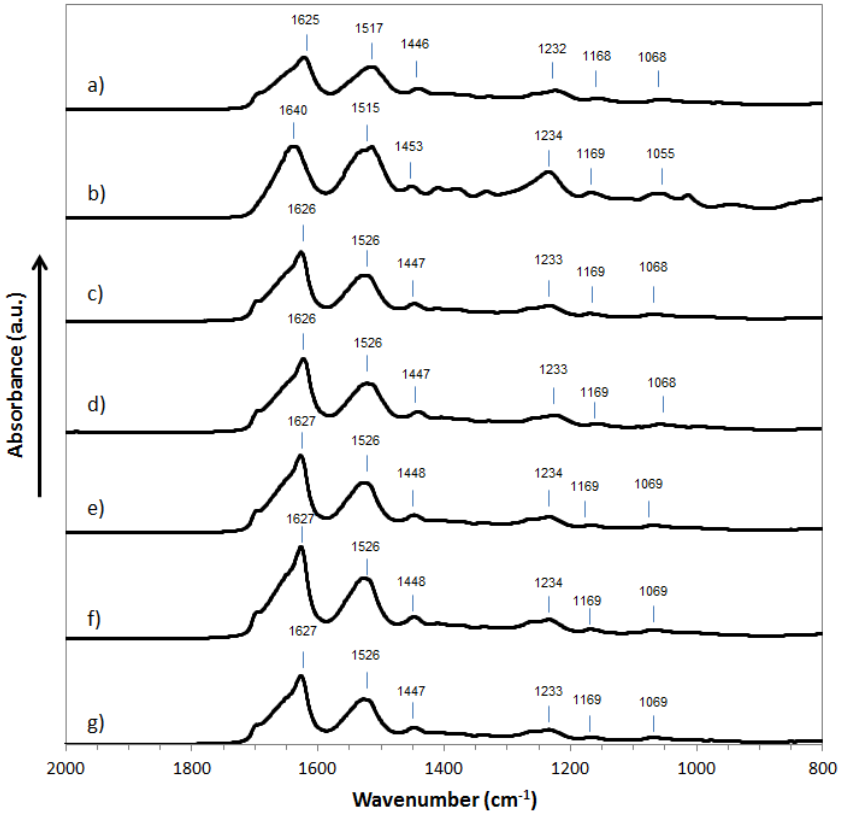

Fig. 5.4: ATR-FTIR spectra of silk fibroin particles: (a) SF nanoparticles (reference of ß-sheet structure), (b) lyophilized SF after dissolution in 9.3M LiBr and dialysis (reference of predominantly random coil structure), and SF-aerogels (c) #1, (d) #2, (e) #3, (f) #4 and (g) #4a.

properties (Fig. 5.2). The ultrasonic treatment accelerates the silk fibroin gelation but there is still a lag time between the end of the mixing process and the gel formation *(Wang et al. 2008)*. CO_2- and ethanol- assisted gelation were used during this lag time to promote the formation of gel particles in the internal phase of the emulsion.

The CO_2-assisted gelation mechanism is a straightforward method of gelation with no need for post-purification processes *(Mallepally et al. 2014)*. Gelation by bubbling of CO_2 was previously reported to be dependent on the SF molecular weight and concentration in the aqueous solution as well as on the CO_2 diffusion kinetics and CO_2-solution contact time. Compressed CO_2 (80 bar, 35 ºC) was bubbled through the SF-containing emulsion at a flow rate of 1 g/min for 30 min to accelerate the CO_2 diffusion process. After depressurization for CO_2 removal and further aerogel processing steps, SF aerogel particles were obtained. The resulting aerogels (#2) had similar secondary structure (Fig. 5.4) and textural properties (Table 5.2) as the aerogels obtained without the CO_2 treatment (#1), but they were more spherical and smaller (Fig. 5.2c) likely due to the homogenizing effect of bubbling in the SF aerogel particle morphology and to reduce their coalescence.

The ethanol-assisted gelation mechanism exploits the miscibility with water to promote gelation through the partial dehydration of the hydrophobic domains of SF *(Moraes et al. 2015)*. The addition of ethanol in a 1:10 volume ratio with respect to the water amount in the emulsion accelerated the SF gelation process as observed by the faster precipitation of the gel particles. After aerogel processing, the resulting particles (#3) had similar secondary structure (Fig. 5.4) and textural properties (Table 5.2) as the ones without post-sonication treatment (#1) but with a broader particle size distribution as well as with the presence of dimples in the surface (Fig. 2d). The changes in particle morphology were related to a two-way mass transfer involving ethanol diffusing into the water droplets of the dispersed phase of the emulsion and the water diffusing out from the said droplets. The formation of deformed SF-gel particles with hollows and dimples were already reported using other organic solvents (ethyl

acetate and diethyl ether) *(Baimark et al. 2010)*. Overall, CO_2- and ethanol-assisted gelation strategies did not improve the SF-aerogel textural properties obtained by ultrasonication-induced gelation. Moreover, an additional step was required in the former strategies to obtain aerogel particles with similar β-sheet structure. Therefore, for the sake of the economy of the process, the SF-gelation by sonication and without further post-gelation treatment was selected for aerogel processing.

Aerogel particle size obtained by emulsion-gelation methods is mainly tuned by the surfactant content used *(García-González et al. 2011)*. Accordingly, higher Span 80 concentration (6 wt.%) led to smaller particles (< 1 μm) and slightly lower textural properties (#4 in Table 5.2). The particle size of the microgel precursor of aerogel particles #4 was of 279±3 nm (Fig. 5.5) and the ζ-potential was of -32.7±0.8 mV according to the zeta potential measurements. A similar or slightly lower particle diameter was obtained for aerogels (Fig. 5.2e,f) due to a limited shrinkage usually taking place during the supercritical drying *(García-González et al. 2011)*. The reduction in particle diameter of SF aerogels #4 to sub-micron sizes with a higher content of surfactant (Span 80) was related to the decrease in the surface tension in the oil/water interface, as was already observed for other biopolymer-based aerogel particles *(García-González et al. 2011, García-González et al. 2012)*. Remaining surfactant molecules in the aerogel structure might result in the reduction in specific surface area (A_{BET}), specific pore volume ($V_{p,BJH}$) and mean pore diameter of SF aerogel particles. To confirm this hypothesis, the surfactant in the gel was removed using diethyl ether, i.e. a solvent for Span 80 and a non-solvent for silk fibroin, before supercritical drying and thus resulted in aerogel #4a with improved textural properties (Table 5.2). Aerogel particles #4 were chosen for scaffold processing (denoted as SA) instead of aerogels #1 since they had smaller particle sizes that resulted in a superior external surface area and in a more homogeneous distribution of the aerogels in the scaffolds. Moreover, aerogels #4 have shown higher Span 80 content, which is a non-ionic surfactant that favors the interaction between the hydrophilic silk fibroin and the hydrophobic matrix of PCL *(Goimil et al. 2017)*.

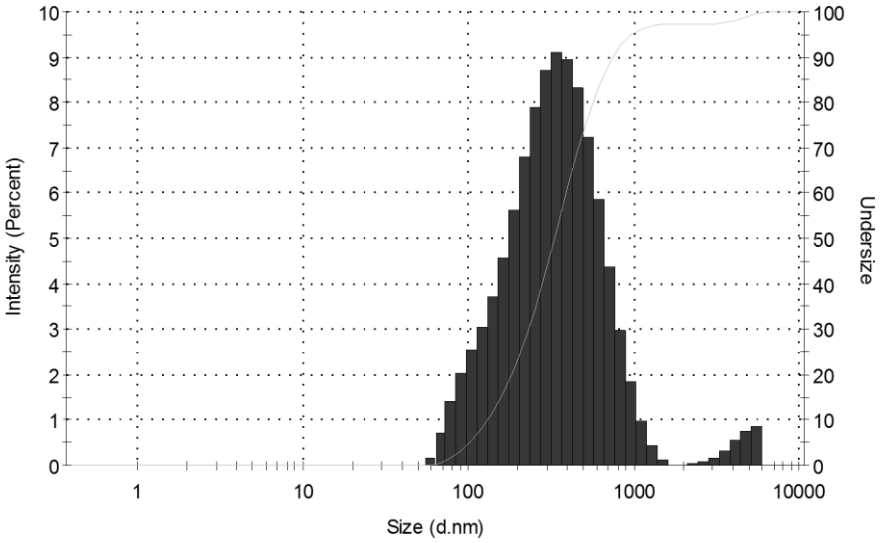

Fig. 5.5: Histogram (dark gray bars, in intensity) and cumulative undersize (gray line, in percentage) of size distribution of silk aerogel particles #4 by dynamic light scattering.

5.3.2. Scaffolds preparation and characterization

Scaffolds were processed using the supercritical foaming process since it is a unique green approach to obtain highly porous polymeric scaffolds incorporating bioactive agents with high incorporation yields and retained activities *(García-González et al. 2015)*. The choice of scCO$_2$ as foaming agent of scaffolds was due to its plasticizing effect in several biopolymers, including PCL *(Kelly et al. 2012, Curia et al. 2015)*, coupled to its GRAS status *(García-González et al. 2015)*. The quadrupole moment of CO$_2$ favors the CO$_2$-polymer interaction leading to high CO$_2$ sorption within the polymer and reduced intermolecular bonding between polymeric chains *(Fanovich and Jaeger 2012, Curia et al. 2015, Goimil et al. 2018)*. As a result, the plasticizing effect of compressed CO$_2$ significantly increases the mobility of the polymer chains, depletes the glass transition and melting temperatures of the polymer and reduces the viscosity of the polymer *(Kelly et al. 2012, Curia et al. 2015, García-González et al. 2015)*. In the case of PCL, the supercritical foaming process liquefies

the polymer at temperatures below its melting point and allows the thermal processing of this polyester at relatively low temperature (37 ºC) and mild pressure (140 bar) compatible with thermally sensitive compounds like dexamethasone among others *(Fanovich and Jaeger 2012, Diaz-Gomez et al. 2017, Goimil et al. 2017, Xin et al. 2018)*. Moreover, supercritical foaming is a solvent-free approach that avoids usual problems of cytotoxicity of scaffolds processed with organic solvents prior to implantation. Supercritical foaming did not alter the textural properties of the aerogel particles present in the formulation as also observed in other processes involving aerogels and $scCO_2$ atmospheres, e.g., supercritical impregnation *(García-González et al. 2015)*. Despite the low (for DX and DS *(Chim et al. 2012, Tang et al. 2014)*) or null (for SA) solubility of the admixtures in $scCO_2$, the compressed fluid favored the dispersion of the aerogel particles and the dexamethasone throughout the scaffold matrix during the supercritical foaming (Fig. 5.6). On other hand, supercritical impregnation of the aerogels with dexamethasone is not expected to take place during the foaming process due to the low solubility of the drug in $scCO_2$ *(Knez et al. 2018)* and the mild pressure and temperature conditions used in the foaming process. Finally, macropores in the 100-300 µm range can be obtained with this technique in the absence of salts as porogens, so that a leaching step leading to not only porogen removal but also bioactive agent washing was avoided and higher incorporation yields (close to 100%) were achieved if compared to the salt leaching scaffold processing (typically lower than 45 % *(Xin et al. 2018)*).

Scaffolds with attractive morphological properties were obtained by using the supercritical foaming technology (Table 5.3 and Fig. 5.6). Scaffolds had a cylindrical shape and a high porosity in the 56-63 % range (Table 5.3). Namely, PCL scaffolds had pores in the 100-200 µm range with a smooth surface (Fig. 5.6a,b) and fairly interconnected (Table 5.3). The presence of SF aerogels (SA) in the scaffolds (PCL-SA) had a noticeable impact on the morphology of the material. The intrinsic light weight of aerogels (*ca.* 85-95 % porosity) contributed to the increase in the porosity of the scaffolds. PCL-SA scaffolds showed

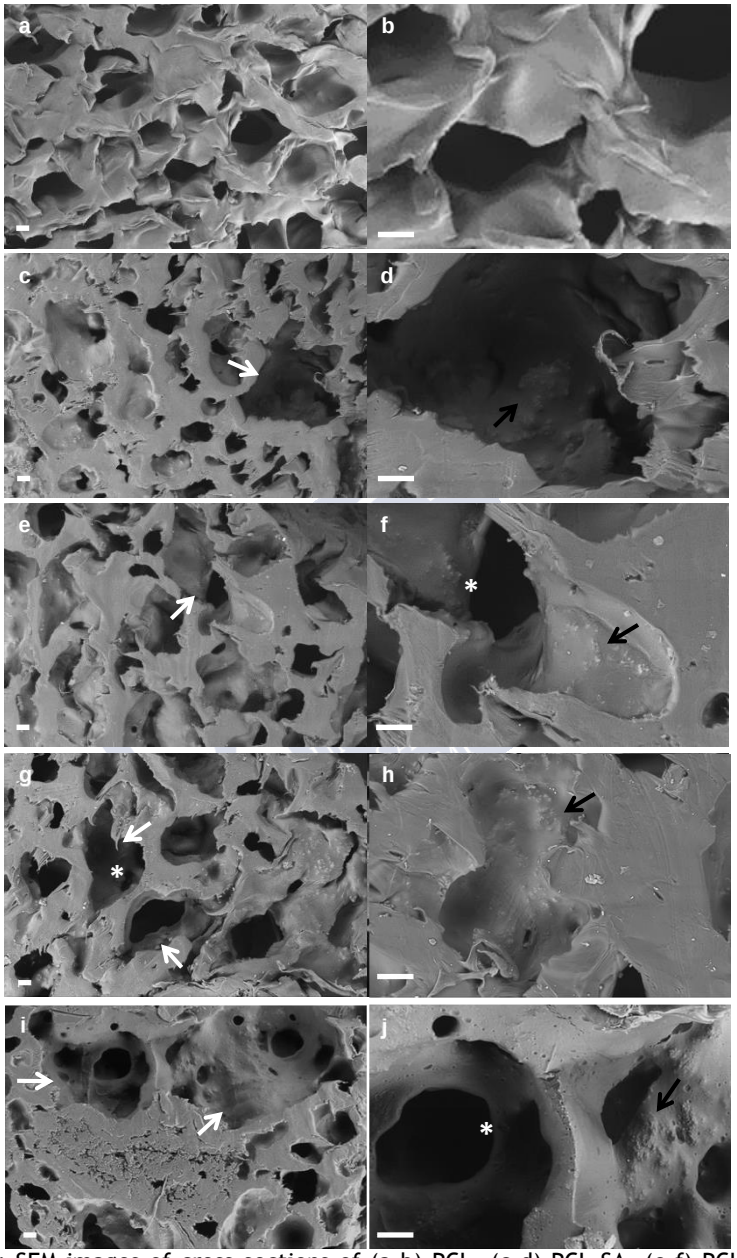

Fig. 5.6: SEM-images of cross sections of (a,b) PCL, (c,d) PCL-SA, (e,f) PCL-SA-DX, (g,h) PCL-SA-DS, and (i,j) PCL-SA-5DX scaffolds. The smooth pore surfaces of PCL scaffolds (a) turn rougher with the presence of silk fibroin aerogel particles in the formulation (d,f,h). Scale bar: 100 µm.

increased sizes of the macropores to values between 150 and 400 µm as unveiled by SEM imaging (Fig. 5.6c,d), falling in the optimum size range for cell ingrowth *(Paul and C.P 2015)* and suitable for angiogenesis. This visual perception was confirmed by the increased discrepancy between the overall porosity ε and the porosity obtained by MIP ε_{MIP} in PCL-SA scaffolds (Table 5.3), which is attributed to the increased amount of pores larger than the maximum measurable pore size by the apparatus (200 µm) with the presence of the aerogel. Finally, the pore surface roughness was increased with the use of aerogel particles in the scaffold formulations and was related to a preferential location of the aerogels close to the pore surface. Aerogels might act as secondary pore nucleation sites during the foaming process *(Collins et al. 2008, de Matos et al. 2013, Goimil et al. 2017)*, thus explaining the topographical distribution of the aerogels throughout the scaffold. This increase in surface roughness of the scaffolds can favor the attachment and proliferation of cells since there are more anchoring sites in the scaffolds for surface adhesion protein receptors of cells like integrins *(Xia et al. 2016)*.

The morphological modifications in the scaffolds with the incorporation of dexamethasone were dependent on the added amount, regardless of the drug form (base or salt) used. At low drug contents (0.1 wt.%), a synergistic effect between the aerogels and the drug took place and the macropores presented larger sizes (Fig. 5.6e-h). Pore sizes are defined during the depressurization stage of the foaming process where pore growth is facilitated by a lower mechanical resistance to the expansion of the polymeric matrix. The increase in the pore sizes of PCL foams with the presence of dexamethasone was also previously reported *(Duarte et al. 2018)* and might be related to the fact that dexamethasone can act as a plasticizer favoring the pore growth in the polymeric matrix. High dexamethasone contents (5 wt.%) in the scaffolds resulted in similar porosities than the PCL scaffolds, although with higher pore medians and pore interconnectivities. The plasticizing effect of the dexamethasone might explain the high pore medians with high interconnectivities observed for PCL-SA-5DX, PCL-SA-5DS and PCL-SA-5DXDS scaffolds. However, dexamethasone acts as a plasticizer up to certain

content and then the remaining drug fraction forms aggregates (Fig. 5.6i,j) with low interaction with the polymeric matrix. The second drug fraction reduces the overall porosity since it increases the bulk density by providing weight and non-foamability (dexamethasone itself has no foamability under $scCO_2$). The addition of SA increased the pore surface roughness (black arrows), pore size (white arrows) and pore interconnectivity (asterisks). The incorporation of dexamethasone dose-dependently incremented pore size.

The scaffolds intended for bone regeneration should have morphologies able to facilitate the accessibility and penetration of cells as well as an adequate permeability of biological fluids for the supply of nutrients and metabolic products and the transport of wastes into or from the cells *(Otsuki et al. 2006, García-González et al. 2015)*. Scaffolds with suitable porosity and pore size would not facilitate tissue growth and transport of fluids if they were not endowed with proper pore interconnectivity properties. The pore interconnectivity properties of a scaffold should take into account the number of connections between pores (i.e., throats) as well as the sizes of the throats and their distribution throughout the scaffolds *(Otsuki et al. 2006)*. These properties would significantly influence a proper colonization and spread of cells (i.e. cell infiltration and tissue integration) and the starvation of cells. Despite the pore interconnectivity in the PCL scaffolds being acceptable, the sizes of the throats are low thus hampering water permeability (k_w) and avoiding cell infiltration for MSCs (Table 5.3). The morphological properties obtained for PCL scaffolds containing SF aerogels played a key role in getting promising water permeabilities (*ca.* 10^{-11}-10^{-12} m^2) and cell infiltration capacities (close to 90-95 %) for bone regeneration. The pore interconnectivity properties of the scaffolds containing dexamethasone (PCL-SA-DX, PCL-SA-DS, PCL-SA-DXDS, PCL-SA-5DX, PCL-SA-5DS and PCL-SA-5DXDS) were of the same order of magnitude and similar to those of PCL-SA scaffolds.

Table 5.3: Structural properties of the PCL-based scaffolds and evaluation of their morphology for cell and aqueous fluid transport. Notation: ρ_{bulk}: bulk density; ρ_{skel}: skeletal density; ε: overall porosity; ε_{MIP}: porosity obtained by MIP, and k_w: water permeability.

Scaffold	ρ_{bulk}, g/cm^3	ρ_{skel}, g/cm^3	ε, %	ε_{MIP}, %	*MIP-Pore median*, µm	*Interconnectivity*, %	k_w,$x10^{12}$ m^2	*Cell infiltration*, %
PCL	0.428±0.006	1.126±0.015	56.4±2.4	48.7	37.4	81.8	<10^{-5}	0
PCL-SA	0.407±0.018	1.059±0.033	61.5±1.7	46.8	70.1	94.0	3.390	91
PCL-SA-5DX	0.464±0.007	1.088±0.018	56.1±0.8	49.6	76.9	87.0	4.712	89
PCL-SA-5DS	0.478±0.009	1.115±0.021	57.3±0.7	47.5	70.8	92.3	5.132	90
PCL-SA-5DXDS	0.468±0.009	1.100±0.027	57.4±0.8	46.6	94.8	89.5	11.358	93
PCL-SA-DX	0.408±0.038	1.060±0.033	61.5±3.6	30.2	77.1	81.8	4.568	93
PCL-SA-DS	0.392±0.004	1.059±0.013	63.0±0.4	35.1	84.1	83.8	12.591	95
PCL-SA-DXDS	0.406±0.005	1.060±0.034	61.7±0.5	32.1	85.2	83.8	11.030	91

The effect of the processing and the composition on the end properties of the foamed scaffolds was evaluated by DSC analysis (Table 5.4). Two heating cycles were used in the DSC-thermograms where the first cycle reflects the effect of the structuration process (thermal history) and the second one indicates the interactions among the components *(Androsits 1999)*. During the supercritical foaming process, PCL is firstly molten in contact with compressed CO_2 and then recrystallized during the CO_2 depressurization *(Fanovich and Jaeger 2012)*. In this work, the slow depressurization rate used for the preparation of the scaffolds (1.8 g CO_2/min) particularly promoted the growth of the PCL crystals, and thus the melting temperature of the PCL scaffolds (T_m) increased with respect to the PCL raw material (PCL_{raw}). This effect of processing on crystallization was confirmed with the results from the second DSC-heating cycle where the melting points (T'_m) of PCL_{raw} and the PCL scaffolds were similar.

Table 5.4: Influence of the foaming process and the composition on the thermal properties of the scaffolds

	1st heating cycle			2nd heating cycle		
Scaffolds	T_m (ºC)	ΔH (J/g)	Crystallinity (%)	T'_m (ºC)	ΔH' (J/g)	Crystallinity (%)
PCLraw	63.1	119.6	84.2	55.9	63.4	44.6
PCL	65.4	63.8	44.9	55.8	60.3	42.5
PCL-SA	67.3	67.0	52.4	57.7	49.9	39.0
PCL-SA-DX	65.3	68.6	53.7	56.1	50.0	39.2
PCL-SA-5DX	66.3	71.3	59.1	55.5	52.7	43.7
PCL-SA-DS	65.3	59.5	46.6	55.8	43.6	34.2
PCL-SA-5DS	67.0	64.2	53.2	55.3	43.6	36.1
PCL-SA-DXDS	66.2	67.3	52.7	56.1	46.6	36.5
PCL-SA-5DXDS	65.3	64.1	53.1	55.1	44.9	37.2

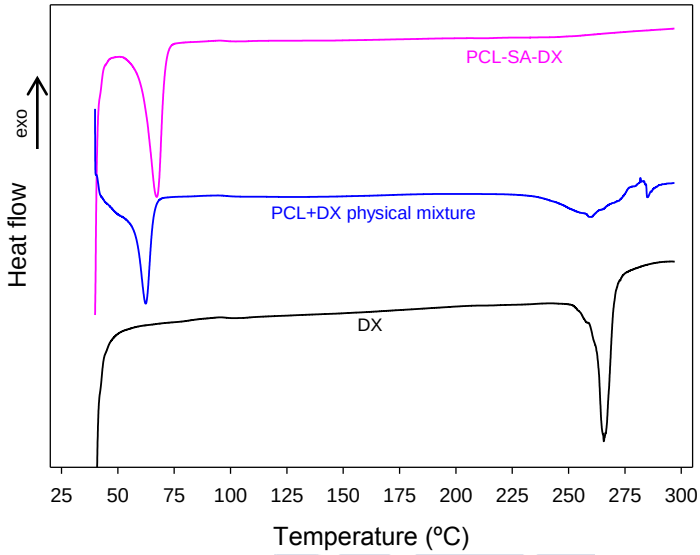

Fig. 5.7: DSC thermograms of pure dexamethasone (bottom), PCL:DX physical mixture (1:1 weight ratio, middle) and PCL-SA-DX scaffold (top).

The presence of SF aerogels and dexamethasone in the formulations changed the crystallinity of PCL in the scaffolds (Table 5.4). Crystallinity and T_m shifted towards higher values in PCL-SA scaffolds with respect to PCL scaffolds, i.e. with and without SF aerogels, respectively, which suggested that the SF aerogels promoted PCL crystallization in the scaffolds upon the foaming process as well as crystal growth. The latter effect was related to the β-sheet conformation of SF in the aerogels that favors the formation of PCL crystals with a fibrillar structure *(Li et al. 2011, Vacanti et al. 2012).* Higher melting temperatures T_m' were also obtained for PCL-SA scaffolds in the second heating cycle thus sustaining the hypothesis of the PCL-SF interaction. A certain interaction between dexamethasone and PCL also took place in the drug-loaded scaffolds (PCL-SA-DX, PCL-SA-DS, PCL-SA-DXDS, PCL-SA-5DX, PCL-SA-5DS and PCL-SA-5DXDS) resulting in changes in the melting point of PCL. The presence of dexamethasone in either of the tested forms (base or salt) counteracted the effect of the aerogel particles on T_m and the values (0.3-2.0 ºC) were lower in all cases. The absence of the melting

peaks of DX and DS in the thermograms of the scaffolds (Fig. 5.7) suggests that dexamethasone-PCL interactions might take place at a molecular level as molecular dispersions of dexamethasone in polyester-based formulations *(Vaishya et al. 2014, Xin et al. 2018).* The formation of this molecular dispersion can be explained by the melting of the polymer to a liquid-like state during the supercritical foaming coupled to the role of $scCO_2$ as a dispersing or mixing agent of admixtures in polymeric matrices *(de Matos et al. 2013).*

5.3.3 Dexamethasone release

Several strategies (encapsulation, adsorption, entrapment) have been proposed for the incorporation of bioactive agents in bone scaffolds, but the optimization of their release kinetics for effective clinical uses is actively prospected *(Mouriño and Boccaccini 2010, Romagnoli et al. 2013, Rambhia and Ma 2015).* In this work, the entrapment of a bioactive agent (dexamethasone) in two different forms (DX and DS) was attempted to modulate its release kinetics. The dexamethasone release patterns from the drug-loaded scaffolds used in the *in vivo* tests (cf. Section 5.3.4) were recorded in PBS pH 7.4 medium (Fig. 5.9). All formulations attained high rates of drug release after three weeks, with payloads of 85-100 % of the initial drug; however, the release profile was strongly influenced by the dexamethasone chemical state. Scaffolds containing DS showed a two-stage release consisting on a burst release during the first hour followed by a sustained release in the following three weeks. The burst was more significant in PCL-SA-DS than in PCL-SA-DXDS scaffolds, which is linked to a higher content in DS of the former. Conversely, more sustained release was observed for the scaffolds containing only DX (PCL-SA-DX). These differences in the release profiles can be related to both the different solubility of the dexamethasone forms in the aqueous medium (0.16 mg/ml for DX *(Jóhannesson G. et al. 2016)* and freely soluble for DS *(Conseil de l'Europe 2008)*) and the different dexamethasone-polymeric matrix interactions depending on the drug form (PCL-DS and PCL-DX binding energies of -7.41 and -8.91 kJ/mol, respectively).

Drug release from the scaffolds containing DX (PCL-SA-DX) fitted well to the Higuchi equation (Eq (5.4) in Table 5.5), indicating that the drug release mechanism was mainly governed by diffusion of the solubilized drug molecules through the porous matrix. The absence of a burst for these scaffolds was confirmed by the low A-value ($<10^{-15}$ %) obtained when the modified Higuchi model (Eq. (5.5)) was applied. According to the Akaike criterion, the modified Higuchi equation was the best model to fit the drug release profile of the scaffolds containing dexamethasone in the form of phosphate salt or the mixture of both DX and DS forms (PCL-SA-DS and PCL-SA-DXDS). The key role of DS during the burst was confirmed by the

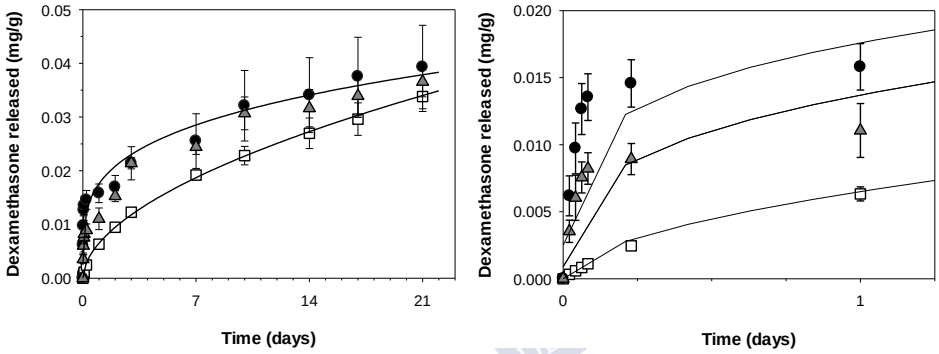

Fig. 5.9: Drug release profiles from PCL-SA-DX (squares), PCL-SA-DS (circles) and PCL-SA-DXDS (triangles) scaffolds containing 0.1 wt.% of dexamethasone in PBS pH 7.4 at 37 °C and 60 rpm for 21 days (left) and close up of the profiles during the first day (right). Lines correspond to the best fitting of experimental data based on Higuchi release kinetics models (Eq. (5.4) for PCL-SA-DX and Eq. (5.5) for PCL-SA-DS and PCL-SA-DXDS as showed in Table 5.5).

fact that the amount of drug released during this step (A-value in Table 5.5) for PCL-SA-DS scaffolds was higher than for PCL-SA-DXDS scaffolds and in a similar ratio to the drug salt weight content for each scaffold formulation. Finally, DS accelerated the drug release rate from the scaffolds since the kinetic coefficient B increased with the drug salt content (i.e. PCL-SA-DS > PCL-SA-DXDS > PCL-SA-DX). Overall, PCL matrices have low hydrophilicity and very slow degradation and erosion rates (in the order of months *(Diaz-Gomez et al. 2017)*) and behave as inert matrices in the drug release medium,

thus explaining the good fitting of the drug release profile to the proposed Higuchi models.

The two-stage release profile obtained for DS-containing scaffolds seems the most promising strategy for bone repair purposes.

Table 5.5: Kinetic fitting parameters of the dexamethasone release profiles from PCL scaffolds containing silk fibroin aerogels in PBS pH 7.4 medium. Values highlighted in bold correspond to the best fitting model for each scaffold formulation applying the Akaike criterion.

Scaffold	Higuchi (Eq. (4))		Higuchi with burst (Eq. (5))		
	B, dose %·$h^{-0.5}$	R^2	A, dose %	B dose %·$h^{-0.5}$	R^2
PCL-SA-DX	**3.89±0.05**	**0.995**	$<10^{-15}$	3.89±0.08	0.995
PCL-SA-DS	6.47±0.33	0.631	**31.16±3.38**	**4.47±0.29**	**0.971**
PCL-SA-DXDS	5.16±0.17	0.883	**15.29±1.77**	**4.17±0.15**	**0.977**

The burst period would be effective in providing a first drug dose at therapeutic levels in the defect site shortly after implantation. Then, the sustained drug release during the second stage would preserve a certain local concentration of the drug in the following weeks.

5.3.4 *In vivo* histological/histomorphometrical results

The effect of the dexamethasone loading in the scaffolds was tested *in vivo* in critical-size calvarial bone defect to unveil the compatibility of the grafts with the bone tissue and their capacity to promote bone tissue formation. The dexamethasone required in the scaffolds was estimated at 0.032 wt.% for the implant disks of 30 mg each, by taking into account the dexamethasone concentration needed to stimulate osteogenic differentiation (100 nM *(Nuttelman et al. 2006)*), the density of a rat (*ca.* 1.025 g/mL *(Hohl et al. 2007)*) and considering an homogenous distribution of the dexamethasone in all the tissues of the animal. Moreover, the drug release profile and clearance that would lower the effective local concentration should be also taken into account to establish the dexamethasone dose in the scaffold formulation. Pilot studies using scaffolds with high doses of dexamethasone (5 wt.%) were performed but animals experimented adverse effects compatible with an intoxication with dexamethasone and 2 out of the 9 rats died 7 days post-implantation, despite the drug concentration being below the LD50 for rats (14 mg/kg). Accordingly,

a dexamethasone content of *ca.* 0.1 wt.% was set for the formulations of the scaffolds in the form of disks to ensure that therapeutic drug levels are achieved and toxicity events are prevented during the *in vivo* tests.

In the *in vivo* tests with the control group (i.e. animals with empty defect), a fibrous capsule surrounding the defect area was not observed. For these animals, repair zones were only observed in the margins of the defect 7 and 14 weeks post-implantation (Fig. 5.9a,b), being more extensive after 14 weeks (Fig. 5.9b,k). The presence of ossification foci in the center of the defect area was not observed in this group.

The analysis of the scaffolds showed an excellent compatibility of the implanted materials (PCL, PCL-SA, PCL-SA-DX, PCL-SA-DS and PCL-SA-DXDS) with the host tissue, with no signs of inflammation or rejection being observed at any time of analysis. In all specimens, the defect area was clearly delimited by a fibrous capsule of dense connective tissue indicating the presence of a tissue-material transition zone (Fig. 5.9c-l). The presence of the scaffolds also favoured the tissue repair throughout the defect and, unlike in the control group, foci of intramembranous ossification were observed within the defect area in all the implanted experimental groups, at both time points of analysis (Fig. 5.9c-l). The presence of the scaffold accelerated the tissue repair since they guided and promoted the cell attachment and colonization at different regions of the defect as well as the formation of extracellular matrix. This hypothesis is sustained by the presence of the scaffolds near or directly in contact with tissue elements in most of the cases (Fig. 5.9n-p). For the groups implanted with PCL and PCL-SA scaffolds, few and incipient ossification foci were observed at 7 and 14 weeks post-implantation (Fig. 5.9c-f,t) and characterized by dense accumulations of extracellular matrix, mainly collagen fibers surrounded by hypertrophic osteoblasts (Fig. 5.9n,o). The PCL-SA-DX scaffold group presented a discrete increase in the number of ossification foci at 7 and 14 weeks post-implantation with respect to the PCL and PCL-SA scaffold groups (Fig. 5.9g,h,t). The newly formed bone in the PCL-SA-DX scaffold group was immature with osteocytes-like cells trapped in an extracellular matrix of loose

and porous appearance (Fig. 5.9p). Significantly higher response of PCL-SA-DS scaffold group than the PCL, PCL-SA and PCL-SA-DX scaffold groups was observed at 7 and 14 weeks post-implantation (Fig. 5.9i,j,s). In this group (PCL-SA-DS), the number of ossification foci was greater at 7 weeks than at 14 weeks (Fig. 5.9i,j,t) due to the increase of the surface area and the confluence of these foci (Fig. 5.9j). The newly formed bone in this group presented a compact appearance and characteristics of mature bone (Fig. 5.9q). The group containing the PCL-SA-DXDS system showed a reparative response similar to the PCL-SA-DX group with slightly lower ossification foci and of larger size at 7 than at 14 weeks post-implantation (Fig. 5.9k,l,t). In the PCL-SA-DXDS scaffold group, the newly formed bone presented intermediate characteristics between the PCL-SA-DX and PCL-SA-DS groups, with regions of compact appearance that are surrounded by regions of loose appearance (Fig. 5.9r). Scaffolds were still present in the defect site 14 weeks post-implantation in all the cases, since the degradation of the main component of the scaffolds (i.e. PCL) takes place in a timeframe of several months *(Diaz-Gomez et al. 2017, García-González et al. 2018)*. The histomorphometric analysis showed that the groups treated with the scaffold formulations containing dexamethasone (PCL-SA-DX, PCL-SA-DS and PCL-SA-DXDS) had repair percentages between 19 % and 39 %, which are significantly higher than the PCL and PCL-SA scaffold groups at the two tested time periods (Fig. 5.9s). Likewise, the best repair response was observed in the group treated with DS (PCL-SA-DS), significantly higher than in the groups treated with DX (PCL-SA-DX) and the combination of DX and DS (PCL-SA-DXDS). A good correlation between the number of ossification foci and the repair data was observed (Fig. 5.9t). Different bone ingrowth can be detected in the X-ray radiographies 7 weeks post-implantation (Fig. 5.10, top) for control and all the tested scaffolds (i.e. implanted animals), being more evident for dexamethasone-loaded scaffolds. After 14 weeks (Fig. 5.10 bottom), there is a notable difference in the bone growth between the control and the animals implanted with scaffolds, being PCL-SA-DS scaffolds the ones that exhibited a higher and more continuous radiological density throughout the implant. The release

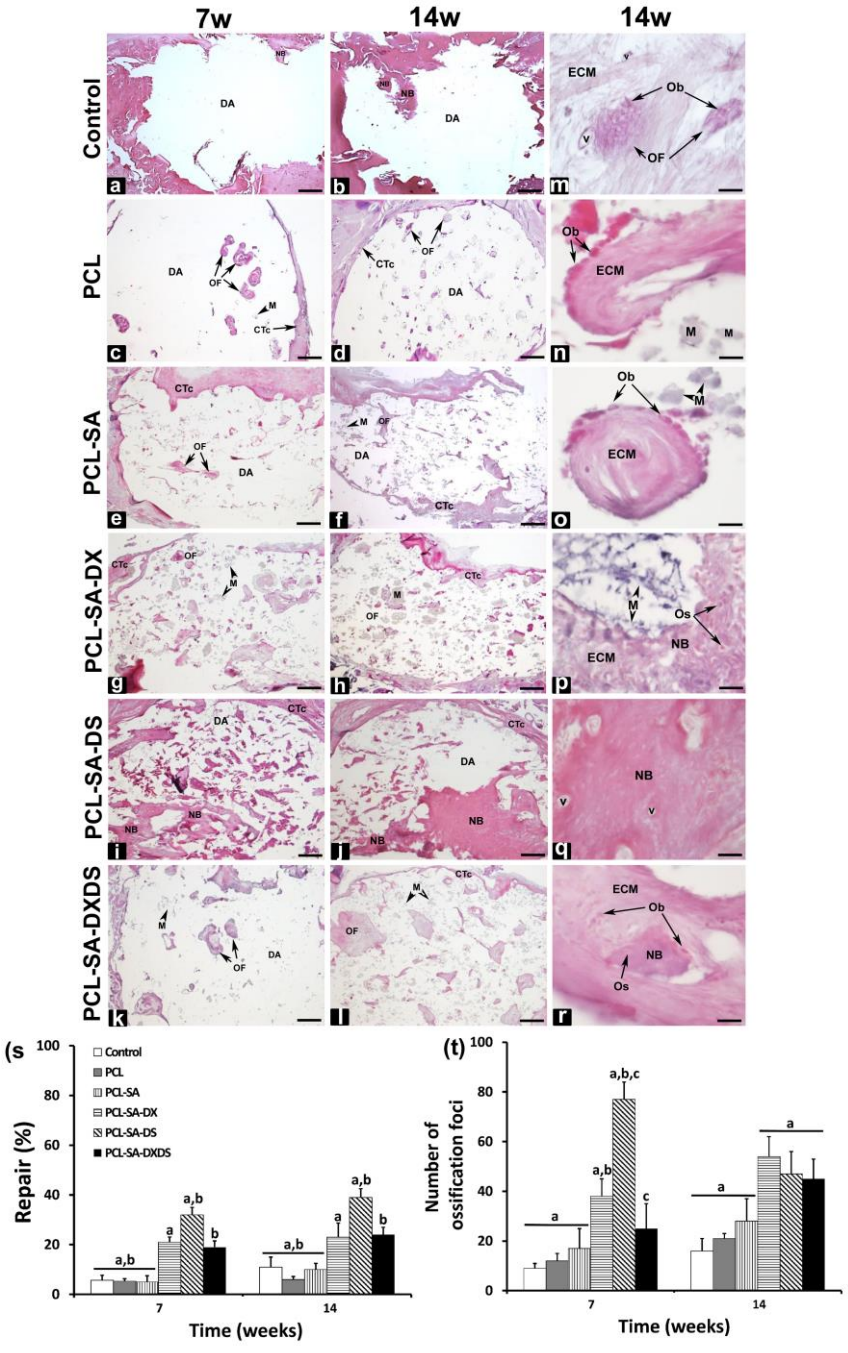
7w
14w
14w
Control
PCL
PCL-SA
PCL-SA-DX
PCL-SA-DS
PCL-SA-DXDS
DA
NB
OF
CTc
M
ECM
Ob
Os
V
(s
Repair (%)
Control
PCL
PCL-SA
PCL-SA-DX
PCL-SA-DS
PCL-SA-DXDS
Time (weeks)
(t)
Number of ossification foci
Time (weeks)

Fig. 5.9: Histological and histomorphometrical analysis of the supercritically processed scaffolds: Horizontal sections in panoramic view of the defect site in the control (a,b) and different experimental groups, at (c,e,g,i,k) 7 and (d,f,h,j,l) 14 weeks after implantation of PCL-based scaffolds. A connective tissue capsule (CTc) was observed surrounding the defect area (DA), and the presence of multiple ossification foci (OF) (arrows) surrounded by rests of material (M) (arrowheads) therein. The column on the right shows at high magnification the morphology and characteristics of the (m,n,o) ossification foci and (p,q,r) newly formed bone in the different experimental groups. Histograms represent (s) the percent of repair and (t) the number of ossification foci in the defect area in the different experimental groups 7 and 14 weeks post-implantation. Values are expressed as mean ± SD (n = 3). The same letter on different histograms indicates significant differences, $p < 0.05$. Notation: CTc: connective tissue capsule, DA: defect area, ECM: extracellular matrix (collagen fibers), M: material, NB: newly formed bone, Ob: osteoblast, OF: ossification foci, Os: osteocyte, v: blood vessel. Scale bars: (a-j): 1 mm. (k-o): 60 µm.

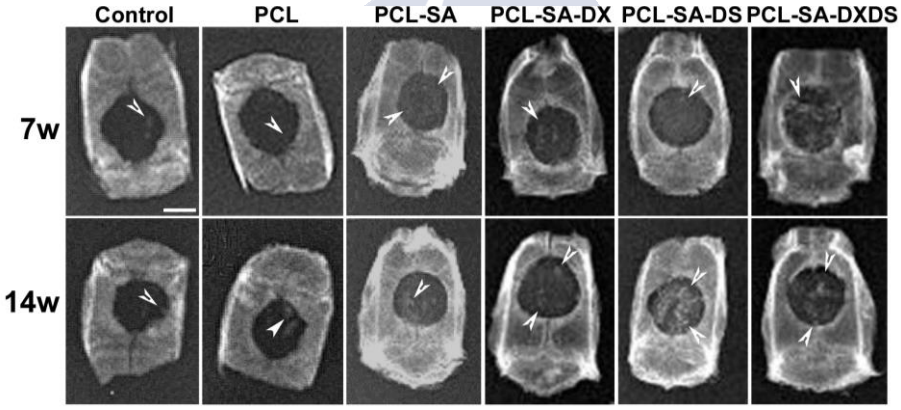

Fig. 5.10: Representative X-ray radiographies of rat crania 7 (top) and 14 (bottom) weeks post-implantation of control and PCL-based scaffolds of different compositions: PCL-SA, PCL-SA-DS, PCL-SA-DX and PCL-SA-DXDS scaffolds. The arrowheads indicate areas of radiological density compatible with bone neoformation. Scale bar: 4 mm.

profile of dexamethasone in PCL-SA-DS with local doses of the osteogenic differentiation agent reaching quickly therapeutic levels and maintaining these concentrations in the timeframe of weeks (*cf.* Section 5.3.3) had a remarkable enhancing effect on bone regeneration.

5.4. CONCLUSIONS

A technological platform based on the use of supercritical carbon dioxide as extraction solvent, gelation promoter, dispersing enhancer and foaming agent was endeavored to prepare nanostructured synthetic scaffolds with osteogenic activity. Submicron-sized aerogel particles of silk fibroin with β-sheet structure were prepared for the first time by combination of an ultrasound-assisted gelation process followed by supercritical CO_2-assisted drying. PCL-based scaffolds processed by supercritical foaming at near room temperature (37 ºC) and in the presence of aerogels had improved physicochemical properties (pore interconnectivity, surface roughness and thermal stability) for cell colonization and transport of biological fluids. Supercritical foaming process allowed the simultaneous scaffold processing and loading of dexamethasone as bioactive agent in a solvent-free approach and under mild operating conditions, which prevents drug leaching or degradation and bypasses the necessity of posterior purification processes, resulting in *ca.* 100 % drug incorporation yield. The importance of the dexamethasone form (base or salt) used in the formulation, a factor that is rarely taken into account, was also highlighted. The release profile of the drug salt from the scaffolds especially favored the *in vivo* biological performance of this formulation in critical-sized calvarial defects. The supercritically-processed scaffolds showed excellent compatibility with the host tissue with no signs of inflammation and promoting cell attachment and colonization at different locations of the defect as well as the development of extracellular matrix. The presence of dexamethasone, particularly in the salt form, in the scaffolds accelerated the osteogenic differentiation activity and promoted the bone repair (repair percentages of 39 % at 14 weeks post-implantation). The critical role of the morphological properties of the medicated scaffolds and the local release profile of bioactive agents, promptly reaching and sustaining therapeutic levels during the bone regeneration process, was herein highlighted. Future studies will focus on the study of the effect of dexamethasone on angiogenesis in the early stages of the reparative process (*ca.* 4 weeks post-implantation) and on the development of scaffolds for tissue regeneration able to customize the

time period keeping local therapeutic levels of bioactive agents at the critical-size bone defect.

5.5. REFERENCES

H. Akaike (1974). "A new look at the statistical model identification." *IEEE Transactions on Automatic Control* **19**(6): 716-723.

B. Androsits (1999). "Thermal Analysis Fundamentals and Applications and Polymer Science (second edition) Editors: T. Hatakeyama and F. X. Quinn." *Journal of Thermal Analysis and Calorimetry* **58**(1): 237-237.

S. D. Aznar-Cervantes, D. Vicente-Cervantes, L. Meseguer-Olmo, J. L. Cenis and A. A. Lozano-Pérez (2013). "Influence of the protocol used for fibroin extraction on the mechanical properties and fiber sizes of electrospun silk mats." *Materials Science and Engineering: C* **33**(4): 1945-1950.

Y. Baimark, P. Srihanam, Y. Srisuwan and P. Phinyocheep (2010). "Preparation of porous silk fibroin microparticles by a water-in-oil emulsification-diffusion method." *Journal of Applied Polymer Science* **118**(2): 1127-1133.

M. Bhamidipati, A. M. Scurto and M. S. Detamore (2013). "The future of carbon dioxide for polymer processing in tissue engineering." *Tissue Engineering - Part B: Reviews* **19**(3): 221-232.

P. Bhattacharjee, B. Kundu, D. Naskar, H. W. Kim, T. K. Maiti, D. Bhattacharya and S. C. Kundu (2017). "Silk scaffolds in bone tissue engineering: An overview." *Acta Biomaterialia* **63**: 1-17.

E. J. Carbone, K. Rajpura, T. Jiang, C. T. Laurencin and K. W. H. Lo (2014). "Regulation of bone regeneration with approved small molecule compounds." *Advances in Regenerative Biology* **1**(1): 25276.

N. J. Collins, G. A. Leeke, R. H. Bridson, F. Hassan and L. M. Grover (2008). "The influence of silica on pore diameter and distribution in PLA scaffolds produced using supercritical CO_2." *Journal of Materials Science: Materials in Medicine* **19**(4): 1497-1502.

Conseil de l'Europe (2008). "European Pharmacopoeia. 6.0." 1667-1668.

S. Curia, D. S. A. De Focatiis and S. M. Howdle (2015). "High-pressure rheological analysis of CO_2-induced melting point depression and viscosity reduction of poly(ε-caprolactone)." *Polymer* **69**: 17-24.

R. B. Chim, M. B. C. de Matos, M. E. M. Braga, A. M. A. Dias and H. C. de Sousa (2012). "Solubility of Dexamethasone in Supercritical Carbon Dioxide." *Journal of Chemical & Engineering Data* **57**(12): 3756-3760.

M. B. C. de Matos, A. P. Piedade, C. Alvarez-Lorenzo, A. Concheiro, M. E. M. Braga and H. C. de Sousa (2013). "Dexamethasone-loaded poly(ε-caprolactone)/silica nanoparticles composites prepared by supercritical CO_2 foaming/mixing and deposition." *International Journal of Pharmaceutics* **456**(2): 269-281.

L. Diaz-Gomez, A. Concheiro, C. Alvarez-Lorenzo and C. A. García-González (2016). "Growth factors delivery from hybrid PCL-starch scaffolds processed using supercritical fluid technology." *Carbohydrate Polymers* **142**: 282-292.

L. Diaz-Gomez, C. A. García-González, J. Wang, F. Yang, S. Aznar-Cervantes, J. L. Cenis, R. Reyes, A. Delgado, C. Évora, A. Concheiro and C. Alvarez-Lorenzo (2017). "Biodegradable PCL/fibroin/hydroxyapatite porous scaffolds prepared by supercritical foaming for bone regeneration." *International Journal of Pharmaceutics* **527**(1): 115-125.

A. R. C. Duarte, J. F. Mano and R. L. Reis (2009). "Supercritical fluids in biomedical and tissue engineering applications: A review." *International Materials Reviews* **54**(4): 214-222.

R. M. Duarte, J. Correia-Pinto, R. L. Reis and A. R. C. Duarte (2018). "Subcritical carbon dioxide foaming of polycaprolactone for bone tissue regeneration." *The Journal of Supercritical Fluids* **140**: 1-10.

P. Dubey, S. Murab, S. Karmakar, P. K. Chowdhury and S. Ghosh (2015). "Modulation of Self-Assembly Process of Fibroin: An Insight for Regulating the Conformation of Silk Biomaterials." *Biomacromolecules* **16**(12): 3936-3944.

T. A. Einhorn and L. C. Gerstenfeld (2015). "Fracture healing: mechanisms and interventions." *Nature Reviews. Rheumatology* **11**(1): 45-54.

M. A. Fanovich, J. Ivanovic, D. Misic, M. V. Alvarez, P. Jaeger, I. Zizovic and R. Eggers (2013). "Development of polycaprolactone scaffold with antibacterial activity by an integrated supercritical extraction and impregnation process." *The Journal of Supercritical Fluids* **78**: 42-53.

M. A. Fanovich and P. Jaeger (2012). "Sorption and diffusion of compressed carbon dioxide in polycaprolactone for the development of porous scaffolds." *Materials Science and Engineering: C* **32**(4): 961-968.

M. L. Floren, S. Spilimbergo, A. Motta and C. Migliaresi (2012). "Carbon dioxide induced silk protein gelation for biomedical applications." *Biomacromolecules* **13**(7): 2060-2072.

C. A. García-González, M. Alnaief and I. Smirnova (2011). "Polysaccharide-based aerogels - Promising biodegradable carriers for drug delivery systems." *Carbohydrate Polymers* **86**(4): 1425-1438.

C. A. García-González, J. Barros, A. Rey-Rico, P. Redondo, J. L. Gómez-Amoza, A. Concheiro, C. Alvarez-Lorenzo and F. J. Monteiro (2018). "Antimicrobial Properties and Osteogenicity of Vancomycin-Loaded Synthetic Scaffolds Obtained by Supercritical Foaming." *ACS Applied Materials & Interfaces* **10**(4): 3349-3360.

C. A. García-González, M. C. Camino-Rey, M. Alnaief, C. Zetzl and I. Smirnova (2012). "Supercritical drying of aerogels using CO_2: Effect of extraction time on the end material textural properties." *Journal of Supercritical Fluids* **66**: 297-306.

C. A. García-González, A. Concheiro and C. Alvarez-Lorenzo (2015). "Processing of Materials for Regenerative Medicine Using Supercritical Fluid Technology." *Bioconjugate Chemistry* **26**(7): 1159-1171.

C. A. García-González, M. Jin, J. Gerth, C. Alvarez-Lorenzo and I. Smirnova (2015). "Polysaccharide-based aerogel microspheres for oral drug delivery." *Carbohydrate Polymers* **117**: 797-806.

C. A. García-González, J. J. Uy, M. Alnaief and I. Smirnova (2012). "Preparation of tailor-made starch-based aerogel microspheres by the emulsion-gelation method." *Carbohydrate Polymers* **88**(4): 1378-1386.

E. Gibon, L. Y. Lu, K. Nathan and S. B. Goodman (2017). "Inflammation, ageing, and bone regeneration." *Journal of Orthopaedic Translation* **10**: 28-35.

L. Goimil, M. E. M. Braga, A. M. A. Dias, J. L. Gómez-Amoza, A. Concheiro, C. Alvarez-Lorenzo, H. C. de Sousa and C. A. García-González (2017). "Supercritical processing of starch aerogels and aerogel-loaded poly(ε-caprolactone) scaffolds for sustained release of ketoprofen for bone regeneration." *Journal of CO_2 Utilization* **18**: 237-249.

L. Goimil, P. Jaeger, I. Ardao, J. L. Gómez-Amoza, A. Concheiro, C. Alvarez-Lorenzo and C. A. García-González (2018). "Preparation and stability of dexamethasone-loaded polymeric scaffolds for bone regeneration processed by compressed CO_2 foaming." *Journal of CO_2 Utilization* **24**: 89-98.

P. J. Harwood, J. B. Newman and A. L. R. Michael (2010). "An update on fracture healing and non-union." *Orthopaedics and Trauma* **24**(1): 9-23.

A. Hernández, E. Sánchez, I. Soriano, R. Reyes, A. Delgado and C. Évora (2012). "Material-related effects of BMP-2 delivery systems on bone regeneration." *Acta Biomaterialia* **8**(2): 781-791.

R. Hohl, R. B. d. Oliveira, D. V. d. Macedo and R. Brenzikofer (2007). "Apparatus for measuring rat body volume: a methodological proposition." *Journal of Applied Physiology* **102**(3): 1229-1234.

X. Hu, D. Kaplan and P. Cebe (2006). "Determining Beta-Sheet Crystallinity in Fibrous Proteins by Thermal Analysis and Infrared Spectroscopy." *Macromolecules* **39**(18): 6161-6170.

M. Jewell, W. Daunch, B. Bengtson and E. Mortarino (2015). "The development of SERI® Surgical Scaffold, an engineered biological scaffold." *Annals of the New York Academy of Sciences* **1358**(1): 44-55.

Jóhannesson G., Stefánsson E and L. T. (2016). Microspheres and nanotechnology for drug delivery *Retinal Pharmacotherapy*. Rodrigues EB, Farah ME and M. WF. Basel, Karger. **55:** 93-103.

D. J. Kang, D. Xu, Z. X. Zhang, K. Pal, D. S. Bang and J. K. Kim (2009). "Well-Controlled Microcellular Biodegradable PLA/Silk Composite Foams Using Supercritical CO_2." *Macromolecular Materials and Engineering* **294**(9): 620-624.

C. A. Kelly, S. M. Howdle, K. M. Shakesheff, M. J. Jenkins and G. A. Leeke (2012). "Viscosity studies of poly(DL-lactic acid) in supercritical CO2." *Journal of Polymer Science Part B: Polymer Physics* **50**(19): 1383-1393.

K. H. Kim, L. Jeong, H. N. Park, S. Y. Shin, W. H. Park, S. C. Lee, T. I. Kim, Y. J. Park, Y. J. Seol, Y. M. Lee, Y. Ku, I. C. Rhyu, S. B. Han and C. P. Chung (2005). "Biological efficacy of silk fibroin nanofiber membranes for guided bone regeneration." *Journal of Biotechnology* **120**(3): 327-339.

Ž. Knez, D. Cör and M. Knez Hrnčič (2018). "Solubility of Solids in Sub- and Supercritical Fluids: A Review 2010–2017." *Journal of Chemical & Engineering Data* **63**(4): 860-884.

C. X. F. Lam, D. W. Hutmacher, J. T. Schantz, M. A. Woodruff and S. H. Teoh (2009). "Evaluation of polycaprolactone scaffold degradation for 6 months in vitro and in vivo." *Journal of Biomedical Materials Research Part A* **90A**(3): 906-919.

D. W. Li, J. He, F. L. He, Y. L. Liu, Y. Y. Liu, Y. J. Ye, X. Deng and D. C. Yin (2018). "Silk fibroin/chitosan thin film promotes osteogenic and adipogenic differentiation of rat bone marrow-derived mesenchymal stem cells." *Journal of Biomaterials Applications* **32**(9): 1164-1173.

L. Li, H. Li, Y. Qian, X. Li, G. K. Singh, L. Zhong, W. Liu, Y. Lv, K. Cai and L. Yang (2011). "Electrospun poly (ε-caprolactone)/silk fibroin core-sheath nanofibers and their potential applications in tissue engineering and drug release." *International Journal of Biological Macromolecules* **49**(2): 223-232.

M. Li and J. Li (2014). Biodegradation behavior of silk biomaterials. *Silk Biomaterials for Tissue Engineering and Regenerative Medicine*. S. C. Kundu. Cambridge, UK, Woodhead Publishing**:** 330-348.

A. A. Lozano-Pérez, M. G. Montalbán, S. D. Aznar-Cervantes, F. Cragnolini, J. L. Cenis and G. Víllora (2015). "Production of silk fibroin nanoparticles using ionic liquids and high-power ultrasounds." *Journal of Applied Polymer Science* **132**(12).

H. Maleki, L. Durães, C. A. García-González, P. del Gaudio, A. Portugal and M. Mahmoudi (2016). "Synthesis and biomedical applications of aerogels: Possibilities and challenges." *Advances in Colloid and Interface Science* **236**: 1-27.

R. R. Mallepally, M. A. Marin and M. A. McHugh (2014). "CO$_2$-assisted synthesis of silk fibroin hydrogels and aerogels." *Acta Biomaterialia* **10**(10): 4419-4424.

R. R. Mallepally, M. A. Marin, V. Surampudi, B. Subia, R. R. Rao, S. C. Kundu and M. A. McHugh (2015). "Silk fibroin aerogels: potential scaffolds for tissue engineering applications." *Biomedical Materials* **10**(3): 035002.

M. A. Marin, R. R. Mallepally and M. A. McHugh (2014). "Silk fibroin aerogels for drug delivery applications." *Journal of Supercritical Fluids* **91**: 84-89.

A. Matsumoto, J. Chen, A. L. Collette, U.-J. Kim, G. H. Altman, P. Cebe and D. L. Kaplan (2006). "Mechanisms of Silk Fibroin Sol−Gel Transitions." *The Journal of Physical Chemistry B* **110**(43): 21630-21638.

J. Melke, S. Midha, S. Ghosh, K. Ito and S. Hofmann (2016). "Silk fibroin as biomaterial for bone tissue engineering." *Acta Biomaterialia* **31**: 1-16.

M. A. d. Moraes, C. R. A. Mahl, M. F. Silva and M. M. Beppu (2015). "Formation of silk fibroin hydrogel and evaluation of its drug release profile." *Journal of Applied Polymer Science* **132**(15).

V. Mouriño and A. R. Boccaccini (2010). "Bone tissue engineering therapeutics: controlled drug delivery in three-dimensional scaffolds." *Journal of the Royal Society, Interface* **7**(43): 209-227.

A. R. Murphy and I. S. Romero (2014). 8 - Biochemical and biophysical properties of native Bombyx mori silk for tissue engineering applications. *Silk Biomaterials for Tissue Engineering and Regenerative Medicine*. S. C. Kundu, Woodhead Publishing**:** 219-238.

C. R. Nuttelman, M. C. Tripodi and K. S. Anseth (2006). "Dexamethasone-functionalized gels induce osteogenic differentiation of encapsulated hMSCs." *Journal of Biomedical Materials Research Part A* **76A**(1): 183-195.

B. Otsuki, M. Takemoto, S. Fujibayashi, M. Neo, T. Kokubo and T. Nakamura (2006). "Pore throat size and connectivity determine bone and tissue ingrowth into porous implants: Three-dimensional micro-CT based structural analyses of porous bioactive titanium implants." *Biomaterials* **27**(35): 5892-5900.

W. Paul and S. C.P (2015). Bioceramic and Composite Scaffolds in Drug Delivery and Bone Tissue Engineering. *Handbook of Intelligent Scaffolds for Tissue Engineering and Regenerative Medicine*. G. Khang. New York.

R. A. Perez, S. J. Seo, J. E. Won, E. J. Lee, J. H. Jang, J. C. Knowles and H. W. Kim (2015). "Therapeutically relevant aspects in bone repair and regeneration." *Materials Today* **18**(10): 573-589.

K. J. Rambhia and P. X. Ma (2015). "Controlled drug release for tissue engineering." *Journal of Controlled Release* **219**: 119-128.

M. Rodríguez-Évora, A. Delgado, R. Reyes, A. Hernández-Daranas, I. Soriano, J. San Román and C. Évora (2013). "Osteogenic effect of local, long versus short term BMP-2 delivery from a novel SPU–PLGA–βTCP concentric system in a critical size defect in rats." *European Journal of Pharmaceutical Sciences* **49**(5): 873-884.

C. Romagnoli, F. D'Asta and M. L. Brandi (2013). "Drug delivery using composite scaffolds in the context of bone tissue engineering." *Clinical cases in mineral and bone metabolism : the official journal of the Italian Society of Osteoporosis, Mineral Metabolism, and Skeletal Diseases* **10**(3): 155-161.

A. Salerno, S. Diéguez, L. Diaz-Gomez, J. L. Gómez-Amoza, B. Magariños, A. Concheiro, C. Domingo, C. Alvarez-Lorenzo and C. A. García-González (2017). "Synthetic scaffolds with full pore interconnectivity for bone regeneration prepared by supercritical foaming using advanced biofunctional plasticizers." *Biofabrication* **9**(3): 035002.

A. Salerno and C. D. Pascual (2015). "Bio-based polymers, supercritical fluids and tissue engineering." *Process Biochemistry* **50**(5): 826-838.

S. K. Samal, D. L. Kaplan and E. Chiellini (2013). "Ultrasound sonication effects on silk fibroin protein." *Macromolecular Materials and Engineering* **298**(11): 1201-1208.

C. Tang, Y. X. Guan, S. J. Yao and Z. Q. Zhu (2014). "Solubility of Dexamethasone in Supercritical Carbon Dioxide with and without a Cosolvent." *Journal of Chemical & Engineering Data* **59**(11): 3359-3364.

S. Thomas, P. Balakrishnan and M. S. Sreekala (2018). *Fundamental Biomaterials: Polymers*. Cambridge, Elsevier Science.

H. Tsuji and Y. Ikada (1998). "Blends of aliphatic polyesters. II. Hydrolysis of solution-cast blends from poly(L-lactide) and poly(E-caprolactone) in phosphate-buffered solution." *Journal of Applied Polymer Science* **67**(3): 405-415.

Z. Ulker and C. Erkey (2014). "An emerging platform for drug delivery: Aerogel based systems." *Journal of Controlled Release* **177**(1): 51-63.

A. ur-Rahman and S. Anjum (2015). *Frontiers in Stem Cell and Regenerative Medicine Research*. Sharjah, Bentham Science Publishers.

N. M. Vacanti, H. Cheng, P. S. Hill, J. D. T. Guerreiro, T. T. Dang, M. Ma, S. Watson, N. S. Hwang, R. Langer and D. G. Anderson (2012). "Localized delivery of dexamethasone from electrospun fibers reduces the foreign body response." *Biomacromolecules* **13**(10): 3031-3038.

R. D. Vaishya, M. Gokulgandhi, S. Patel, M. Minocha and A. K. Mitra (2014). "Novel dexamethasone-loaded nanomicelles for the intermediate and posterior segment uveitis." *AAPS PharmSciTech* **15**(5): 1238-1251.

M. Wang, H. J. Jin, D. L. Kaplan and G. C. Rutledge (2004). "Mechanical Properties of Electrospun Silk Fibers." *Macromolecules* **37**(18): 6856-6864.

W. Wang and K. W. K. Yeung (2017). "Bone grafts and biomaterials substitutes for bone defect repair: A review." *Bioactive Materials* **2**(4): 224-247.

X. Wang, J. Kluge, G. G. Leisk and D. L. Kaplan (2008). "Sonication-Induced Gelation of Silk Fibroin for Cell Encapsulation." *Biomaterials* **29**(8): 1054-1064.

L. Xia, W. Xiupeng, J. Xiangfen, Y. Maho, I. Atsuo, B. Yoshio and G. Dmitri (2016). "Boron nitride nanotube-enhanced osteogenic differentiation of mesenchymal stem cells." *Journal of Biomedical Materials Research Part B: Applied Biomaterials* **104**(2): 323-329.

X. Xin, Y. X. Guan and S. J. Yao (2018). "Sustained release of dexamethasone from drug-loading PLGA scaffolds with specific pore structure fabricated by supercritical CO_2 foaming." *Journal of Applied Polymer Science* **135**(17): 46207.

Ying Deng and J. Kuiper (2018). *Functional 3D Tissue Engineering Scaffolds: Materials, Technologies and Applications*. Chippenham, UK, Woodhead publishing.

Y. Q. Zhang, W. D. Shen, R. L. Xiang, L. J. Zhuge, W. J. Gao and W. B. Wang (2007). "Formation of silk fibroin nanoparticles in water-miscible organic solvent and their characterization." *Journal of Nanoparticle Research* **9**(5): 885-900.

M. Zhao, P. Li, H. Xu, Q. Pan, R. Zeng, X. Ma, Z. Li and H. Lin (2018). "Dexamethasone-Activated MSCs Release MVs for Stimulating Osteogenic Response." *Stem Cells International* **2018**: 12.

USC
UNIVERSIDADE
DE SANTIAGO
DE COMPOSTELA

6. CONCLUSIONS

The development of biodegradable scaffolds for bone tissue regeneration was carried out taking advantage of the properties of compressed and supercritical CO_2, minimizing or avoiding the use of organic solvents and high temperatures. The work of this Ph. D Thesis was performed in three different steps focusing on various relevant aspects for the implementation of these techniques, leading to the following conclusions:

1. Regarding the scaffolds prepared with PCL and low intrinsic viscosity PLGA, the compressed CO_2 assisted-foaming technique was optimized with the addition of liquid CO_2 during depressurization as a means to control the expansion of the polymeric foam. This approach allowed the control of the porosity and pore size of the scaffolds. Besides, magnetic suspension balance was used as an analytical technique to assess CO_2 sorption profile with time under the processing conditions, 26 ºC and 60 bar, determining the most appropriate soaking period. The resulting scaffolds presented a dual porosity, with a population of 50-200 μm and other with 10 μm mean pore size, that is prospected to favor cell attachment and growth and to promote vascularization. The release profile of dexamethasone was mainly governed by the erosion of the matrix and the swelling effect of starch and could be sustained for up to 3 weeks, matching the natural bone regeneration process. Storage for 1 to 3 months under zone II ICH-climatic conditions (25 ºC and 65 % RH) revealed that the addition of starch and dexamethasone resulted in less crystalline

structures that were more sensitive to environmental humidity. As a result, prolonged exposition to zone II ICH-climatic conditions had detrimental effects on the capability of pregelified starch to regulate drug release. Overall, the findings of this part of the Thesis highlight the versatility of the compressed CO_2 foaming technique to combine polymers with different biodegradation profiles and to obtain precisely designed porous structures capable of providing sustained drug release. Moreover, the study calls attention on the impact that storage may have on properties relevant for the performance of the scaffolds in bone regeneration.

2. Application of emulsion-gelation followed by supercritical drying allowed obtaining micron-sized starch aerogels with specific surface areas of up to 188 m^2/g. The effect of the incorporation of starch aerogel particles into PCL scaffolds by supercritical foaming was described for the first time. Their addition caused an increase in the porosity from 54 to 66 %, and up to 70 % with the presence of ketoprofen. Maximum pore sizes obtained by supercritical CO_2 foaming for PCL scaffolds were also increased from 200-300 μm to 300-600 μm with the inclusion of starch aerogels in the formulation, as well as pore interconnectivity and surface roughness, key parameters for scaffolds in bone regeneration. An anti-inflammatory drug, ketoprofen, was loaded into the scaffolds, providing a sustained release during the span of days, which may be suitable to avoid a prolonged inflammation due to foreign body response after implantation. Besides, the mild operating conditions of supercritical CO_2 foaming, 37 ºC and 140 bar, enabled the incorporation of thermolabile bioactive compounds without the need of organic solvents and achieving *ca.* 100 % incorporation yields.

3. The gelation method of silk fibroin to obtain submicron-sized silk fibroin gel particles was optimized by testing different gelation-

promoters, ultrasounds, ethanol and CO_2, aimed at inducing a change in conformation from soluble random coil to a stable β-sheet structure. As a result, an ultrasound-assisted emulsion-gelation protocol followed by supercritical drying was selected as the most suitable approach for the preparation of silk fibroin aerogels with surface specific areas above 330 m^2/g. These microparticles not only improved the physicochemical properties of the PCL-based scaffolds processed by supercritical foaming, as previously seen with the addition of starch aerogels, obtaining pore sizes in the range of 100 to 400 μm and cell infiltration values of 89-95 %, but also incorporate the capacity of promoting tissue regeneration of silk fibroin. Two forms of dexamethasone, as base (DX) and salt (DS), in two concentrations (0.1 and 5 wt.%) were included in the formulation to evaluate the distinct release profiles and effect on the properties of the scaffolds. Different drug release behaviours were observed owing to their distinct PCL-drug interactions. Drug delivery was sustained for 3 weeks in all cases, but DS showed a two-stage release, with a burst release during the first hour and a sustained release in the following weeks, while there was no such burst release for DX. The presence of dexamethasone in either of its forms had a plasticizing effect, especially when incorporated in low concentrations (0.1 wt.%), favouring pore growth and interconnection. *In vivo* tests in critical calvarial defects in Sprague-Dawley rats were conducted for the scaffolds with and without dexamethasone and revealed a more favouring performance for scaffolds containing DS, reaching repair percentages of 39 % at 14 weeks after implantation, almost doubling the results for the scaffolds containing DX. The results for PCL and PCL-SA grafts did not show significant differences from control group (empty defect), which evidences the importance of the incorporation of osteoinductive factors and the choice of the drug form administered in enhancing bone repair.

USC
UNIVERSIDADE
DE SANTIAGO
DE COMPOSTELA

ANNEX

CONFLICT OF INTEREST

I declare no conflict of interest with the subject, matter or materials discussed in this Thesis.

Miss Leticia Goimil García

Departamento de
Ingeniería Química y
Tecnología Farmacéutica
Universidad de La Laguna

La Laguna a 29 de mayo de 2019

Carmen Mª Évora García (DNI: 42017429V) Catedrática de la Universidad de La Laguna del área de Farmacia y Tecnología Farmacéutica e Investigadora principal del proyecto de investigación MAT201455657-R

Hago constar que:

El estudio de investigación realizado por Leticia Goimil et al., con scaffolds tipo aerogel en un defecto óseo crítico de rata, publicado en la revista científica Journal of CO_2 Utilization
31 (2019) 51–64 con el título "scCO2-foamed silk fibroin aerogel/poly(ε-caprolactone) scaffolds containing dexamethasone for bone regeneration" fue realizado respetando los requerimientos vigentes éticos y legales de la investigación con animales. Éste trabajo fue llevado a cabo bajo el amparo del informe positivo emitido por el Comité de Ética de la Investigación y Bienestar Animal de la Universidad de La Laguna para el proyecto MAT201455657-R (se adjunta).

CEIBA

Comité de Ética de la Investigación y Bienestar Animal
Vicerrectorado de Investigación y Transferencia de Conocimiento Universidad de La Laguna. 38071, La Laguna
ceiba@ull.es

Proyecto de Investigación: Sistemas inyectables para regeneración ósea en osteoporosis Investigador Principal: CARMEN MARIA EVORA GARCIA
Organismo: Ministerio de Ciencia e Innovación Número de Registro: CEIBA2014-0128

En su reunión del 05 de noviembre de 2014, el Comité de Ética de la Investigación y Bienestar Animal de la Universidad de La Laguna ha revisado el proyecto de investigación arriba mencionado. Tras adecuada deliberación emite el siguiente informe:

Tanto el protocolo como los procedimientos para la utilización de animales respetan los requerimientos éticos y legales de la investigación con animales.

Por tanto el proyecto presentado satisface los requerimientos

de la ética de la investigación y el Comité emite un informe **positivo** y da la autorización solicitada para la realización del estudio en los términos propuestos.

La Secretaria del CEIBA

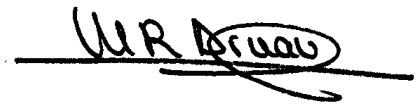

Dr. María Rosa Arnau
En La Laguna, a 05 de noviembre de 2014

Comité de Ética de la Investigación y Bienestar Animal.
Vicerrectorado de Investigación y Transferencia de Conocimiento. Universidad de La Laguna. 38071, La Laguna.

FE DE ERROS

-Lenda da figura 4.7:

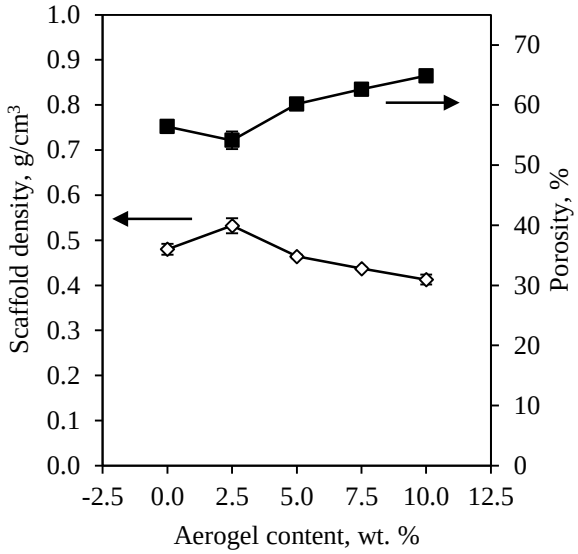

Fig. 4.7: Effect of starch aerogel content in PCL-based scaffolds on the bulk density and porosity of the scaffolds. Statistical comparison regarding scaffold density: 1-way ANOVA test ($F_{4,5d.f.}$=35.37; α<0.01); Tukey's multiple comparisons test: 0 2.5 5.0 7.5 10. Statistical comparison regarding scaffold porosity: 1-way ANOVA ($F_{4,5d.f.}$=45.03; α<0.01); Tukey's multiple comparisons test: 2.5 0 5.0 7.5 10 . Notation: the groups connected by an underline are not significantly different.

-Conclusións:

1. A compressed CO_2 assisted-foaming technique was optimized with the addition of liquid CO_2 during depressurization to control the expansion of the polymeric foam of PCL and low intrinsic viscosity PLGA, allowing the control of the porosity and pore size of the scaffolds. Also, the most appropriate soaking period was determined by magnetic suspension balance, assessing CO_2 sorption profile with

time under the processing conditions, 26 ºC and 60 bar. The resulting scaffolds presented a dual porosity, with a population of 50-200 μm and other with 10 μm mean pore size, which should favor cell attachment and growth and promote vascularization. The release profile of dexamethasone was mainly governed by the erosion of the matrix and the swelling effect of starch, and could be sustained for up to 3 weeks. Storage for 1 to 3 months under zone II ICH-climatic conditions (25 ºC and 65 % RH) revealed that the addition of starch and dexamethasone resulted in less crystalline structures, more sensitive to environmental humidity. As a result, prolonged exposition to zone II ICH-climatic conditions had detrimental effects on the capability of pregelified starch to regulate drug release. Overall, the findings of this part of the Thesis highlight the versatility of the compressed CO_2 foaming technique to combine polymers with different biodegradation profiles and to tune the porous structure, and also call attention on the impact that storage conditions have on properties relevant for the performance of the scaffolds.

2. Application of emulsion-gelation followed by supercritical drying allowed obtaining micron-sized starch aerogels with specific surface areas of up to 188 m^2/g. The effect of the incorporation of starch aerogel particles into PCL scaffolds by supercritical foaming was described for the first time. Their addition caused an increase in the porosity from 54 to 66 %, and up to 70 % with the presence of ketoprofen. Maximum pore sizes obtained by supercritical CO_2 foaming for PCL scaffolds were also increased from 200-300 μm to 300-600 μm with the inclusion of starch aerogels in the formulation, as well as pore interconnectivity and surface roughness, key parameters for scaffolds in bone regeneration. An anti-inflammatory drug, ketoprofen, was loaded into the scaffolds, providing a sustained release during the span of days, which may be suitable to avoid a prolonged inflammation due to foreign body response after

implantation. Besides, the mild operating conditions of supercritical CO_2 foaming, 37 ºC and 140 bar, enabled the incorporation of thermolabile bioactive compounds without the need of organic solvents and achieving *ca.* 100 % incorporation yields.

3. The gelation method of silk fibroin to obtain submicron-sized silk fibroin gel particles was optimized by testing different gelation-promoters, ultrasounds, ethanol and CO_2, aimed at inducing a change in conformation from soluble random coil to a stable β-sheet structure. An ultrasound-assisted emulsion-gelation protocol followed by supercritical drying was selected as the most suitable approach, and silk fibroin aerogels with surface specific areas above 330 m^2/g were obtained. These microparticles improved the physicochemical properties of the PCL-based scaffolds processed by supercritical foaming, obtaining pore sizes in the range of 100 to 400 μm and cell infiltration values of 89-95 %, and also incorporate the capacity of promoting tissue regeneration of silk fibroin. Two forms of dexamethasone, as base (DX) and salt (DS), in two concentrations (0.1 and 5 wt.%) were included in the formulation to evaluate the distinct release profiles and effect on the properties of the scaffolds. Drug delivery was sustained for 3 weeks in all cases, but DS showed a burst release during the first hour and a sustained release in the following weeks, while there was no such burst release for DX. The presence of dexamethasone in either of its forms had a plasticizing effect, especially when incorporated in low concentrations (0.1 wt.%), favouring pore growth and interconnection. *In vivo* tests in critical calvarial defects in Sprague-Dawley rats were conducted for the scaffolds with and without dexamethasone and revealed a better performance for scaffolds containing DS, reaching repair percentages of 39 % at 14 weeks after implantation, almost doubling the results for the scaffolds containing DX. The results for PCL and PCL-SA grafts

did not show significant differences from control group (empty defect).